ELSEVIER

Journal of Non-Crystalline Solids 169 (1994) 211–266

JOURNAL OF NON-CRYSTALLINE SOLIDS

Review Paper

Enthalpy relaxation and recovery in amorphous materials

I.M. Hodge *

Eastman Kodak Company, Imaging Research Laboratories, Rochester, NY 14650-2116, USA

(Received 28 July 1993; revised manuscript received 1 November 1993)

Abstract

The field of enthalpy relaxation is reviewed. Current phenomenologies for dealing with the non-linear and non-exponential character of enthalpy relaxation are presented, and their successes and shortcomings are discussed. Qualitative experimental data and quantitative parameterizations are summarized, and some directions for future research are suggested.

1. Introduction

This review summarizes developments in enthalpy relaxation in amorphous materials up to the end of 1992. The field is intimately associated with the glass transition, and an abbreviated account of the glass transition phenomenon is included. A comprehensive account of the glass transition as an independent field of scientific endeavor is not attempted, however. Excellent accounts of the glass transition and glassy state are available [1–5].

The review is divided into seven sections. The introduction begins with some brief comments on nomenclature, followed by a summary of those aspects of linear response theory that provide a foundation for the non-linear phenomenology of enthalpy relaxation, and a brief account of the kinetics of the glass transition. An account of experimental techniques is given in Section 2, with emphasis given to experimental difficulties that can affect data quality. Phenomenological equations for describing enthalpy relaxation are introduced in Section 3, and calculation procedures for implementing them are described in Section 4. Experimental results are summarized in Section 5, and enthalpy relaxation parameters are discussed in Section 6. A summary and some thoughts for future research are given in Section 7.

1.1. Nomenclature

Many experiments described as enthalpy relaxation would be better described as enthalpy recovery, because it is the enthalpy recovered during heating that is recorded and analyzed. Enthalpy is also a retardation function rather than a relaxation one (Section 1.2.2). To be consistent with entrenched usage in the literature, however, the terms enthalpy relaxation or simply relaxation will be used here in statements of a general nature. The more precise terms 'enthalpy recov-

* Corresponding author. Tel: +1-716 477 3165. Telefax: +1-716 722 2327.

SSDI 0022-3093(93)E0614-E

ery' and 'retardation times' are used where these are specifically appropriate. Relaxation in the glassy state is referred to in the literature as structural relaxation, physical aging, stabilization or annealing. The phrase 'structural relaxation' refers to inferred changes in atomic arrangement that occur during relaxation, although these are not known in any detail for most materials. The term 'physical aging' was introduced by Struik [6], to distinguish relaxation effects from those produced by chemical reactions, degradation or changes in crystallinity. The variety of terminologies reflects the considerable practical importance of glassy state relaxation, to both inorganic and organic high polymer glass science and technology. We choose the term structural relaxation here, and refer to relaxation in the glassy state as annealing. Annealing time and temperature are written as t_a and T_a, respectively. For convenience, the supercooled liquid or rubbery state above the glass transition temperature range is referred to as the equilibrium state, to distinguish it from the non-equilibrium glassy state, even though supercooled liquids and some rubbers are metastable with respect to the crystalline state (except for most atactic polymers). Differential scanning calorimetry is referred to as DSC.

The thermodynamic or ideal glass temperature, at which excess properties such as entropy vanish, is referred to in the literature as T_0 (introduced by Fulcher), T_∞ (introduced by Vogel and also used by Tamman and Hesse), T_2 (introduced by Gibbs and DiMarzio) and T_K (identified by Kauzmann). Theoretical and experimental reasons can be given for believing that T_0, T_2 and T_K are equal for several materials (discussed below), but this belief is not uniformly accepted. Here, T_0 denotes the adjustable parameter in the empirical linear Vogel–Tamman–Fulcher equation, T_2 is the temperature of zero excess entropy in theoretically derived non-linear kinetic equations and T_K is the thermodynamically determined Kauzmann temperature of zero excess entropy. Sets of subscripted variables or material parameters are enclosed in braces, e.g., $\{T_i\}$. Braces are also used as the highest member in the hierarchy of parentheses, $\{[(\ldots)]\}$. Averaged quantities are denoted by $\langle \ldots \rangle$.

1.2. Kinetics of the glass transition

1.2.1. General aspects

The calorimetrically observed glass transition is a kinetic phenomenon, and it is the kinetics of the transition with which enthalpy relaxation is concerned. The observed glass transition is essentially a Deborah number (DN) effect, named after the prophetess Deborah who declared that what appeared to mortals to be stationary, such as non-volcanic mountains and the size of the oceans, are not necessarily so to an eternal deity. The Deborah number is defined as the ratio of timescales of the observed and the observer, and the glass transition is seen when these two timescales for structural relaxation cross over and DN passes through unity. Thus, the glass transition can be studied by changing the timescale of either the experimental probe, or the system under study. The experimental timescale can be varied by changing either the frequency of an applied sinusoidal perturbation, or the observation time for a time-dependent property. The timescale of structural relaxation can be controlled by temperature or pressure, or by various applied stresses if the system is non-linear. In the temperature domain that is explored most thoroughly, a DN of unity that defines an average glass transition temperature, T_g, can be expressed in terms of the rate of change of some characteristic timescale, τ, determined during cooling:

$$\mathrm{DN} \equiv \frac{\mathrm{d}\tau}{\mathrm{d}t} = \frac{\mathrm{d}\tau}{\mathrm{d}T}\frac{\mathrm{d}T}{\mathrm{d}t} = \frac{\Delta H_{\mathrm{eff}}}{RT_g^2} Q_c \tau \approx 1.0, \qquad (1)$$

where ΔH_{eff} is the effective average activation energy at T_g, defined as $(\partial \ln \tau/\partial(1/T))|_{T_g}$ (e.g., Eq. (5) below), R is the ideal gas constant and Q_c is the cooling rate. The derivative $\mathrm{d}\tau/\mathrm{d}t$ has also been termed the Lillie number by Cooper [7], and has been discussed by Cooper and Gupta [8] and Scherer [9]. Equating it to unity is implicit in earlier work, however, and has been used to estimate $\tau(T_g)$ in terms of the activation energy and scan rate, for example in Ref. [10]. It will enter again into the discussion of the fictive temperature in Section 1.2.3. It is not advisable to define DN (and therefore T_g) in terms of the

heating rate, Q_h, alone, because the kinetics of recovery are partly determined by the previous history, such as cooling rate (often not specified, a practice that is to be discouraged), and annealing. It can be shown from quite general arguments that T_g increases in proportion to log Q_c [9,11,12], but the value of ΔH_{eff} near T_g is usually so large (typically several hundred kJ mol^{-1})

Table 1
Averaged Tool–Narayanaswamy and KAHR parameters

Material	$\Delta h^*/R$ (kK)	x	β	$-\ln A$ (s)	T_g (K)	$x\,\Delta h^*/R$ (kK)	$\Delta h^*/RT_g^2 = \theta$ (K^{-1})	Ref.
PVAc	71	0.35	0.57	224.5	310	25	0.74	[250]
	71	0.41	0.51	223.6		29	0.74	[133]
	88	0.27	0.51	277.5		24	0.92	[130]
PS	80	0.46	0.71	216.0	373	37	0.58	[130,161]
	70	0.48	–	–	373	34	0.56	[91]
	53–71	0.52	0.8	–	373	32	0.44	[153]
	76–110	*0.44*	*0.55*	–	373	*37*	*0.60*	*[246]*
PVC	225	0.10	0.23	622.0	353	23	1.74	[130]
BPAPC	150	0.19	0.46	355.8	415	29	0.87	[130]
a-PMMA	138	0.19	0.35	357.8	375	26	0.98	[130]
	150	0.20	0.35		375	21	0.75	[162]
i-PMMA	80	0.22	0.43		325	18	0.76	[162]
s-PMMA	135	0.20	0.35		395	27	0.87	[162]
B_2O_3	*45*	*0.40*	*0.65*	75.6	535	*18*	*0.16*	*[160]*
As_2Se_3	41	0.49	0.67	85.5	450	20	0.20	[257]
5P2E	39	0.40	0.70	153.1	243	16	0.65	[42]
NBS710 [a]	74	0.44	0.63	82.8	840	33	0.105	[129,141]
NBS711 [b]	45	0.65	0.65	57.4	670	29	0.10	[260]
ZBLA	168	0.23	0.43	282.9	580	39	0.50	[112,113,157]
	165	0.19	0.50	282.6		31	0.50	[130]
ZBLALiPb	*124*	*0.23*	*0.53*		*510*	*28*	*0.48*	*[112]*
ZBLALi	132	0.30	0.55		520	40	0.49	[112]
ZBLAN	112	0.35	0.56		535	39	0.39	[112]
ZBL	184	0.27	0.54		570	50	0.57	[112]
BZnYbT	137	0.35	0.48		620	48	0.36	[112]
LiAc	200	0.17	0.56	490.7	405	34	1.22	[133]
Glycerol	26	0.29	0.51		190	7.5	0.73	[113]
EG [c] (bulk)	*12*	*0.49*	*0.64*	*81.50*	*140*	*5.9*	*0.61*	*[218]*
EG [c] (gel) [d]	12	0.46	0.39	75.45	150	5.5	0.53	[218]
LiCl [e] (bulk)	12	0.68	0.93	82.10	145	8.2	0.57	[218]
LiCl [e] (gel) [d]	12	0.67	0.39	70.53	155	8.0	0.50	[218]
$40Ca(NO_3)_2$–$60KNO_3$	70	0.31	0.46	202.5	335	22	0.62	[258]
$24.4[yNa_2O\cdot(1-y)K_2O]$–$75.6SiO_2$ ($y = 0$ to 1.0)	49	0.70	0.66	62.8	750	34	0.087	[259]
$40AgI$–$60Ag_2MoO_4$	77	0.50	–	–	365	39	0.58	[245]
$50AgI$–$50Ag_2MoO_4$	61	0.55	–	–	345	34	0.51	[245]
$60AgI$–$40Ag_2MoO_4$	43	0.65	–	–	325	28	0.41	[245]
$75AgPO_3$–$25Ag_2MoO_4$	61	0.68	–	–	539	41	0.21	[244]
$30AgI$–$52.5AgPO_3$–$17.5Ag_2MoO_4$	49	0.68	–	–	471	33	0.22	[244]
$50AgI$–$37.5AgPO_3$–$12.5Ag_2MoO_4$	54	0.68	–	–	418	37	0.31	[244]

[a] Soda–lime–silicate.
[b] Lead silicate.
[c] Ethylene glycol (22 mol% in H_2O).
[d] Imbibed in poly(hydroxyethyl-methacrylate).
[e] LiCl (16 mol% in H_2O).

that T_g is defined to within a few K for cooling rates that vary over several orders of magnitude. Another definition of DN is

$$\mathrm{DN} \equiv \tau/\langle t \rangle \approx 1, \tag{2}$$

where $\langle t \rangle$ is some average time of observation. If $\langle t \rangle$ is numerically equated to the inverse of Q_c (i.e., $Q_c\tau \approx 1$ K), Eqs. (1) and (2) are consistent only when the factor $\Delta H_{eff}/RT_g^2$ is of order unity. Such consistency is indeed found for a wide variety of glasses (Table 1), although there is a tendency for some inorganic glasses to have values of $\Delta H_{eff}/RT_g^2$ closer to 0.1. The last observation is the source of the frequently quoted generalization that $\tau(T_g) \approx 10^2$ s, since from Eq. (1) $\tau(T_g) \approx (RT_g^2/\Delta H_{eff})(1/Q_c) \approx 10/Q_c \approx 60$ s, for a typical cooling rate of 10 K min^{-1}. The quantity $\Delta H_{eff}/RT_g^2$ is equal to the KAHR parameter θ (Section 3.2.2.).

In this review, T_g is generally used to denote the temperature at which the heat capacity measured during heating reaches half of its ultimate increase through the glass transition region (the 'midpoint' definition frequently used in DSC scans). More specific definitions and additional nomenclature are introduced in the discussion of fictive temperature in Section 1.2.3. The average relaxation time at T_g for typical DSC scans depends on history, and on how T_g is defined from DSC data. Calculations using the Tool–Narayanaswamy phenomenology (Section 4.2.) confirm the Lillie number analysis given above: for $Q_c = Q_h = 10$ K min^{-1}, $\tau(T_g) \approx 100$ s for the 'onset' definition of T_g (where the heat capacity first starts to rise above the glassy state background). This onset value is the temperature at which the tangent drawn through the inflection point in the middle of the transition intersects the extrapolated glass heat capacity. The 'onset' and 'midpoint' definitions of T_g are illustrated in Fig. 1(A).

In the isobaric liquid or rubbery state above T_g, where molecular motion is rapid compared with experimental observation times, the temperature dependence of the average relaxation time for many dynamic processes is given by the empirical Vogel–Tamman–Fulcher (VTF) equation [13–15],

$$\langle \tau \rangle = A \exp(B/(T - T_0)), \tag{3}$$

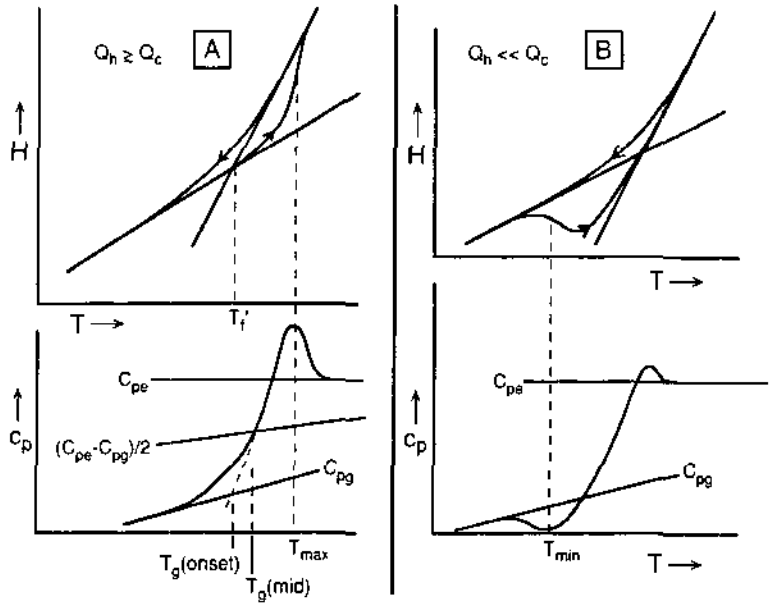

Fig. 1. (A) Definition of onset and midpoint values of T_g, and of T_f', for a heating rate comparable with or greater than the cooling rate. (B) Illustration of exothermic excursion below T_g resulting from a heating rate that is much less than the cooling rate.

in which A, B and T_0 are positive constants. The VTF equation can be derived from the configurational entropy theory of Adam and Gibbs [16] (Section 3.2.3.), and in terms of free volume. The free volume version is exemplified by the Williams–Landel–Ferry (WLF) equation [17] that is ubiquitous in the polymer literature. The WLF equation expresses T_0 as $T_g - C_2$, and defines a shift factor, a_T, relative to some reference temperature (usually T_g):

$$a_T \equiv \frac{\tau(T)}{\tau(T_g)} = \exp\left(\frac{C_1(T-T_g)}{T-T_g+C_2}\right). \tag{4}$$

An extended discussion of the WLF equation is given in the classic book by Ferry [18], in which C_1 and C_2 are defined in terms of free volume. Ferry, and many others, have noted that Eq. (3) is more objective than Eq. (4), because the values of C_1 and C_2 depend on the choice of T_g. Accordingly, Eq. (3) is used here in preference to Eq. (4). The effective VTF activation energy is

$$\frac{\Delta H_{\text{eff}}}{R} \equiv \frac{\mathrm{d}\ln\tau}{\mathrm{d}\,1/T} = \frac{BT^2}{(T-T_0)^2} = \frac{B}{(1-T_0/T)^2}. \tag{5}$$

The VTF equation can be fitted to data using reiterative linear least-squares or non-linear regression techniques. The parameters are usually correlated, because changes in B can be partly compensated by changes in T_0. These changes can be estimated by exploiting the fact that ΔH_{eff} is tightly constrained by the data, so that relative changes in B and T_0 can be determined from Eq. (5). The WLF equation suffers the same problem, as does the extension of the VTF equation into the glassy state (Section 3.2.3.).

Another expression for $\tau(T)$, deduced from mode coupling theory, is

$$\langle\tau\rangle = A'(T/T_c - 1)^{-\gamma}, \tag{6}$$

where $T_c > T_g$. It is difficult to distinguish between Eqs. (3) and (6) for $T > T_g$. Their near equivalence arises from the 'Bardeen identity', discussed briefly by Anderson [19]:

$$\exp(-1/x) \approx (2/e)^2 x - 0.13. \tag{7}$$

Eq. (7) is accurate to within a few percent near $x = 0.5$, so that for $T \approx 2T_0$ Eqs. (3) and (6) are essentially indistinguishable. However, it is not possible to apply Eq. (6) to enthalpy relaxation within and below the glass transition temperature range, because it would have to be extrapolated through the singularity at $T = T_c$. The relevance of mode coupling theory to the glass transition has been questioned by Angell [20,21], and is discussed in the proceedings of an international discussion meeting [22].

The glassy state below T_g is generally a non-equilibrium one [23], and glassy state relaxation results from the thermodynamic driving force towards (metastable) equilibrium. An early discussion of the glass transition and non-equilibrium glassy state was given by Simon [24]. Relaxation in the glassy state below T_g generally has an Arrhenius temperature dependence. Any theory or phenomenology must account for, or describe, the change from VTF behavior above T_g to Arrhenius behavior below T_g. Secondary β relaxations do not affect the glassy heat capacity, and there is no evidence that they directly influence enthalpy relaxation. However, Goldstein [25,26] has argued that they can affect the change in heat capacity at T_g, because of the entropy associated with the corresponding degrees of freedom.

1.2.2. Non-exponentiality

Most relaxation processes in condensed matter are non-exponential, and enthalpy relaxation is no exception. Non-exponentiality produces the memory effect, which strongly influences enthalpy recovery after annealing. The memory effect is discussed below, but first we consider some aspects of linear response theory for non-exponential decay functions, and summarize the more common mathematical expressions used to describe them.

A non-exponential decay function, $\phi(t)$, is mathematically equivalent to a distribution of relaxation or retardation times, $g(\ln\tau)$:

$$\phi(t) = \int_{-\infty}^{\infty} g(\ln\tau)\exp(-t/\tau)\,\mathrm{d}\ln\tau, \tag{8}$$

$$\int_{-\infty}^{\infty} g(\ln\tau)\,\mathrm{d}\ln\tau = 1.0. \tag{9}$$

Because of this equivalence it is not possible, in the absence of independent experimental information, to determine if the essential physics lie in $\phi(t)$ or in $g(\ln \tau)$. Averages of the relaxation or retardation time, $\langle \tau^n \rangle$, are defined by the moments of $g(\ln \tau)$ and $\phi(t)$:

$$\langle \tau^n \rangle = \int_{-\infty}^{\infty} \tau^n g(\ln \tau)\, \mathrm{d} \ln \tau, \tag{10}$$

$$= \frac{1}{\Gamma(n)} \int_0^{\infty} t^{n-1} \phi(t)\, \mathrm{d}t, \tag{11}$$

where Γ is the gamma function. In the frequency domain, the corresponding expressions for the complex retardation function, $R^*_{\mathrm{ret}}(i\omega)$, are

$$R^*_{\mathrm{ret}}(\mathrm{i}\omega) - R_{\mathrm{U}} = (R_{\mathrm{R}} - R_{\mathrm{U}}) \times \int_{-\infty}^{\infty} \frac{1}{(1 + \mathrm{i}\omega\tau_{\mathrm{ret}})} g_{\mathrm{ret}}(\ln \tau_{\mathrm{ret}})\, \mathrm{d} \ln \tau_{\mathrm{ret}}, \tag{12}$$

$$= (R_{\mathrm{R}} - R_{\mathrm{U}}) \int_0^{\infty} -(\mathrm{d}\phi/\mathrm{d}t) \exp(\mathrm{i}\omega t)\, \mathrm{d}t, \tag{13}$$

where $i = (-1)^{1/2}$, ω is the angular frequency, $R'(\omega)$ and $R''(\omega)$ are the real and imaginary components of $R^*_{\mathrm{ret}}(i\omega)$, respectively, R_{U} is the unrelaxed (real) component of $R^*_{\mathrm{ret}}(\mathrm{i}\omega)$, and R_{R} is the relaxed component of $R^*_{\mathrm{ret}}(i\omega)$ (also real).

The value of R_{U} corresponds to the limiting high frequency or short time response, and R_{R} is the limiting low frequency or long time response. For exponential decay functions, $g_{\mathrm{ret}}(\ln \tau_{\mathrm{ret}})$ is a Dirac delta function $\delta(\tau_{\mathrm{ret}} - \tau_0)$, and $R^*_{\mathrm{ret}}(\mathrm{i}\omega) - R_{\mathrm{U}}$ is proportional to $1/(1 + i\omega\tau_0)$. The quantity τ_{ret} in Eq. (12) is subscripted as a retardation time, because in the time domain it determines the rate of retardation as R increases from R_{U} to R_{R} following a step perturbation:

$$R(t) = R_{\mathrm{U}} + (R_{\mathrm{R}} - R_{\mathrm{U}})[1 - \phi(t)]. \tag{14}$$

In Eq. (14), the response $R(t)$ corresponds to the change in a measurable property, $P(t)$, following an instantaneous increase (Heaviside function) in a forcing perturbation from 0 to F: $R(t) = P(t)/F$. In the frequency domain, this is generalized to $R^*(\mathrm{i}\omega) = P^*(\mathrm{i}\omega)/F^*(\mathrm{i}\omega)$. Familiar examples of $R^*_{\mathrm{ret}}(\mathrm{i}\omega)$ are the complex relative permittivity $\epsilon^*(\mathrm{i}\omega)$ and the shear compliance $J^*(\mathrm{i}\omega)$. A less familiar example is the complex isobaric heat capacity, $C_p^*(\mathrm{i}\omega)$, discussed below. In this last case the forcing function is the temperature, and the measured response is the enthalpy (or isobaric heat, see Section 2.2.). Since the limiting high frequency (short time, low temperature, or glassy) heat capacity is less than the limiting low frequency (long time, high temperature, liquid or rubber) heat capacity, the enthalpic τ is a retardation time.

If $R_{\mathrm{U}} > R_{\mathrm{R}}$, the rate of relaxation of $R(t)$ from R_{U} to R_{R} is determined by the relaxation time, τ_{relax}:

$$R(t) = R_{\mathrm{R}} + (R_{\mathrm{U}} - R_{\mathrm{R}})\phi(t), \tag{15}$$

and

$$R^*_{\mathrm{relax}}(i\omega) - R_{\mathrm{R}} = (R_{\mathrm{U}} - R_{\mathrm{R}}) \times \int_{-\infty}^{\infty} \frac{\mathrm{i}\omega\tau_{\mathrm{relax}}}{(1 + \mathrm{i}\omega\tau_{\mathrm{relax}})} g_{\mathrm{relax}}(\ln \tau_{\mathrm{relax}})\, \mathrm{d} \ln \tau_{\mathrm{relax}}. \tag{16}$$

An example of $R^*_{\mathrm{relax}}(\mathrm{i}\omega)$ is the shear modulus, $G^*(\mathrm{i}\omega) \equiv 1/J^*(\mathrm{i}\omega)$. For properties that are the complex inverses of one another (such as G^* and J^*), specific relations exist between $g_{\mathrm{relax}}(\ln \tau_{\mathrm{relax}})$ and $g_{\mathrm{ret}}(\ln \tau_{\mathrm{ret}})$[18].

The distinction between relaxation and retardation times can be important for non-exponential decays, because their average values differ substantially if the dispersion $|R_{\mathrm{U}} - R_{\mathrm{R}}|$ is large. For $G^*(\mathrm{i}\omega)$ and $J^*(\mathrm{i}\omega)$, for example,

$$\tau_{ret} = \tau_{relax}(J_{\mathrm{R}}/J_{\mathrm{U}}) \geq \tau_{relax}, \tag{17}$$

where the factor $J_{\mathrm{R}}/J_{\mathrm{U}}$ increases with increasing non-exponentiality as

$$\frac{J_{\mathrm{R}}}{J_{\mathrm{U}}} = \frac{\tau_{\mathrm{ret}}}{\tau_{\mathrm{relax}}} = \frac{\langle \tau^2_{\mathrm{relax}} \rangle}{\langle \tau_{\mathrm{relax}} \rangle^2} \geq 1. \tag{18}$$

For strongly non-exponential relaxations, or very broad distributions of relaxation times, the two moments of $g_{relax}(\ln \tau_{relax})$ in Eq. (18) can differ by several orders of magnitude. The distinction

between retardation and relaxation times also enters into any comparison between the characteristic times of different properties, and it is important that a relaxation time for one property not be compared with a retardation time for another. For the rest of this review, however, we omit the subscripts with the understanding that we are discussing enthalpy retardation times.

An important consequence of non-exponentiality is the memory effect, which arises from Boltzmann superposition of non-exponential response functions (as discussed by Goldstein [27] and others). The memory effect refers to the dependence of relaxation on the path by which the starting state was reached, i.e., the system 'remembers' its earlier history. The development of sub-T_g heat capacity peaks in some annealed glasses is due to the memory effect, for example. Another striking manifestation is the initial move away from equilibrium after two temperature steps of opposite sign, followed by the inevitable approach to equilibrium at long times. This results in a maximum in the departure from equilibrium, first observed for volume by Ritland [28] and Kovacs [29], and later by Hofer et al. [30] for enthalpy [31]. It is instructive to analyze these observations, the relevance of which to enthalpy recovery has been discussed by Hodge [32]. Consider a specific example of the thermal history just mentioned: a downward step in temperature from the equilibrium state at T_0 to T_1 at time t_1, followed by an upward step from T_1 to T_2 at time t_2. Boltzmann superposition of the responses to these two temperature steps yields the time-dependent enthalpy, $H(t)$:

$$H(t) = H_0 + \sum_i \Delta H_i(1 - \phi(t - t_i)), \tag{19}$$

$$= H_1 + (H_0 - H_1)\phi(t - t_1) + (H_2 - H_1)[1 - \phi(t - t_2)], \tag{20}$$

$$= H_1 + (H_0 - H_1)\phi[(t_2 - t_1) + (t - t_2)] + (H_2 - H_1)[1 - \phi(t - t_2)], \tag{21}$$

where $\{H_i\}$ are the equilibrium enthalpies at temperatures $\{T_i\}$, and $\{\Delta H_i\}$ are the enthalpy changes corresponding to the temperature steps at times $\{t_i\}$. If $\phi(t)$ is exponential and the retardation times at $\{T_i\}$ are $\{\tau_i\}$, then

$$H(t) = H_1 + (H_0 - H_1) \times \exp\left(-\frac{(t_2 - t_1)}{\tau_1} - \frac{(t - t_2)}{\tau_2}\right) + (H_2 - H_1)\left(1 - \exp\left(-\frac{(t - t_2)}{\tau_2}\right)\right), \tag{22}$$

$$= H_2 + \left\{(H_0 - H_1)\exp\left(-\frac{(t_2 - t_1)}{\tau_1}\right) - (H_2 - H_1)\right\}\exp\left(-\frac{(t - t_2)}{\tau_2}\right). \tag{23}$$

The expression in braces in Eq. (23) is independent of time, so that $H(t)$ decays exponentially from its value at $t = t_2$, with a retardation time τ_2 appropriate for the temperature T_2. Thus, if an observer's clock started at $t = t_2$, there would be nothing in the subsequent behavior to indicate how the starting value was reached, i.e., the system would retain no 'memory' of the earlier temperature step at $t = t_1$. This occurs only when $\phi(t)$ is exponential, because the transformation from Eq. (22) to (23) depends on the relation

$$\phi[(t_2 - t_1) + (t - t_2)] = \phi(t_2 - t_1)\phi(t - t_2), \tag{24}$$

which is unique to the exponential function.

Another history that demonstrates the memory effect is exemplified in the 'crossover' experiment of Spinner and Napolitano [33]. A sample was equilibrated near T_g, taken to a lower temperature, and annealed until the refractive index reached an arbitrary value equal to that of a sample equilibrated at temperature, T_x. The annealed sample was then placed in a furnace at temperature T_x, and the refractive index monitored as a function of time. It was observed to pass through a minimum, corresponding to a maximum in the volume. Thus, although the non-equilibrium annealed sample had a refractive index equal to a sample equilibrated at T_x, the subsequent time dependence indicated that the

non-equilibrium and equilibrated glasses had different structures.

The memory effect can also be described in terms of the components of a distribution of retardation times. Although each component decays exponentially and exhibits no memory effect, the overall departure from equilibrium at any time can be partitioned between the components in several ways, depending on the path by which the non-equilibrium state was reached, and these different partitionings will produce different relaxation behavior.

The memory effect is seen only if the response to the first temperature step still has a significant time dependence after the second step. This condition is not fulfilled for the two limiting cases of very small and very large values of $(t_2 - t_1)/\langle\tau_1\rangle$. If $(t_2 - t_1)$ is very long, and/or $\langle\tau_1\rangle$ is very short, then $\phi(t - t_1) \approx \phi(t_2 - t_1) \approx 0$ and the response to the first temperature jump will have decayed to zero. On the other hand, if $(t_2 - t_1)$ is very short and/or $\langle\tau_1\rangle$ is very long, then $\phi(t - t_1) \approx \phi(t - t_2)$ and no term containing t_1 will appear in Eqs. (19)–(21). In both cases, the effects of thermal history for $t < t_2$ on subsequent relaxation is small.

The memory effect occurs in any non-exponentially relaxing system, regardless of (although modified by) any possible non-linearity in the system, described next.

1.2.3. Non-linearity

In 1936, Lillie [34] reported a time-dependent zero frequency viscosity, $\eta_0(t)$, in inorganic glasses. Since the viscosity is proportional to the average stress relaxation time

$$\eta_0 = G_U\langle\tau_{rel}\rangle, \tag{25}$$

where G_U is the (essentially time invariant) limiting high frequency modulus, Lillie's observation is equivalent to a viscosity- and time-dependent $\langle\tau_{rel}\rangle$, so that glassy relaxation is non-linear. Viscosity is usually associated with structural relaxation in inorganic glasses (their activation energies are often the same), implying that structural relaxation is also non-linear. Non-linearity was confirmed in 1955 by Hara and Suetoshi [35], who found that, for an equilibrated soda–lime–silicate glass subjected to temperature jumps of opposite sign and magnitude ≥ 2 K, the form of the volume relaxation function depended on the sign of the temperature step: the approaches to equilibrium from above and below occurred at different rates. A similar asymmetric approach to volumetric equilibrium was observed in poly(vinyl acetate) (PVAc) by Kovacs [36]. These observations are independent of the memory effect and non-exponentiality, because relaxation occurred from the equilibrium state. The dependence of $\phi(t)$ on the departure from equilibrium is equivalent to the structural relaxation kinetics depending on the time-dependent structure of the relaxing system, so that in order to quantify non-linearity it is necessary to specify the structural state mathematically. Two equivalent methods are in general use.

One measure of structure is the fictive temperature, T_f, introduced into the literature by Tool and Eichlin in 1931 [37] and Tool in 1946 [38], but presented orally in 1924 [39]. Thus, non-linearity was recognized more than 30 years before the memory effect was observed by Ritland [28] and Kovacs [29], and some 45 years before non-linearity and non-exponentiality were first combined in a consistent way by Narayanaswamy [40,41]. This very early introduction of T_f indicates the considerable practical importance of non-linearity to annealing behavior. Excellent discussions of the definition and use of T_f have been given by Narayanaswamy [41], Moynihan et al. [42] and Scherer [9]. The definition of T_f for enthalpy is

$$H(T) = H_e(T_f) - \int_T^{T_f} C_{pg}\, dT', \tag{26}$$

where $H_e(T_f)$ is the equilibrium value of H at temperature T_f and C_{pg} is the non-structural, unrelaxed, glassy state heat capacity. The equilibrium state is defined by the condition $T_f = T$, in addition to the general requirement of time invariance, $dT_f/dt = 0$. The value of T_f defined by Eq. (26) corresponds to the temperature of intersection of the equilibrium H_e–T curve, with a line drawn parallel to the glassy H_g–T curve and passing through the (H, T) point of interest. This construction is shown in Fig. 2, which also illustrates how T_f is the relaxational part of the

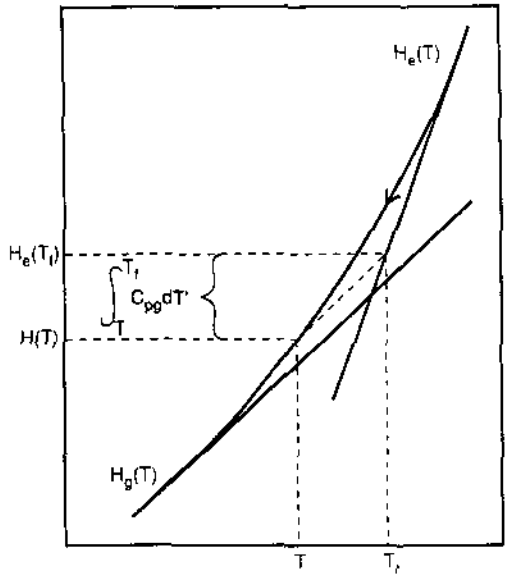

Fig. 2. Definition of fictive temperature from experimental enthalpy versus temperature data (Eq. (26)).

enthalpy expressed in temperature units. The structural contribution to the heat capacity is obtained by differentiating Eq. (26):

$$\frac{dT_f}{dT} = \frac{(C_p - C_{pg})|_T}{(C_{pe} - C_{pg})|_{T_f}} = \frac{(C_p - C_{pg})|_T}{\Delta C_p(T_f)} \tag{27}$$

$$\approx \frac{(C_p - C_{pg})|_T}{\Delta C_p(T)} \equiv C_p^N, \tag{28}$$

where C_{pe} is the equilibrium liquid or rubber heat capacity, C_p is the observed heat capacity and C_p^N is the normalized heat capacity. Both C_{pe} and C_{pg} are generally temperature-dependent, and must be obtained by extrapolation into the relaxation temperature range. It is often assumed (although rarely stated explicitly) that ΔC_p in the denominator of Eq. (27), specified at the fictive temperature, T_f, is the same as that at temperature T, so that dT_f/dT equals C_p^N. The accuracy of this approximation is demonstrated by noting that $|T - T_f|$ rarely exceeds 10 K or so during scanning through the relaxation region, so that for the representative hyperbolic relation $\Delta C_p \sim 1/T$ (Eq. (55) below) the error is about 3% for $T_g = 373$ K. The glassy value of T_f, denoted by T_f', is obtained by integration of the normalized heat capacity measured during heating:

$$T_f' = T_{max} - \int_{T_{min}}^{T_{max}} \left(\frac{dT_f}{dT} \right) dT \approx T_{max} - \int_{T_{min}}^{T_{max}} C_p^N \, dT, \tag{29}$$

where $T_{min} \ll T_g \ll T_{max}$. Since T_f' is defined in terms of the integrated normalized heat capacity measured during heating, its value for annealed glasses can be affected by possible relaxation during cooling from the annealing temperature to the starting temperature for heating. For glasses equilibrated at $T_a \approx T_g$, such relaxation results in values of T_f' that are less than T_a. The numerical value of T_f' provides a definition of T_g that is preferred over those given in terms of the heat capacity curve measured during heating, either as the onset or midpoint temperatures [11,43–45]. The relative values of T_f' and these definitions of T_g are unambiguous for unannealed glasses, but for annealed glasses the two definitions give T_g values that move in opposite directions as the amount of annealing increases: T_f' decreases, but the heat capacity curve measured during heating moves to higher temperatures. The definition of T_g from the Deborah condition $d\tau/dt \approx 1$ (eq. (1)) has been shown by Cooper and Gupta [8] to be approximately equivalent to $dT_f/dT \approx 1$ during cooling ($d\tau/dt \approx 2.0$ and $dT_f/dT \approx 0.4$ when $T = T_g$).

The fictive temperature concept becomes more complex when the memory effect associated with non-exponential relaxation functions is considered. In these cases the structure of a material must be formally defined by more than one fictive temperature, and the global fictive temperature for one property may not equal that for another. Thus the fictive temperature is usually subscripted with the property being considered, e.g., $T_{f,H}$ for enthalpy and $T_{f,V}$ for volume. In this review, however, we deal almost exclusively with the enthalpic fictive temperature and the subscript is omitted for convenience. An example of different values of T_f for different properties was described by Ritland [28], who observed that two glasses with the same refractive index arrived at by different paths (rate cooling and annealing)

had different electrical conductivites. Thus, at least one of these glasses was characterized by different fictive temperatures for refractive index and electrical conductivity. Ritland concluded that a single fictive temperature gives an inadequate description of a non-equilibrium glass, and this is supported by the thermodynamic analysis of Davies and Jones [46]. Another example of a different path to the same T_f is a rapid quench, compared with a slow cool under pressure followed by pressure release (see Section 5.1.3.2.). In this case the glasses have different densities and their structures are clearly different. The temptation to equate T_f with a definite molecular structure should therefore be avoided, and too much physical significance should not be attached to the numerical value of what is essentially a phenomenological convenience.

A second method for specifying the structural state, pioneered by Kovacs and co-workers [36,47,48], is to define the departure from equilibrium in terms of a quantity, δ_H, defined for enthalpy as

$$\delta_H(t) = H(t) - H(\infty) \tag{30}$$

$$\approx \Delta C_p\left[T_{f,H}(t) - T\right], \tag{31}$$

where $H(\infty)$ is the limiting long time (equilibrium) value of $H(t)$. As with the fictive temperature, we dispense with the enthalpic subscript here. The use of δ is discussed further in Section 3.2.2., when the KAHR equation is introduced.

It is often more convenient to describe the excess enthalpy of a glass using T_f rather than δ, because T_f is a direct measure of excess enthalpy whereas δ differs for the same excess enthalpy, depending on the thermodynamic temperature.

Non-linearity is handled by making the average retardation time a function of both T and T_f (or δ). The application of this method to non-exponential relaxations is intricate, because the memory effect can generate different relaxation behavior from systems that have the same instantaneous values of T and T_f. This problem was first solved by Gardon and Narayanaswamy [40] and Narayanaswamy [41], using the Tool fictive temperature, and the resulting phenomenology is best described as the Tool–Narayanaswamy (TN) formalism. A key concept introduced by Gardon and Narayanaswamy is the reduced time, ζ, defined as

$$\zeta(t) = \int_{-\infty}^{t} \frac{\mathrm{d}t'}{\tau(t')} = \int_{-\infty}^{t} \frac{\mathrm{d}t'}{\tau\left[T(t'); T_f(t')\right]}. \tag{32}$$

The integral is path-dependent, because it includes the time dependence of both T and T_f. Generally speaking, $T(t')$ is specified experimentally by the thermal history and $T_f(t')$ is the observed response to that history, although in some cases non-thermal perturbations can change T_f directly (Section 4.7.). The reduced time linearizes the kinetics, and the methods of linear response theory can be applied by replacing the time t with ζ. In particular, Boltzmann superposition of responses to all past perturbations can be employed, using a generalized form of thermorheological simplicity in which the shape of $\phi(t)$ or $g(\ln \tau)$ is invariant with respect to both T and T_f. Thermorheological simplicity has been derived for glasses from the principle of equivalency between time and temperature (both thermodynamic and fictive) [49]. Thermorheological complexity, in which the shape of $\phi(t)$ or $g(\ln \tau)$ changes with T or T_f, has been introduced into the TN phenomenology by Mazurin and Startsev [50] and others, but is rarely used. Further details of how the TN formalism is implemented are given in Section 3.2.

Spurious relaxation parameters can result if non-linearity is incorrectly incorporated into the reduced time. An example of such an incorrect analysis has been discussed by Hodge and O'Reilly [51], using unpublished observations of Scherer [52]. For short annealing times, $\tau(t)$ can be approximated as

$$\tau(t) = \tau_0 t^{\mu}, \tag{33}$$

where $\mu \equiv \mathrm{d} \ln \tau / \mathrm{d} \ln t_a$ is the shift factor introduced by Struik [6]. Eq. (33) has the important consequence that the non-linear stretched exponential retains its functional form, with an exponent and retardation time modified by the shift

factor, μ:

$$\phi = \exp(-\zeta^{\beta}) = \exp\left(-\left(\int_0^t \frac{dt'}{\tau_0 t'^{\mu}}\right)^{\beta}\right)$$

$$= \exp\left(-\left(\frac{t^{1-\mu}}{\tau_0(1-\mu)}\right)^{\beta}\right) = \exp\left(-\left(\frac{t}{\tau'}\right)^{\beta'}\right), \tag{34}$$

where

$$\beta' = (1-\mu)\beta \tag{35}$$

and

$$\tau' = [(1-\mu)\tau_0]^{1/(1-\mu)}. \tag{36}$$

Eqs. (33)–(36) will be referred to here as the Scherer relations. They imply that, if a non-linear stretched exponential is treated as a linear function, a good fit may still be obtained but with β' and τ' parameters that are determined in part by the non-linearity parameter, μ. Eq. (33) is often a reasonably good approximation, so that these results may be fairly general. In any event, the Scherer relations provide an excellent illustration of the pitfalls of neglecting, or incorrectly incorporating, non-linearity in the analysis of enthalpy relaxation data. Analyses based on decay functions that omit, or incorrectly incorporate, non-linearity [53–60] must be considered unreliable. For example, it is clearly inconsistent to estimate a non-linearity parameter from τ' data obtained from linear fits to the stretched exponential.

In recent years, another formalism for handling non-linearity has been introduced by Ngai and Rendell. This approach differs most significantly from that of Tool–Narayanaswamy in that the time variable is not simply replaced by ζ, and that non-linearity and non-exponentiality are less easily separated. It is discussed in Section 4.3.

1.3. Thermodynamic aspects of the glass transition

1.3.1. The thermodynamic case

The kinetics of the glass transition have a thermodynamic foundation, and enthalpy relaxation therefore has a thermodynamic dimension. This dimension is discussed here.

The isobaric heat capacity of a supercooled liquid or rubber exceeds that of the crystal at the same temperature, so that the excess entropy of a liquid or rubber over that of the crystal decreases with decreasing temperature. Extrapolations for many materials imply that the excess entropy would vanish at a temperature well above absolute zero. At this temperature, the entropy of the supercooled liquid equals that of the crystal, and if the same trend were to extend down to absolute zero the entropy of the liquid would be less than that of the crystal, in conflict with the third law of thermodynamics. This difficulty was first recognized by Kauzmann [61], and the extrapolated temperature at which the supercooled liquid and crystal entropies become equal is known as the Kauzmann temperature, T_K. The problem is often referred to as the Kauzmann paradox, because it seems paradoxical that the intervention of a kinetic event, the observed glass transition, averts rather than resolves a thermodynamic impossibility. The value of T_K is calculated by equating the excess entropy of the liquid, relative to the crystal, to the entropy of melting ΔS_m:

$$\Delta S_m = \int_{T_K}^{T_m} \frac{\Delta C_p(T)}{T} dT, \tag{37}$$

where T_m is the melting temperature, and $\Delta C_p(T)$ is now the difference in isobaric heat capacity of the liquid or rubber and that of the crystal (equal to that of the glass within 5–10%). Because $\Delta C_p(T)$ must be obtained by extrapolation from T_m or T_g down to T_K, the value of T_K can be very uncertain. For polymers, this difficulty is compounded by the need to correct for tacticity and partial crystallinity. Further, as noted already, Goldstein [25,26] has argued that ΔC_p is not entirely configurational and may contain significant contributions from vibrational and secondary relaxation sources. He estimated that between 20 and 80% of ΔC_p could originate from non-configurational sources, and noted that this renders even more uncertain the extrapolations required to assess T_K. Calculated values of T_K are always found to be less than T_g, although in some cases the difference can be as small as 20 K [62–65].

The value of T_K is often close to T_0 of the VTF equation [65], suggesting that the kinetic and thermodynamic aspects of the glass transition are related. The link between thermodynamics and kinetics is an important aspect of the glass transition phenomenon, and is discussed below in more detail.

Three resolutions of the thermodynamic difficulties imposed by $T_K > 0$ have been proposed. One is that the extrapolation of excess entropy to low temperatures is not well defined and has no firm theoretical basis, so that the prediction $T_K > 0$ is a spurious result of incorrect extrapolation [66,67]. As noted already, however, the extrapolation is only 20 K or so for some materials, and a non-zero T_K seems inescapable in these cases. A second resolution, suggested by Kauzmann [61], is that the extrapolation is irrelevant because the thermodynamic driving force for crystallization would always intervene before the entropy problem manifested itself. However, this intervention has been shown to be extremely unlikely in some systems [68], and it may actually be impossible in two rather bizarre systems (CrO_3–H_2O [69] and RbAc–H_2O [70]), in which T_g (and possibly T_K) exceeds the eutectic temperature (the Kauzmann analysis can be applied to eutectic mixtures [68]). The third resolution is that a thermodynamic second-order transition occurs at T_K, at which ΔC_p falls rapidly to zero in a manner similar to that which is observed kinetically at T_g. Thus, T_K is interpreted as a second-order thermodynamic transition temperature (in the Ehrenfest sense, see below), but is unobservable because of kinetic factors. It seems difficult to refute this hypothesis other than to dismiss it as an artifact of extrapolation but, as has just been noted, this objection is itself weakened by the fact that very short extrapolations are needed in some cases. Further, an entropically based second-order transition at T_K has been derived for polymers by Gibbs and DiMarzio [71]. Although this theory has been criticized [72], its predictions agree well with experimental observations near T_g, including recent ones on the effect of molecular weight on T_g for polymeric rings [73,74]. The case for a thermodynamic foundation for the glass transition is therefore quite strong, and it is appropriate to summarize here some of the properties of thermodynamic second-order transitions.

1.3.2. Ehrenfest relations

Ehrenfest [75] classified thermodynamic transitions according to the smallest order of the derivative of the free energy that exhibits a discontinuity at the transition temperature. Thus, discontinuities in second derivative quantities such as the heat capacity, compressibility and expansivity are classified as second-order transitions. Several thermodynamic relations can be derived for second-order transitions, of which only those for the pressure dependence of the transition temperature will be considered here. The purpose of these derivations is to introduce expressions that are relevant to treatments of pressure-dependent kinetics to be discussed later, and that can be compared with experimental data to identify the most important thermodynamic variables controlling the glass transition and annealing phenomena. The relations are derived by setting the differences between the liquid and glassy values of the various first derivatives of the free energy equal to zero. For volume,

$$0 = \mathrm{d}(\Delta V) = \left(\frac{\partial \Delta V}{\partial T}\right)_P \mathrm{d}T + \left(\frac{\partial \Delta V}{\partial P}\right)_T \mathrm{d}P, \tag{38}$$

$$= V\,\Delta\alpha\,\mathrm{d}T - V\,\Delta\kappa\,\mathrm{d}P, \tag{39}$$

where $\Delta\alpha$ and $\Delta\kappa$ are the changes in expansivity and compressibility at T_g, respectively. Thus,

$$\left(\frac{\partial T}{\partial P}\right)_V = \frac{-(\partial \Delta V/\partial P)_T}{(\partial \Delta V/\partial T)_P} \tag{40}$$

$$= \Delta\kappa/\Delta\alpha. \tag{41}$$

For entropy,

$$0 = \mathrm{d}(\Delta S) = \left(\frac{\partial \Delta S}{\partial T}\right)_P \mathrm{d}T + \left(\frac{\partial \Delta S}{\partial P}\right)_T \mathrm{d}P, \tag{42}$$

$$= \left(\frac{\partial \Delta S}{\partial T}\right)_P \mathrm{d}T - \left(\frac{\partial \Delta V}{\partial T}\right)_P \mathrm{d}P, \tag{43}$$

$$= T\,\Delta C_p\,\mathrm{d}T - V\,\Delta\alpha\,\mathrm{d}P, \tag{44}$$

and

$$(\partial T/\partial P)_S = VT(\Delta\alpha/\Delta C_p). \tag{45}$$

For enthalpy,

$$0 = \mathrm{d}(\Delta H) = \left(\frac{\partial \Delta H}{\partial T}\right)_P \mathrm{d}T + \left(\frac{\partial \Delta H}{\partial P}\right)_T \mathrm{d}P, \tag{46}$$

$$= \Delta C_p \,\mathrm{d}T + \left(\Delta V - T\left(\frac{\partial \Delta V}{\partial T}\right)_P\right) \mathrm{d}P, \tag{47}$$

$$= \Delta C_p \,\mathrm{d}T - TV\,\Delta\alpha \,\mathrm{d}P, \tag{48}$$

where $\Delta V = 0$ because the transition is second-order. Thus

$$(\partial T/\partial P)_H = VT(\Delta\alpha/\Delta C_p). \tag{49}$$

Eqs. (45) and (49) are identical, so that entropy and enthalpy cannot be distinguished as controlling variables. Goldstein (cited in Ref. [76]) has derived an expression from the condition that TS_c is constant:

$$\left(\frac{\partial T}{\partial P}\right)_{TS_c} = VT\frac{\Delta\alpha}{(S_c + \Delta C_p)}, \tag{50}$$

where S_c is the configurational entropy.

1.3.3. Prigogine–Defay ratio

Experimental values of $\mathrm{d}T_g/\mathrm{d}P$ generally agree with Eqs. (45) and (49) [76,77], and are smaller than those given by Eq. (41) [76], suggesting that enthalpy or entropy and not volume determines T_g. However, O'Reilly [77] has pointed out that the $\Delta\kappa$ is strongly pressure-dependent, and that reasonable values of $\Delta\kappa$ can be found that satisfy Eq. (41). McKenna [78] has also suggested that the usually quoted values of $\Delta\alpha$, ΔC_p and $\Delta\kappa$ are not obtained under the proper conditions and that, if they were, Eqs. (41) and (45) would both be satisfied. However, enthalpy or entropy alone cannot determine T_g. Davies and Jones [46] showed, from considerations of thermodynamic stability that are independent of any assumption about a second-order transition, that more than one thermodynamic variable must determine T_g if the Prigogine–Defay ratio, Π, (Eq. (51)) is greater than unity. Experimental values of Π generally do exceed unity [42,79]:

$$\Pi \equiv \frac{\Delta C_p\,\Delta\kappa}{TV\,\Delta\alpha^2} = \frac{(\partial T/\partial P)_V}{(\partial T/\partial P)_S} \geq 1. \tag{51}$$

If it is assumed for simplicity that one variable is dominant, however, it is evidently better to use enthalpy or entropy rather than volume. The superiority of enthalpy or entropy over volume can be rationalized by noting that the isobaric heat capacity has contributions from internal energy sources (the isochoric heat capacity), as well as from volume changes (the term $\alpha^2 TV/\kappa$). Gupta [80] has argued that a fictive pressure, P_f, in addition to T_f, is all that is needed to account for $\Pi > 1$.

1.3.4. Heat capacity change at T_g

Heat capacity is an extensive variable, and the appropriate mass unit for configurational heat capacity has been a subject of debate. A frequently used unit is the 'bead', introduced by Wunderlich and Jones [81]. The bead is defined for organic high polymers as a main chain or side chain segment or functional group. Wunderlich observed that ΔC_p per bead is approximately constant for polymers. A review by Mathot [82] summarizes the number of beads per repeat unit, and values of ΔC_p per bead, for several polymers. Another method for dealing with mass is to normalize ΔC_p (or C_{pe}) by C_{pg}. Values of $\Delta C_p/C_{pg}$ vary greatly, from about zero for silica to about 2.0 for some hydrogen-bonded liquids [62].

The value of $\Delta C_p(T_g)$ often decreases with increasing T_g. For polymers, this can be rationalized in terms of the Gibbs–DiMarzio theory of the glass transition [71], that predicts an increase in T_g with chain stiffness (amongst other factors). Since stiffness can reasonably be supposed to decrease the mean-square fluctuations in configurational entropy, $\langle S_c^2 \rangle$, it follows from the statistical mechanical relation

$$k_B C_p = \langle S^2 \rangle \tag{52}$$

that ΔC_p should also decrease (k_B is Boltzmann's constant). A similar argument can be invoked to rationalize the decrease in ΔC_p with increasing cross-link density in polymers. The value of $\Delta C_p(T_g)$ has been discussed by Angell [5,20,21,62] in terms of the breakdown in structure with temperature. Materials whose structures break down rapidly with temperature have large values of $\Delta C_p(T_g)$ (hydrogen-bonded liquids, for example),

and are termed 'fragile'. Materials whose structure is resistant to breakdown have correspondingly small values of $\Delta C_p(T_g)$ (silicates, for example), and are termed 'strong'. The variability in $\Delta C_p(T_g)$ contrasts with the approximate constancy of the excess entropy at T_g, for which there is abundant evidence, so it can be anticipated that small values of ΔC_p correspond to large ratios of T_g/T_K [76]. This observation will enter into later discussions of the physical origin of non-linearity. The value of ΔC_p also generally decreases with increasing thermodynamic temperature. An illuminating discussion of $\Delta C_p(T_g)$ has been given by Alba et al. [83]. Empirically, ΔC_p is often fitted to the linear equation

$$\Delta C_p = a_0 - a_1 T \quad (a_1 > 0). \tag{53}$$

Analysis of the data in Ref. [82] reveals that, for most polymers, the values of a_1/a_0 are such that ΔC_p has a temperature dependence lying between

$$\Delta C_p = C = \text{constant} \tag{54}$$

and the hyperbolic form

$$\Delta C_p = C' T_g/T = CT_2/T, \tag{55}$$

where C' is the value of ΔC_p at T_g and C is the value at T_2. The intermediate behavior of polymers supports the speculation by Angell [5] that the temperature dependence of ΔC_p should be weaker than hyperbolic for larger molecules. For some materials, such as bisphenol A polycarbonate (BPAPC, often referred to simply as 'polycarbonate'), Eq. (53) parameters predict that ΔC_p would be zero near the melting temperature, an unlikely result. For other materials, ΔC_p is predicted to be negative some 100–200 K above T_g. Negative values are unphysical, and serve to emphasize the empiricism of Eq. (53). On the other hand, the hyperbolic form of Eq. (55) is accurate for many non-polymeric materials [83-85], and never becomes negative. It should be noted, however, that Eqs. (53) and (55) are approximately equivalent for $T \approx T_g$, provided $a_1/a_0 \approx 1/(2T_g) < 10^{-3}\ \mathrm{K}^{-1}$ [86]:

$$\frac{CT_2}{T} = \frac{CT_2}{T_g}(1+\Delta)^{-1} \approx \frac{CT_2}{T_g}(1-\Delta) = \frac{2CT_2}{T_g} - \frac{CT_2}{T_g^2}T. \tag{56}$$

where $\Delta \equiv T/T_g - 1 \ll 1$.

2. Experimental techniques

2.1. Scanning calorimetry

The most frequently used technique for studying enthalpy relaxation is differential scanning calorimetry (DSC). Indeed, the introduction of commercial DSC instruments essentially made the field of enthalpy relaxation possible. In this technique, the difference in electrical power needed to heat a sample and a reference material to the same temperature is assessed, produced and measured (hence the term differential). The reference (usually alumina) is heated at a controlled, known and uniform heating rate (thus the term scanning). The differential current is proportional to the heat capacity difference between the sample and reference, and is a direct measure of the sample heat capacity if the reference exhibits no transitions and is thermally stable. Quantitative heat capacities can be obtained if the heat capacity of the reference is known as a function of temperature. These data are necessary only if the approximate equality between C_p^N and dT_f/dT (Eq. (28)) breaks down, however, and even in this case only heat capacity values in excess of $C_{pg}(T)$ are needed. As noted already, however, Eq. (28) is sufficiently accurate in most cases that absolute heat capacities are not needed. Thus, the measurement of absolute heat capacities will not be described here.

Experimental heat capacity data must be normalized in order to compare them with calculated curves. As noted in Section 1.2.3., both $C_{pg}(T)$ and $C_{pe}(T)$ must be extrapolated through and beyond the glass transition temperature range, and this places a premium on experimental precision. One potential cause of poor reproducibility in $C_p^N(T)$ is a baseline shift between scans that

changes the absolute values of C_{pg} and C_{pe}, but not their difference. Thus, it is advisable to compute C_p^N using C_{pg} and C_{pe} data from the same scan, rather than averaged values for several scans (desirable for the most accurate absolute heat capacities). The liquid (rubber) heat capacity, being an equilibrium property, is not sensitive to thermal history (apart from the real possibilities of chemical decomposition or crystallization). The glassy heat capacity is more problematic, because relaxation effects can affect it to quite low temperatures, so that $C_{pg}(T)$ should be determined at temperatures as far below the glass transition range as possible.

It is important that good thermal contact be made between the sample and sample pan, and between the pan and the instrument cup. Good sample-to-pan contact is readily achieved by forming samples into thin disks that fit snugly into the pan. Thermal contact between the sample pan and instrument cup can be improved by applying silicone grease between the pan and the cup. Thermal contacts can be important in determining the dynamic response of the measurements, and thermal transfer corrections are a constant source of uncertainty in all enthalpy recovery experiments. Some researchers insist that corrections should always be applied before any data analyses are attempted, while others have restricted their analyses to low overshoot data obtained at relatively slow heating rates (Section 4.6.). Thermal transfer is probably a more important issue for polymers than for inorganics, because polymers have lower thermal conductivities and their glass transitions usually occur over a smaller temperature range. Two aspects of thermal transfer will be addressed here. The first is the time constant for heat transfer to the sample, arising from the heat capacity of the sample plus pan, and the total thermal resistance between the instrument cup and sample. The effects of this time constant on the scanned heat capacity have been estimated by Gray [87]:

$$C_p(t) = C_p^*(t) + \tau_{th}\left(dC_p^*/dt\right) \quad (57)$$

$$= C_p^*(t) + \tau_{th}\left(dC_p^*/dT\right)\left(dT/dt\right) \quad (58)$$

$$= C_p^*(t) + \tau_{th}\left(dC_p^*/dT\right)Q_h \quad (59)$$

$$= C_p^*(t) + R_0 C_p^* M\left(dC_p^*/dT\right)Q_h \quad (60)$$

where $C_p(t)$ and $C_p^*(t)$ are the observed and true heat capacities per unit mass, respectively, τ_{th} is the thermal time constant, M is the sample mass and R_0 is the total thermal resistance between instrument cup and sample. A predicted baseline shift due to sample mass has been omitted. Eqs. (57)–(60) quantify the intuitive notions that large thermal resistance, large sample mass, fast heating rates and rapidly changing heat capacity will all adversely affect transient data. The thermal resistance, R_0, can be estimated from melting endotherms, which are predicted to rise linearly with slope $dC_p/dT = 1/R_0Q_h$, and to decrease exponentially with time constant, τ_{th}. For good thermal conductors such as indium, R_0 obtained in this way is dominated by the contact resistance between the pan and cup, and this dominance can also be expected for poorer conductors such as polymers and inorganic glasses. Contact resistance is affected by the flatness of the sample pan bottom, which can be distorted by small misadjustments of sample preparation devices such as crimping presses. The application of silicone grease to the interface between the cup and sample pan, mentioned above, reduces this problem by decreasing R_0. Applying Eqs. (57)–(60) to experimental data is problematic, because it is dC_p/dt that is measured, not dC_p^*/dt. Equating these two quantities at constant heating rate is approximately equivalent to neglecting $\tau_{th}(d^2C_p^*/dT^2)$, assuming τ_{th} to be constant. The accuracy of this approximation can only be assessed a posteriori by evaluating $d^2C_p^*/dT^2$ from the computed temperature dependence of $C_p^*(T)$. Eqs. (57)–(60) have not yet been applied to enthalpy relaxation analyses, although Hutchinson and co-workers [90,91] used a similar procedure (see below).

The thermal resistance of the sample also produces a temperature gradient across the sample. The first measurement of this appeared in the thesis of DeBolt [88], in which temperature differences of up to 1 K across ~1 mm thick samples of Vycor glass were reported. These data were obtained by placing slivers of indium at the bottom and top of the sample, and measuring the two melting temperatures. O'Reilly and Hodge [89] applied the same technique to polystyrene and observed temperature differences across a

0.5 mm sample ranging from 0.3 K at a heating rate of 1.25 K min^{-1}, to 1.3 K at 20 K min^{-1}. These differences increased linearly with heating rate for both 0.15 and 0.5 mm thick samples, but the variation with sample thickness depended on heating rate (qualitatively consistent with Eq. (60)). Since high overshoots can have a 'full width at half height' of just a few K (using $C_p^N = 1.0$ as a 'baseline'), such gradients can be expected to be significant. Hutchinson and co-workers [90,91] proposed that transfer effects be assessed by assuming the heat capacities are exactly described by the KAHR (and TN [92]) models (Section 3.2.2.), and to ascribe all deviations to thermal transfer effects. The KAHR and TN models predict that, for a constant ratio of cooling to heating rate, the heat capacity measured during heating shifts along the temperature axis with changes in heating rate, but does not change shape. This approach depends on the KAHR or TN formalisms being correct, which is a reasonable assumption for the simple rate cool and reheat histories that the method uses.

Thermal transfer effects have also been discussed by Lagasse [93], Mraw [94], Richardson and Burrington [95] and Hutchinson [96]. Richardson and Burrington determined a temperature difference between the temperature sensor and the bottom of a sapphire sample of about 4 K at a heating rate of 30 K min^{-1}, that decreased linearly with decreasing heating rate and passed through the origin. Sample mass has been reported to affect the temperature difference between the sample and temperature sensor [95], as well as the normalized heat capacity overshoot [97], consistent with Eq. (60). Lagasse [93] described a technique for overcoming thermal transfer in the measurement of enthalpy loss during annealing. It exploits the transients induced by starting and stopping scans, and is similar to the technique used by Richardson [98] and Gray [99] for measuring the enthalpy of melting of crystalline polymers.

2.2. AC calorimetry

This recent technique has been applied to the glass transition by Birge and Nagel [100,101], Menon et al. [102] and Birge [103]. It is an extension of techniques used to measure static heat capacities of organic liquids (see Refs. [7–9] in Ref. [102]), and is an important development because it measures enthalpy relaxation in the linear region of small temperature changes, thus avoiding the intricate non-linear phenomenology and data analysis needed in scanning calorimetry. The experiments are tedious and demanding, however, and to date only a few materials have been characterized.

Birge [103] has given an excellent discussion of the frequency-dependent heat capacity. The heat capacity is proportional to the mean-square fluctuations in entropy (Eq. (52)), and since these fluctuations have an associated spectral density it follows from the fluctuation–dissipation theorem that the frequency-dependent heat capacity, $C_p^*(i\omega)$, is complex. The imaginary component of a complex response function is normally associated with the absorption of energy from the applied field, but in ac calorimetry there is no net exchange of energy between the sample and its surroundings. However, there is a change in the entropy of the surroundings that is proportional to C_p'', and the second law of thermodynamics ensures that $C_p'' \geq 0$. The experimental technique is to drive a sinusoidal current, $I(t)$, through a thin heater made from a material with a large temperature coefficient of electrical resistance (usually nickel). The magnitude of the temperature oscillations depends on thermal diffusion from the heater into the sample, and is a function of the heat capacity, thermal conductivity and geometry of the sample. Information on $C_p^*(i\omega)$ is obtained from the magnitude of the temperature oscillations. The electrical power, $P(t)$, is proportional to the square of the current, so that the temperature, $T(t)$, has a dc component and a phase shifted oscillation at twice the current frequency:

$$I(t) = I_0 \cos(\omega t/2), \tag{61}$$

$$P(t) = (I_0^2 R/2)[1 + \cos(\omega t)], \tag{62}$$

$$T(t) = T_{dc} + T_\omega \cos(\omega t - \phi). \tag{63}$$

The oscillating temperature produces an oscillating heater resistance, $R(t)$, which with the cur-

rent at frequency $\omega/2$ produces a voltage, $V(t)$, across the heater with a component at frequency $3\omega/2$:

$$R(t) = R_{dc} + R_{\omega} \cos(\omega t - \phi), \tag{64}$$

$$R_{\omega} = \alpha R_{dc} T_{\omega}, \tag{65}$$

$$V(t) = I(t)R(t) = V_{\omega/2} \cos(\omega t/2 - \phi') + V_{3\omega/2} \cos(3\omega t/2 - \phi), \tag{66}$$

$$V_{3\omega/2} = I_0 R_{\omega}/2, \tag{67}$$

where α in Eq. (65) is the temperature coefficient of resistance of the heater. Accurate measurement of the third-harmonic signal requires considerable care. An important element of the technique is the use of a Wheatstone bridge to cancel the fundamental component of the signal, which is much stronger than the third-harmonic. An out-of-phase component at the fundamental (Eq. (66)) is not cancelled by the bridge, but does not present a problem to any good lock-in amplifier. If the bridge is purely resistive over the frequency range of interest, any third-harmonic distortion in the source signal is also nulled. The frequency range is 10^{-2} to 6×10^3 Hz. For most boundary conditions, the product $C_p\kappa$ is obtained from T_{ω}, rather than C_p alone (where κ is the thermal conductivity).

3. Phenomenological expressions

A minimum of four parameters is needed to describe enthalpy relaxation. An effective activation energy is required to specify the cooling rate dependence of T_f', a pre-exponential factor fixes the absolute value of T_f' and a minimum of one parameter each is needed to specify non-exponentiality and non-linearity. In this section we summarize the mathematical expressions used to express these different aspects of relaxation behavior. Activation energies are discussed with non-linearity, because the non-linearity parameters define the activation energies above and below T_g.

3.1. Non-exponentiality

Many empirical functional forms for non-exponentiality have been suggested. A widely used, versatile, convenient and generally accurate decay function is the stretched exponential

$$\phi(t) = \exp\left(-(t/\tau_0)^{\beta}\right) \quad (1 \geq \beta > 0). \tag{68}$$

This is referred to as the Kohlrausch [104,105], Williams–Watt [106,107] or Kohlrausch–Williams–Watt (KWW) function, and statisticians will find it (and its derivative) familiar as the Weibull distribution (albeit with $\beta > 1$). It has been said with considerable justification [9] that Eq. (68) has been in use for so long, and in so many different applications, that it seems inappropriate to attach individual names to it. We adopt this position here, and refer to Eq. (68) as the stretched exponential. The average retardation times are

$$\langle \tau^n \rangle = (\tau_0^n/(\beta\Gamma(n)))\Gamma(n/\beta), \tag{69}$$

$$= (\tau_0^n/\Gamma(n+1))\Gamma(1+(n/\beta)), \tag{70}$$

and the ratio of retardation to relaxation times is (cf. Eq. (18))

$$\frac{\tau_{ret}}{\tau_{relax}} = \frac{\langle \tau_{relax}^2 \rangle}{\langle \tau_{relax} \rangle^2} = \frac{\beta\Gamma(2/\beta)}{[\Gamma(1/\beta)]^2}. \tag{71}$$

Neither $g(\tau)$ nor $R^*(i\omega\tau)$ is expressible in terms of named functions, except for $\beta = 0.5$:

$$g(\tau) = \frac{\exp[-\tau/4\tau_0]}{2(\pi\tau\tau_0)^{1/2}}, \tag{72}$$

and

$$R^*(i\omega\tau) - R_U = \frac{(R_R - R_U)}{2}\left(\frac{\pi}{\tau_0}\right)^{1/2} \frac{1}{(i\omega)^{1/2}} \times \exp\left(\frac{k^2}{i\omega}\right) \operatorname{erfc}\left(\frac{k}{(i\omega)^{1/2}}\right) \tag{73}$$

$$= (R_R - R_U)\pi^{1/2}\left(\frac{1-i}{\rho}\right) \times \exp(-z^2) \operatorname{erfc}(-iz), \tag{74}$$

where $2k = (\tau_0)^{-1/2}$, $\rho = (8\omega\tau_0)^{1/2}$ and $z = ((1 + i)/\rho)$. Tables of $\exp(-z^2)\,\mathrm{erfc}(-iz)$ are available [108], and are included as library functions in some software products. Tables of both $g(\tau)$ and $R^*(i\omega\tau)$ for $0.3 \le \beta \le 1.0$ have been prepared by expressing Eq. (68) as a sum of exponentials [109,110]. The value of β can be obtained from the full width at half height of the loss component $R''(\omega\tau)$, Δ, expressed in decades of $\omega\tau$ [111]:

$$\beta^{-1} = -0.08984 + 0.96479\Delta - 0.004604\Delta^2 \quad (0.3 \le \beta \le 1.0;\ 1.14 \le \Delta \le 3.6), \tag{75}$$

which gives β to within ± 0.001 for $\beta \le 0.7$, and within ± 0.002 for $0.7 \le \beta \le 0.95$. The stretched exponential has also been applied to enthalpy relaxation in a truncated form, in which the short time components of $g(\tau)$ are suppressed [112,113].

An empirical function often used in dielectric relaxation spectroscopy is the Davidson–Cole function [114]. It is characterized by a nearly single relaxation time (Debye) low frequency response, and an extended high frequency tail in the loss. This function is unusual in having simple forms in the frequency, retardation time and real time domains. In the frequency domain,

$$R^*(i\omega\tau) - R_U = \frac{(R_R - R_U)}{(1 + i\omega\tau_0)^\gamma}, \quad 1 \ge \gamma > 0, \tag{76}$$

from which

$$R'(\omega\tau) - R_U = (R_R - R_U)(\cos\phi)^\gamma \cos(\gamma\phi), \tag{77}$$

$$R''(\omega\tau) = (R_R - R_U)(\cos\phi)^\gamma \sin(\gamma\phi), \tag{78}$$

where $\tan\phi = \omega\tau_0$. The distribution function is

$$g(\ln \tau/\tau_0) = \frac{\sin\gamma\pi}{\pi}\left(\frac{\tau}{\tau_0 - \tau}\right)^\gamma \quad (\tau \le \tau_0)$$
$$= 0 \quad (\tau > \tau_0), \tag{79}$$

and the decay function is

$$\phi(t) = 1 - G(\gamma, t/\tau_0), \tag{80}$$

where

$$G(\gamma, t/\tau_0) \equiv \frac{1}{\Gamma(\gamma)}\int_0^{t/\tau_0} \exp(-x)x^{\gamma-1}\,dx \tag{81}$$

is the incomplete gamma function [108]. Eq. (80) has not been very useful in the past, because of the inaccessibility of $G(\gamma, t/\tau_0)$, but this function is now increasingly available in Fortran mathematical libraries. A numerical approximation to $\phi(t)$ can be made by discretizing $g(\tau)$ and expressing $\phi(t)$ as a discretized version of Eqs. (8) and (9), and such discretized functions have been applied to enthalpy relaxation [112,113]. The parameter γ can also be expressed in terms of the full width at half height of the loss peak $R''(\omega\tau)$ [111]:

$$\gamma^{-1} = -1.2067 + 1.6715\Delta + 0.222569\Delta^2 \quad (0.15 \le \gamma \le 1.0;\ 1.14 \le \Delta \le 3.3), \tag{82}$$

which gives γ to within ± 0.002 for $\gamma \le 0.9$. Maximum values of $R''(\omega\tau)$ are given by Eq. (78) for $\phi_{max} = \pi/[2(1 + \gamma)]$. Lindsey and Patterson [110] have given a detailed comparison of the Davidson–Cole and stretched exponential functions. They found that the two decay functions are surprisingly similar, given the quite different distribution functions.

A logarithmic Gaussian distribution for $g(\ln\tau)$ has been fitted to enthalpy relaxation data [112,113]:

$$g(\ln\tau) = \left(\frac{b}{\pi^{1/2}}\right)\exp\left(-\left(b^2\ln^2(\tau/\tau_0)\right)\right). \tag{83}$$

It is derived from the reasonable assumption of a Gaussian distribution of activation energies. The latter implies that $g(\ln\tau)$ changes with temperature and/or fictive temperature, although neither of these possibilities is usually incorporated into enthalpy relaxation calculations.

Box and wedge distribution functions have also been applied to enthalpy relaxation. As introduced by Tobolsky [115], the single box distribution is

$$g(\ln\tau) = 1/\ln(\tau_2/\tau_1) \quad (\tau_2 \ge \tau \ge \tau_1)$$
$$= 0 \quad (\tau_2 < \tau < \tau_1). \tag{84}$$

Expressions for $R^*(i\omega\tau)$ corresponding to the box distribution have been given by Frohlich [116]. The wedge distribution is

$$g(\ln\tau) = \frac{1}{\tau^{1/2}}\left(\frac{\tau_1^{1/2}\tau_2^{1/2}}{\tau_2^{1/2}-\tau_1^{1/2}}\right) \quad (\tau_2 \geq \tau \geq \tau_1)$$
$$= 0 \quad (\tau_2 < \tau < \tau_1). \tag{85}$$

The double box distribution,

$$g(\ln\tau) = \frac{A}{\ln(\tau_2/\tau_1)} \quad (\tau_2 \geq \tau \geq \tau_1)$$
$$= \frac{(1-A)}{\ln(\tau_3/\tau_2)} \quad (\tau_3 \geq \tau \geq \tau_2)$$
$$= 0 \quad (\tau_3 < \tau < \tau_1), \tag{86}$$

has been used in the analysis and parameterization of enthalpy relaxation data by Kovacs, Hutchinson and co-workers [47]. The decay functions corresponding to certain double box distributions are remarkably similar to the stretched *exponential function for* $\beta = 0.5$.

Other functions, used principally in the frequency domain of dielectric relaxation, include the Cole–Cole [117], Havriliak–Negami [118] and Glarum [119] functions. However, these are inconvenient to use in the time domain, and have not yet been applied to enthalpy relaxation.

3.2. Non-linearity

3.2.1. Narayanaswamy–Moynihan equation

Narayanaswamy [41] introduced a generalized version of the Arrhenius equation of the form

$$\tau_0 = A\exp\left(\frac{H_g}{RT} + \frac{H_s}{RT_f}\right), \tag{87}$$

where A, H_g and H_s are constant parameters and R is the ideal gas constant [120]. In the equilibrium state above T_g where $T_f = T$, Eq. (87) transforms to the familiar Arrhenius form with an *activation energy* $H_g + H_s$. *Moynihan et al.* [12] rewrote this equation as

$$\tau_0 = A\exp\left(\frac{x\,\Delta H^*}{RT} + \frac{(1-x)\,\Delta h^*}{RT_f}\right)$$
$$(1 \geq x \geq 0), \tag{88}$$

where x is a partitioning parameter that defines the degree of non-linearity, and this is the form in which the equation is now used. We refer to Eq. (88) as the Narayanaswamy–Moynihan (NM) equation. It has been recognized since its introduction that Eq. (88) is only approximately true near T_g, because it predicts an Arrhenius temperature dependence in the equilibrium state above T_g that is inconsistent with the VTF equation. However, the range in T and T_f over which the glass transition occurs is sufficiently small that the effective VTF activation energy (Eq. (5)) is almost constant. In some cases, the equilibrium temperature dependence just above T_g reverts to the Arrhenius form, rather than continuing a VTF dependence, and Eq. (88) is not inconsistent. Such a return to Arrhenius behavior just above T_g is observed for the viscosity of B_2O_3 [121], Ca/KNO_3 [122] and some simple organic compounds [123], and is discussed below (Section 6.3.).

3.2.2. The KAHR equation

Kovacs, Aklonis, Hutchinson and Ramos (KAHR) [47] introduced the expression

$$\ln\tau_0(T,\delta) - \ln\tau_0(T_r,\delta)$$
$$= -\theta(T-T_r) - (1-x)\theta\delta/\Delta C_p, \tag{89}$$

where δ is given by Eqs. (30) and (31), T_r is a reference temperature close to T_g, θ is a form of activation energy and x is a parameter that partitions T and δ. As noted in the Introduction, θ lies in the range 0.1–1 K^{-1} for a wide variety of materials. Eq. (89) is referred to as the KAHR equation. The relation between θ and the NM parameter Δh^* is derived by equating the temperature derivatives of τ_0 in the equilibrium state ($T = T_f$, $\delta = 0$), and making the approximation $T \approx T_f \approx T_g$:

$$\theta \approx \frac{\Delta h^*}{RT^2} \approx \frac{\Delta h^*}{RT_f^2} \approx \frac{\Delta h^*}{RT_g^2}. \tag{90}$$

Within the same approximation, the x parameters of Eqs. (88) and (89) are equivalent:

$$-\theta T - (1-x)\theta(T_f - T)$$

$$\approx \frac{\Delta h^*}{RT} + \frac{(1-x)\,\Delta h^*}{RT_f} - \frac{(1-x)\,\Delta h^*}{RT}$$

$$\approx \frac{x\,\Delta h^*}{RT} + \frac{(1-x)\,\Delta h^*}{RT_f}. \quad (91)$$

Dimensionless and normalized parameters and variables have been defined for the KAHR equation. The dimensionless temperature, $\mathscr{T}$, is

$$\mathscr{T} = \theta T = \frac{\Delta h^* T}{RT_g^2}, \quad (92)$$

and the normalized heating or cooling rate, $\mathscr{E}$, is

$$\mathscr{E} = \theta Q = \frac{\Delta h^*}{RT_g^2} Q. \quad (93)$$

The dimensionless amount of annealing, $\mathscr{D}_H$, is

$$\mathscr{D}_H = \frac{\theta\,\Delta\delta}{\Delta c_p} = \frac{\Delta h^*\,\Delta T_f}{RT_g^2}, \quad (94)$$

where $\Delta\delta$ and ΔT_f denote changes during annealing. An effective retardation time, τ_{eff}, is often associated with the KAHR phenomenology:

$$\frac{1}{\tau_{eff}} = \frac{1}{\delta}\frac{d\delta}{dt}. \quad (95)$$

The value of τ_{eff} equals the retardation time for an exponential decay, but for a non-exponential decay function such as the stretched exponential function, with a constant retardation time, τ_0, it is time-dependent:

$$\frac{1}{\tau_{eff}} = \beta\left(t^{\beta-1}/\tau_0^{\beta}\right). \quad (96)$$

Thus, its use complicates the treatment of non-linearity, in which τ_0 is also time-dependent.

3.2.3. Adam–Gibbs equation

The Adam–Gibbs theory for linear relaxations [16] is based on transition state theory, and predicts that configurational entropy determines the average relaxation time. It gives rise to equations that are almost indistinguishable from the VTF equation, and for the hyperbolic form of $\Delta C_p(T)$ (Eq. (55)) it reproduces the VTF equation exactly. The ease with which this equation can be extended through the glass transition to the glassy state was quickly recognized by Macedo and Napolitano [121], Goldstein [124], Kovacs et al. [125], Plazek and Magill [126], Magill [127] and Howell et al. [128], but was not used explicitly for enthalpy relaxation until the pioneering work of Scherer [129], and in later studies by Hodge [130]. Because it invokes general concepts that have had an important influence on thinking about the cooperative nature of molecular motions in the glass transition region, a derivation of the equation is given here.

The central assumption is that relaxation involves the cooperative rearrangement of many 'particles' (defined below). The transition state activation energy, E_a, is expressed as

$$E_a = z\,\Delta\mu, \quad (97)$$

where $\Delta\mu$ is the elementary excitation energy per particle, and z is the number of particles that cooperatively rearrange. It can be shown mathematically that only the minimum value of z, z^*, significantly contributes to the relaxation time. The value of z^* is determined by equating two expressions for the configurational entropy per particle:

$$\frac{S_c(T)}{N_A} = \frac{s_c^*}{z^*(T)}, \quad (98)$$

where $S_c(T)$ is the macroscopic configurational entropy (defined below), N_A is Avogadro's number and s_c^* is the configurational entropy of the smallest number of particles capable of rearranging. Thus

$$\tau_0 = A\exp(E_a/RT), \quad (99)$$

$$= A\exp\left(\frac{z^*\,\Delta\mu}{k_B T}\right), \quad (100)$$

$$= A\exp\left(\frac{N_A s_c^*\,\Delta\mu}{k_B T S_c}\right), \quad (101)$$

where a pre-exponential factor $(1-\exp(-\Delta\mu/k_BT))^{-1}$ has been suppressed because of its weak temperature dependence relative to the exponential term. There must be at least two configurations available to the smallest rearranging group (those before and after rearrangement), so that

$$s_c^* = k_B \ln W^* \geq k_B \ln 2, \quad (102)$$

where W^* is the minimum number of configurations needed for rearrangement. The value of S_c is given by

$$S_c = \int_{T_2}^{T} (\Delta C_p/T)\, dT, \tag{103}$$

where T_2 is the temperature at which S_c extrapolates to zero, i.e., the Kauzmann temperature. As noted in the Introduction, we refer to it here as T_2 rather than T_K to emphasize that it is an adjustable parameter connected with the non-linear kinetics of the glass transition. Assessment of $\Delta C_p(T)$ requires care. It is common to equate it with the difference between the liquid or rubber and glass heat capacities, on the assumption that this difference is totally configurational but, as noted already, this assumption has been challenged by Goldstein [25,26]. Moreover, the temperature dependence of ΔC_p must be obtained from extrapolated data, and these extrapolations are uncertain. For example, C_{pg} must be obtained at temperatures well below T_g, to ensure that relaxation effects are not included in its temperature dependence. These low temperature data require lengthy extrapolations that place high demands on experimental precision. In addition, C_{pg} must be measured over a significant temperature range in order that its temperature dependence be accurately determined. Huang and Gupta [131] evaluated expressions for $C_{pg}(T)$ suitable for extrapolation into and above the glass transition temperature range, for a soda lime silicate glass.

The functional form for $\tau_0(T)$ depends on the temperature dependence of ΔC_p (see Section 1.3.4.). For $\Delta C_p = C$ = constant (eq. (54)),

$$\tau_0 = A \exp(Q/T \ln(T/T_2)), \tag{104}$$

where

$$Q = \frac{N_A s_c^* \Delta\mu}{k_B C}. \tag{105}$$

Eq. (104) is almost indistinguishable from the VTF equation, and in fact retaining only the first term in the expansion of the logarithmic term reproduces the VTF form. For the hyperbolic form of Eq. (55),

$$S_c = C(1 - T_2/T), \tag{106}$$

and the VTF form is reproduced exactly [76,132]:

$$\tau_0 = A \exp\left(\frac{Q}{T(1 - T_2/T)}\right) = A \exp\left(\frac{Q}{T - T_2}\right). \tag{107}$$

As noted already (Section 1.3.4.), the hyperbolic Eq. (55) has a somewhat stronger temperature dependence than that observed for most polymers, according to plots of the data compiled in Ref. [82], and thus should be regarded only as a mathematically convenient approximation for polymers.

Eqs. (98) and (106) imply that z^* is proportional to $(1 - T_2/T)^{-1}$. Thus, z^* and the barrier height $z^* \Delta\mu$ diverge as $T \to T_2$, and this divergence can be expected to prevent T_g approaching T_2 [130,133,134]. Since z^* is conceivably associated with some form of correlation length, it is of interest that the correlation length computed from a random field Ising model also diverges, albeit as $(1 - T_c/T)^{-\nu}$ [135]. However, no evidence for a structural correlation length was observed in a viscosity study of glycerol by Dixon et al. [136], nor in a molecular dynamics simulation by Ernst et al. [137]. On the other hand, if z^* is interpreted in dynamic terms, for example as the minimum number of particles needed for the ensemble averaged time correlation function to be independent of size, it would not necessarily be seen structurally. It is also possible that z^* corresponds in some way to the 'dynamic characteristic length', defined by the ratio of the frequency of the Raman 'boson' peak to the speed of sound [138,139]. Adam–Gibbs behavior has been observed in a spin-facilitated kinetic Ising model developed by Frederickson [140].

As noted above, the AG equation has been extended through the glass transition to the glassy state by several investigators, by replacing T with T_f in the expression for S_c. In applying this extension to enthalpy relaxation, it must be assumed that the entropic T_f is the same as the enthalpic T_f that enters into the non-linear forms of $\tau_0(T, T_f)$. This equality is a good approximation, however, because the temperature factor relating enthalpy and entropy does not vary more than about 20 K over the glass transition temper-

ature range of integration. Scherer [129] inserted the empirical eq. (53) form of $\Delta C_p(T)$ into Eqs. (101) and (103), using experimental values of the coefficients a_0 and a_1, and obtained good agreement with the enthalpy relaxation data for NBS-710 glass reported by Sasabe et al. [141]. Satisfactory fits (within experimental uncertainty) were also obtained for published viscosity data [142]. For $\Delta C_p = C$, the non-linear form of Eq. (104) is

$$\tau_0(T, T_f) = A \exp(Q/(T \ln(T_f/T_2))). \quad (108)$$

For $\Delta C_p = CT_2/T$,

$$\tau_0(T, T_f) = A \exp(Q/(T(1 - T_2/T_f))). \quad (109)$$

Eq. (108) has been termed AGL [130] (L denoting the logarithmic term), and Eq. (109) has been referred to as AGF ('Adam–Gibbs–Fulcher') [130]. Approximate relations between the Narayanaswamy and Adam–Gibbs parameters are derived from the temperature derivatives of τ_0 in the equilibrium ($T_f = T$) and glassy ($T_f = T_f'$) states. For Eq. (108),

$$\frac{d \ln \tau_0}{d\, 1/T} = \frac{\Delta h^*}{R} \approx Q(L^{-1} + L^{-2}) \approx \frac{Q(1-x)}{x^2} \text{ (see Eq. (113))}, \quad (110)$$

and

$$\left.\frac{\partial \ln \tau_0}{\partial\, 1/T}\right|_{T_f'} = \frac{x\, \Delta h^*}{R} \approx QL^{-1}, \quad (111)$$

where

$$L \approx \ln(T_f'/T_2) \quad (112)$$

and the approximation $T \approx T_f'$ has been used. Thus

$$x \approx L/(1 + L). \quad (113)$$

Eqs. (110) and (111) were first obtained, using a different notation, by Plazek and Magill [126]. For Eq. (109),

$$\frac{\Delta h^*}{R} = \frac{Q}{(1 - T_2/T)^2} \approx \frac{Q}{(1 - T_2/T_f')^2} \approx \frac{Q}{x^2} \text{ (see Eq. (116))}, \quad (114)$$

$$x\, \Delta h^*/R \approx Q/(1 - T_2/T_f'), \quad (115)$$

and

$$x \approx 1 - (T_2/T_f'). \quad (116)$$

Eqs. (114) and (115) were first obtained by Macedo and Napolitano [121], albeit using a different route. They considered the ratio of glassy and liquid state activation energies, and inferred the Eq. (106) form for S_c by equating the VTF and entropic AG equations. They did not invoke the hyperbolic form of $\Delta C_p(T)$, first applied to enthalpy relaxation by Hodge [130] but having much earlier roots [76,132]. Eqs. (110)–(116) are special cases of the general expressions first derived by Howell et al. [128]:

$$\frac{\Delta h^*}{R} \approx \frac{E}{S_c(T)} + \frac{ET}{S_c^2}\frac{dS_c}{dT} \quad (117)$$

and

$$x\, \Delta h^*/R \approx E/S_c(T_f'), \quad (118)$$

where $E = \Delta\mu\, s_c^*$. Thus, the general expression for x is, in the approximation $T \approx T_f'$,

$$x \approx \left(1 + \frac{T}{S_c(T_f')}\left(\frac{dS_c}{dT}\right)_{T=T_f'}\right)^{-1}. \quad (119)$$

The difference in T_f'/T_2 evaluated from Eqs. (113) and (116) depends on the value of x. For small x the difference is small, but for large x it can be substantial. For $x = 0.15$, $T_f'/T_2 = 1.19$ and 1.18 from Eqs. (113) and (116), respectively, whereas for $x = 0.70$ values of 10.3 and 3.33 are obtained.

3.2.4. Free volume equations

Free volume theories are less easily generalized to the non-linear domain because, although a fictive temperature can be associated with the free volume, it is not clear how a sufficiently strong temperature factor can be introduced. This deficiency was first emphasized by Goldstein and Nakonecznyi [143], in their analysis of volume relaxation data for PVAc reported by Kovacs [36], and has also been discussed by Macedo and Napolitano [121]. The close-packed or occupied volume, V_0, that is subtracted from the observed volume to give the free volume, is temperature-dependent [18], but this temperature dependence

arises from the anharmonicity of vibrational modes, and as Ferry [18] has pointed out "... its magnitude and thermal expansion coefficient, α_0,... remain a matter of conjecture and can be estimated only indirectly".

Free volume theories have been derived that introduce an explicit temperature term, but the resulting equations contain undesirable extra adjustable parameters. These (and other) equations *have been discussed by Scherer [129] and Hodge* [130]. Macedo and Litovitz [144] derived a hybrid equation by modifying the Doolittle equation [145] (rationalized by Cohen and Turnbull [146]):

$$\tau = A \exp(b/f), \tag{120}$$

where b is a constant of order unity and f is the free volume fraction defined as

$$f = \frac{V - V_0}{V_\infty} = \frac{V_\infty - V_0}{V_\infty} + \frac{V - V_\infty}{V_\infty} = f_T + \delta_v, \tag{121}$$

where V_∞ and V_0 are the equilibrium (limiting long time) and 'occupied' volumes, respectively. The quantity δ_v has been discussed above in the context of the KAHR phenomenology, and can be identified here with the recoverable part of the fractional free volume. Macedo and Litovitz suggested that an activation energy be added to *the free volume term, to account for the thermal* activation needed for a particle to move from one pocket of free volume to another:

$$\tau = A' \exp\left(\frac{b}{V_f} + \frac{E}{RT}\right). \tag{122}$$

If V_f is assumed to vary as $T_f - T_2$, this becomes

$$\tau = A' \exp\left(\frac{B'}{T_f - T_2} + \frac{E}{RT}\right), \tag{123}$$

whose linear form ($T_f = T$) was first proposed by Dienes [147]. The Dienes equation was reported by Macedo and Litovitz to give a good fit to viscosity data for B_2O_3, SiO_2, alkali silicates, alcohols and poly(isobutylene).

Mazurin et al. [148] proposed the equation

$$\tau = A'' \exp\left(\frac{B''}{R(T_f - T_2)} + \frac{Q}{R}\left(\frac{1}{T} - \frac{1}{T_f}\right)\right), \tag{124}$$

which becomes the VTF equation above T_g where $T_f = T$, and is Arrhenius in the glassy state. This equation is not attractive, however, because it contains an additional adjustable parameter.

Free volume concepts have been applied through and below T_g by Kovacs et al. [125]. They wrote the equilibrium fractional free volume, f_T (Eq. (121)), as

$$f_T = f_g + \alpha_f (T - T_g), \tag{125}$$

where α_f is the coefficient of fractional free volume thermal expansivity, and f_g is the fractional free volume of the glassy state. Thus,

$$\tau(T, \delta) = \tau_g \exp\left(\frac{b\delta/f_T}{f_T + \delta}\right) \times \exp\left(\frac{(b/f_g)(T - T_g)}{(f_g/\alpha_f) + T - T_g}\right). \tag{126}$$

Comparing Eq. (126) with the KAHR equation (Eq. (89)) yields

$$\theta = b\alpha_f / f_g^2 \tag{127}$$

and

$$(1 - x)\theta = (b\,\Delta\alpha)/f_T^2, \tag{128}$$

where $\Delta\alpha$ is the change in free volume expansivity at T_g. For $T \approx T_g$,

$$x \approx (\alpha_f - \Delta\alpha)/\alpha_f. \tag{129}$$

A free volume expression can also be formulated using Adam–Gibbs concepts, by defining z^* in terms of the free volume per particle rather than the entropy per particle. This approach is straightforward, but does not appear to have been described before. Eq. (98) is replaced by

$$V_f(T)/N_A = v^*/(z^*(T)), \tag{130}$$

so that

$$z^*(T) = \frac{N_A v^*}{V_f(T)}, \tag{131}$$

where v^* is the minimum volume needed for rearrangement. The non-linear free volume ver*sion of the Adam–Gibbs equation then becomes*

$$\tau_0(T, T_{f,v}) = A \exp\left(\frac{N_A v^* \Delta\mu}{k_B T V_f(T_{f,v})}\right). \tag{132}$$

It seems natural to interpret v^* as the activation volume for the pressure dependence of τ_0. For polystyrene, this is about 300 ± 100 cm^3 per mol of monomer [149].

3.3. Pre-exponential factor

This is determined by T_f' and the TN and KAHR activation energies, Δh^* and θ:

$$\ln A = -\frac{\Delta h^*}{RT_f'} + \ln \tau(T_f')$$

$$\approx -\frac{\Delta H_{\text{eff}}}{RT_f'} + 4.6\left[(\tau(T_f') \approx 100 \text{ s})\right] \quad (133)$$

$$\approx \theta T_g + 4.6. \quad (134)$$

For thermal histories without annealing, changing $\ln A$ moves the T_f vs. T curve along the $T_f = T$ equilibrium line, and the dT_f/dT vs. T curve along the T axis by an amount

$$\Delta T \approx \left(RT_g^2/\Delta h^*\right) \Delta \ln A \approx (\Delta \ln A)/\theta. \quad (135)$$

Changes in $\ln A$ affect annealing behavior, because the difference between T_f' and T_a determines, in part, the rate of annealing.

4. Calculation procedures

4.1. The KAHR method

Kovacs, Aklonis, Hutchinson and Ramos [47] described a procedure for solving the set of coupled non-linear differential equations that arises in the KAHR phenomenology. The non-exponential decay function is written as a finite series of exponentials, where the retardation times, $\{\tau_i\}$, are defined by the KAHR equation (89):

$$\phi(t) = \sum_i g_i \exp\left[-t/\tau_i(T, \delta)\right]. \quad (136)$$

The coefficients g_i also define the weighting factors dividing the total departure from equilibrium, δ, of Eqs. (30) and (31), into components δ_i that correspond to each τ_i. Thermorheological simplicity is enforced by keeping the $\{g_i\}$ constant. The differential equations are those defining the exponential function:

$$\frac{d\delta_i}{dt} = \frac{-\delta_i}{\tau_i(T, \delta)}, \quad (137)$$

where

$$\delta = \sum_i g_i \delta_i; \quad \sum_i g_i = 1. \quad (138)$$

Eq. (137) is the same as that used in the pioneering work of Tool [38]. However, Tool used the equation to define the complete decay function, whereas in the KAHR phenomenology it defines only one component of a non-exponential decay function. Eqs. (136) and (137) are coupled because the τ_i are defined in terms of the global value of δ, rather than the components δ_i. The numerical solution of these coupled non-linear differential equations is computationally expensive, in part because the time increments must be very small in the equilibrium state above T_g, where the retardation times are short. Thus, considerable time is spent on calculating the equilibrium heat capacity, before the departures from equilibrium that are of interest are observed during cooling. This formalism was the first to be applied to rate cooling and heating histories with intervening annealing, and gave the first prediction and explanation of sub-T_g endotherms in scans of annealed glasses [47], but it has been used to fit only a limited number of experimental heat capacity data.

4.2. The Tool–Narayanaswamy (TN) method

The TN method is based on Boltzmann superposition of responses that have been linearized using the reduced time method of Gardon and Narayanaswamy [40] (Section 1.2.3.). It was used to describe annealing effects by Narayanaswamy [40,41] and others [150], but was first applied to thermal histories that included rate cooling and heating in 1975 by Mazurin et al. [151] and Moynihan et al. [150]. The TN method has since been used by many groups. The method is computationally more efficient and more easily implemented than the KAHR method, and has been extensively used to extract enthalpy relaxation

parameters from experimental data. Both the Boltzmann and reduced time integrals must be evaluated numerically. Numerical evaluation of the Boltzmann integral is accomplished by expressing the thermal history, $T(t)$, as a series of temperature steps, ΔT_k, that are small enough to ensure a linear response (generally 1 K, but see below). For uniform cooling and heating without intervening annealing, $T_f(t)$ is given by

$$T_{f,n} = T_0 + \sum_{j=1}^{n} \Delta T_j \left\{1 - \phi(\zeta_{j,n})\right\} \tag{139}$$

$$= T_0 + \sum_{j=1}^{n} \Delta T_j \left(1 - \phi\left(\sum_{k=j}^{n} (\Delta T_k/(Q_k \tau_{0,k}))\right)\right), \tag{140}$$

where T_0 ($\gg T_g$) is the temperature from which cooling starts, Q_k is the cooling or heating rate (negative for cooling), and $\tau_{0,k}$ is a function of $T_{f,k-1}$ and $T_k = T_0 + \Sigma_{j=1}^{n} \Delta T_j$. During annealing, the upper index of the Boltzmann summation is fixed at n_A, and the reduced time summation becomes [152]

$$\zeta_{j,n} = \sum_{k=n_A}^{n_A+n} \frac{\Delta t_k}{\tau_{0;k}} \quad (n = 1, n_B), \tag{141}$$

where Δt_k are subintervals of the annealing time, t_a, such that

$$t_a = \sum_{k=n_A}^{n_A+n_B} \Delta t_k. \tag{142}$$

To ensure linearity, the intervals Δt_k must be small enough that T_f decays by less than about 1 K. Dividing the annealing time into five logarithmically even increments per decade is usually satisfactory, so that $n_B = 5 \log_{10} t_a(s)$. However, time increments of 0.2 decades can be too large to ensure linearity during initial relaxation in some rapidly relaxing systems, such as those formed by extremely rapid cooling rates, or for the last stages of relaxation after very long annealing times. These cases draw attention to themselves by changes in T_f that exceed ~ 1 K per time subinterval, and can be corrected by using shorter time increments.

For the commonly computed combination of a stretched exponential for $\phi(\zeta)$ and the NM expression for τ_0, the explicit expression for $T_{f,n}$ for rate cooling and heating is

$$T_{f,n} = T_0 + \sum_{j=1}^{n} \Delta T_j \left(1 - \exp\left(-\left(\sum_{k=j}^{n} \Delta T_k / Q_k \tau_{0;k}\right)^{\beta}\right)\right), \tag{143}$$

$$\tau_{0;k} = A \exp\left(\frac{x\,\Delta h^*}{RT_n} + \frac{(1-x)\,\Delta h^*}{RT_{f;n-1}}\right). \tag{144}$$

There is no requirement that ΔT_k or Q_k be constant, although they are usually made so for convenience. The value of dT_f/dT is discretized as

$$\frac{dT_f}{dT} \approx \frac{T_{f;n} - T_{f;n-1}}{T_n - T_{n-1}}. \tag{145}$$

The maximum values of dT_f/dT can be very large for annealed glasses, and in these cases a temperature step of 1 K in Eq. (143) is too large. Hodge [130] corrected this problem by making ΔT_k an inverse function of $(dT_f/dT)_{k-1}$ for the previous step:

$$\Delta T_k = \left(\frac{dT_f}{dT}\right)_{k-1}^{-1} = \frac{T_{k-1} - T_{k-2}}{T_{f;k-1} - T_{f;k-2}} \quad \left(\frac{dT_f}{dT} > 1\right)$$

$$= 1 \qquad (dT_f/dT \le 1). \tag{146}$$

This procedure broke down when the rate of change of dT_f/dT was too large, which occurred when dT_f/dT exceeded 6 or so. Prest et al. [153] used a self-consistency test for each calculation of $T_{f,n}$, in which the magnitude of each temperature step was changed until the computed value of $\tau_{0,k}$ became independent of ΔT_k to within a specified error amount. The maximum number of iterations was usually two or three and the computation time did not increase substantially.

Integration of Eq. (143) is considerably faster than solving the KAHR differential equations, but it is still CPU intensive because the double exponentiation needed to evaluate the stretched exponential function occurs in the innermost of two nested DO loops (corresponding to the reduced time and Boltzmann summations). Scherer [154] and Rekhson [155] have reported (and the

present writer can confirm) that a considerable saving in computing time is gained if the decay function $\phi(\zeta)$ is expressed as a weighted sum of exponentials. This procedure is computationally more efficient because the memory effect is absent for each exponential component. Each term for each component of the distribution is obtained by multiplying the value at the beginning of a time step by $\exp(-\Delta\zeta^i)$, where i indexes the component of the decay function. This is much faster than the addition of $\Delta\zeta^i$ to the argument of the stretched exponential, followed by exponentiation to the power β and computation of the exponential function. In the program used by Hodge [130], a two-dimensional array of $g_i(\beta)$ values is specified in a DATA statement for values of β differing by 0.05, with intermediate values of $g_i(\beta)$ obtained by linear interpolation. Alternatively, $\{g_i(\beta)\}$ can be obtained by a subroutine that least-squares fits $\sum_i g_i(\beta)\exp(-(t/\tau_i))$ to $\exp(-(t/\tau)^\beta)$ for each iteration.

The stretched exponential expression for $\phi(t)$ was first incorporated into the TN formalism by Rekhson et al. [156]. However, it should be clear from the exposition just given that any form for $\phi(t)$ can be used, and the box, wedge, Davidson–Cole, truncated stretched exponential, and log Gaussian forms for $g(\tau)$ have all been applied to enthalpy relaxation [112,113,157]. The stretched exponential has been used with the TN formalism more often than these other expressions only because of its convenience and general accuracy, and not because the phenomenology demands it.

4.3. The Ngai–Rendell (NR) theory

This theory [158] derives the stretched exponential decay function from basic principles, and thus attaches a fundamental significance to its functional form. The relaxation time, τ_0, in Eq. (68) is a function of β:

$$\tau_0 = \left(\beta\omega_c^{1-\beta}\tau_0^0\right)^{1/\beta}, \tag{147}$$

where ω_c, τ_0^0 and β may depend on T_f (or δ). If only τ_0^0 or ω_c depends on T_f or δ, non-linearity in the TN sense is produced. The theory identifies the relaxation rate as the relevant variable, and the rate equation for the isothermal decay function $\phi(t)$ is

$$\frac{d\ln\phi}{dt} = \frac{-1}{\tau_0^0}(\omega_c t)^{\beta-1} = \frac{-\beta t^{\beta-1}}{\tau_0^\beta}, \tag{148}$$

where β and ω_c have been assumed to be independent of time. In the linear case where τ_0 and τ_0^0 are also independent of time, integration of Eq. (148) yields the stretched exponential function. The non-linear decay function is obtained by inserting the isothermal time dependence of τ_0 into Eq. (148) and integrating:

$$\phi(t) = \exp\left(-\beta\int_0^t dt'(\omega_c t')^{\beta-1}/[\tau_0(t')]^\beta\right). \tag{149}$$

This differs from the TN non-linear form

$$\phi(t) = \exp\left(-\left(\int_0^t dt'/\tau_0(t')\right)^\beta\right). \tag{150}$$

whose differential

$$\frac{d\ln\phi}{dt} = -\beta\left(\int_0^t \frac{dt'}{\tau_0(t')}\right)^{\beta-1}\frac{d}{dt}\left(\int_0^t \frac{dt'}{\tau_0(t')}\right) \tag{151}$$

$$= -\frac{\beta}{\tau_0(t)}\left(\int_0^t \frac{dt'}{\tau_0(t')}\right)^{\beta-1} \tag{152}$$

is not the same as Eq. (148) when $(d\tau_0/dt) = d\tau_0[T_f(t)]/dt \neq 0$.

There is recent evidence that Eq. (149) is inconsistent with Boltzmann superposition [111,159], even for the linear case where $d\tau_0/dT_f = 0$. For a simple thermal history of two opposite temperature steps, between which the temperature is so low that no significant relaxation can occur, Eq. (149) predicts a relaxation function that depends on the time between temperature steps, which is inconsistent with experimental observation. Consider a special case of the history leading to Eqs. (19)–(21), in which $T_2 = T_0$ is sufficiently above T_g that equilibrium prevails [159]. The fictive temperature is given by an appropriately modified version of Eq. (19):

$$T_f(t) = T_0 - \Delta T(1-\phi(t,t_1)) + \Delta T(1-\phi(t,t_2)), \tag{153}$$

where $\Delta T = T_0 - T_1 = T_2 - T_1$. Insertion of the NR expression for $\phi(t)$ (Eq. (149)) into Eq. (153) yields

$$T_f(t) = T_0 - \Delta T\left(1 - \exp\left(-\int_{t_1}^{t}\frac{\beta(t'-t_1)^{\beta-1}}{\tau^{\beta}}dt'\right)\right) + \Delta T\left(1 - \exp\left(-\int_{t_2}^{t}\frac{\beta(t'-t_2)^{\beta-1}}{\tau^{\beta}}dt'\right)\right) \quad (154)$$

The first integral of Eq. (154) may be written as

$$\int_{t_1}^{t}\frac{\beta(t'-t_1)^{\beta-1}}{\tau^{\beta}}dt = \int_{t_1}^{t_2}\frac{\beta(t'-t_1)^{\beta-1}}{\tau_1^{\beta}}dt' + \int_{t_2}^{t}\frac{\beta(t'-t_1)^{\beta-1}}{\tau_2^{\beta}}dt'. \quad (155)$$

If T_1 is sufficiently low that no relaxation occurs in the time interval t_2–t_1, the first term on the right-hand side of Eq. (155) is zero and Eq. (154) becomes

$$T_f(t) = T_0 + \Delta T\exp\left(-\int_{t_2}^{t}\frac{\beta(t'-t_1)^{\beta-1}}{\tau_2^{\beta}}dt'\right) - \Delta T\exp\left(-\int_{t_2}^{t}\frac{\beta(t'-t_2)^{\beta-1}}{\tau_2^{\beta}}dt'\right). \quad (156)$$

The two integrals in Eq. (156) are not the same for $\beta \neq 1$, so that a time dependence of T_f is incorrectly predicted for $t > t_2$. Thus, the NR formalism predicts a memory effect even when the response to the first temperature step has a negligible time dependence (Section 1.2.2.). The TN result for the same history is

$$T_f = T_0 + \Delta T\exp\left(-\left(\int_{t_2}^{t}\frac{dt'}{\tau_2}\right)^{\beta}\right) - \Delta T\exp\left(-\left(\int_{t_2}^{t}\frac{dt'}{\tau_2}\right)^{\beta}\right) = T_0, \quad (157)$$

in accord with experiment. The Boltzmann superposition problem for NR is seen from Eq. (156) to reside in the choice of a correct zero for time, that seems inherent in the selection of the time-dependent relaxation rate as the physically relevant variable.

If $\phi(t)$ is expressed as a sum of exponentials, the integrated version of Eq. (148) can be expressed as [113]

$$\phi(t) = 1 - \sum_i \int_0^t \left(\frac{1}{\tau_i}\left(\frac{d\tau}{dt'}\right)\exp(-t'/\tau_i)\right)dt'. \quad (158)$$

However, if the $\{\tau_i\}$ are isothermally time-dependent this expression does not go to zero in the limit of long time [159]. This particular difficulty appears to arise from integrating the partial derivative of $\phi(t)$ rather than the full derivative. It can be shown [111], for the simplified form of $\tau(t)$

$$\tau(t) = \tau_1 + (\tau_2 - \tau_1)(t/t_m) \quad (0 \le t < t_m)$$
$$= \tau_2 \quad (t_m \le t < \infty), \quad (159)$$

that

$$\phi(t) = 1 - \sum_i \int_0^t \left(\left(\frac{1}{\tau_i} - \frac{t'}{\tau_i^2}\frac{d\tau}{dt'}\right)\exp(-t'/\tau_i)\right)dt' \quad (160)$$

gives the correct physical limit $\phi(t \to \infty) \to 0$. This difficulty is a separate issue from the Boltzmann superposition problem.

It must be emphasized that these difficulties with the NR approach are the subject of ongoing research, and may yet be resolved. They serve to emphasize once again, however, the need for special care when dealing with relaxations that are both non-linear and non-exponential.

4.4. Evaluation of parameters from experimental data

4.4.1. Activation energy

Values of Δh^* or θ are best evaluated from the cooling rate dependence of T_f', determined before any annealing has occurred:

$$\theta T_f'^2 \approx \Delta h^*/R = -\frac{d\ln Q_c}{d(1/T_f')}. \quad (161)$$

Eq. (161) is valid over a larger range of cooling rates than that expected from the approximations

used in its derivation. Scherer [9] has discussed this and associated issues related to the temperature dependence of τ_0. The theoretical consistency between Eq. (161) and the TN formalism has been demonstrated by Moynihan and co-workers [12,160], and for the KAHR formalism by Kovacs et al. [47]. Eq. (161) generally gives Δh^* to within 2%, although larger errors of the order of 10% occur when x and β are very small [111]. As noted by Richardson and Savill [43], DeBolt et al. [160] and Hodge [130,161], the evaluation of Δh^* or θ from Eq. (161) has three experimental advantages over other methods. First, thermal transfer effects are largely integrated out. Second, temperature calibration is simplified because T_f' is determined from data measured at a single heating rate. In fact, temperature calibration is not required at all, provided any temperature discrepancy is constant over the temperature range of integration and does not drift with time. The need for temperature calibration is vitiated because differentiation with respect to $(T_f' + \delta T)$ rather than T_f' produces errors of the order $\delta T/T_f'$, or a few percent for $\delta T \leq 5$ K, and experimental uncertainties in the derivative in Eq. (161) are usually larger than this. The third advantage is that the usable range of cooling rates is wider than that for heating rates, because no instrumental sensitivity limits are met at low cooling rates. A large range in cooling rates is needed for accurate determinations of high values of Δh^*, because the uncertainties in T_f' are fairly large (typically ± 0.5 K for polymers, smaller for inorganics).

A second method for determining Δh^* is to determine the heating rate dependence of T_g (defined either as the midpoint or the onset value), for glasses heated at the same rate as the cooling rate used to form them [90,160]. This method does not require integration of the heat capacity curves, but has some disadvantages. These include the need for temperature calibration at several heating rates, and a possible shift in T_g resulting from thermal transfer effects at high heating rates (Section 2.1.).

Values of Δh^* can also be obtained in principle from least squares fits of the normalized heat capacity, but this method has its own special set of problems (Section 4.5.). Values of Δh^* obtained by curve fitting are often less than those obtained from Eq. (161).

There are conflicting claims about whether accurate values of Δh^* can be obtained from the heating rate dependence of T_g of glasses formed at a constant cooling rate. Tribone et al. [162] reported that this method gave values for Δh^* that agreed with those obtained by keeping $Q_c = Q_h$, but Hodge [130] challenged this by asserting that calculations using known input values of Δh^* yielded constant Q_c activation energies that were substantially less than the input Δh^*.

4.4.2. Pre-exponential factor

The pre-exponential parameter, A, is fixed by Δh^* and T_f'. It is given to a first approximation by Eq. (133), but best values are obtained by matching calculated values of T_f' with experimental values, for whatever history is being parameterized (including those with annealing). As has been emphasized by Moynihan and co-workers [42,160], it is very important that the experimental and calculated values of T' be matched to ensure a self-consistent set of parameters (Section 4.5.).

4.4.3. Non-exponentiality

By far the most frequently used method for obtaining non-exponentiality parameters from experimental data is the curve fitting method, described below. Because of the intricacy of the phenomenology, and the possibility of systematic experimental error, it is probably asking too much at the present level of development to determine the components of $g(\tau)$ from experimental data. To date, a specific functional form for $g(\tau)$ or $\phi(t)$ has always been used (most often the stretched exponential function), and best fit estimates obtained for a single shape parameter (e.g., β). The assumption of a specific functional form for $\phi(t)$ or $g(\tau)$ is not ideal, but seems inescapable at the present time. Hutchinson and Ruddy [163] suggested that, given values of x and θ, a non-exponentiality parameter can be estimated from the value of C_{pmax}^N as a function of Q_c/Q_h. This method is attractive, because it uses the same histories as those needed to determine

θ or Δh^*. It has been used by Hutchinson [96] to determine the stretched exponential parameter for poly(vinylchloride) (PVC), polystyrene (PS) and three Ag–T–MoO_4 glasses.

4.4.4. Non-linearity

Several methods have been proposed for determining the KAHR and NM non-linearity parameter, x, from heat capacity data obtained for different thermal histories. Some of the proposed methods are incorrect, and others have particular difficulties or a restricted range of validity.

4.4.4.1. Annealing method. Moynihan et al. [164] used a method that exploited thermal histories for which the decay function could be approximated as an exponential. As with some of the other methods described here, this has so far only been applied to one material. In this case, however, the value of x agreed with that found by curve fitting, under conditions in which the curve fitting method was believed to be valid. The annealing method is based on the expansion of a non-exponential decay function as a weighted sum of exponentials. For short annealing times only the shortest retardation time component, τ_1, contributes to the relaxation, and the decay is approximately exponential. The weighting factor for this component, g_1, is the same as that for the component of T_f, T_{f1}, that relaxes with time constant τ_1, and is estimated from the fraction of relaxation that occurs after long annealing times:

$$g_1 \approx \frac{T_f(0) - T_f(t_a)}{T_f(0) - T_a}. \tag{162}$$

The time dependence of $T_f(t)$ is then given by

$$T_f(t) \approx T_a + g_1(T_{f1}(0) - T_a)\exp\left(-\int_0^t \frac{dt'}{\tau_1(t')}\right) + \sum_{i=2}^{n} g_i(T_{fi}(0) - T_a), \tag{163}$$

where $\tau_1(t)$ is given by

$$\tau_1(t) = A_1 \exp\left(\frac{x\,\Delta h^*}{RT_a} + \frac{(1-x)\,\Delta h^*}{RT_{f1}(t)}\right). \tag{164}$$

For the material being studied (a ZBLA glass), the value of Δh^* obtained from Eq. (161) was sufficiently large that differences in τ_i gave rise to relatively small changes in T_{fi} compared with $T_f(0) - T_f(t_a)$. Thus,

$$T_{f,i} \approx T_f \quad \text{(for all } i\text{)}, \tag{165}$$

and Eq. (163) simplified to

$$T_f(t) = g_1 T_a + (1 - g_1)T_f(0) + g_1(T_f(0) - T_a)\exp\left(-\int_0^t \frac{dt'}{\tau_1(t')}\right). \tag{166}$$

The parameters x and A_1 are now the only unknowns, and can be obtained by fitting Eqs. (164) and (166) to experimental values of $T_f(t)$. Note that Eqs. (162) and (166) are consistent because, for long annealing times, the exponential decay falls to zero and

$$T_f(t \to \infty) = g_1 T_a + (1 - g_1)T_f(0) = T_f(0) - g_1[T_f(0) - T_a], \tag{167}$$

so that a fraction g_1 of the maximum possible change in T_f has occurred. Some judgment must be made as to how short the annealing time needs to be for Eq. (158) to be valid. In principle, different values for t_a could be chosen to establish a range in x, but this has not yet been attempted.

4.4.4.2. Method of curve shifting. Hutchinson and Ruddy [91] determined x by exploiting two theoretical results. Both the KAHR and TN phenomenologies predict that, for scans of unannealed glasses for which the ratio of cooling to heating rates is constant, the normalized heat capacity curves shift to higher temperatures with increasing heating rate but do not change shape. Deviations from this prediction are attributed to thermal transfer effects. After corrections for these effects have been applied, x is obtained from a second theoretical result, that a unique function, $F(x)$, describes the shift in peak temperature, T_p, with respect to Q_c, Q_h, T_a, and the enthalpy lost during annealing [90,162,165–167]:

$$F(x) = -\frac{\theta\,\partial T_p}{\partial \ln|Q_c|} = \frac{\theta\,\partial T_p}{\partial \ln Q_h} - 1 = \Delta C_p \frac{\partial T_p}{\partial \bar{\delta}}, \tag{168}$$

$$\partial T_p / \partial T_a = 0, \tag{169}$$

where $\bar{\delta}$ (Eq. (30)) is the enthalpy lost during annealing between times t_1) and t_2:

$$\bar{\delta} = \frac{\Delta H_a}{\Delta C_p} = H(t_1) - H(t_2). \tag{170}$$

The partial derivatives are by definition evaluated by holding all other variables constant, and this can be done with experimental ease only for the derivatives with respect to $\bar{\delta}$ and Q_h, or with respect to Q_c if no annealing occurs between cooling and reheating. The Q_h derivative is subject to all the disadvantages associated with heating rate methods (see above), but the derivative with respect to Q_c can be obtained from the same experiments needed to determine Δh^* or θ (Eq. (161)). The derivative with respect to $\bar{\delta}$ has only the minor disadvantage, shared by most of the methods described here, that time-consuming long anneals are needed to ensure (a) the shift in T_p is large enough for an accurate determination of the derivative, and (b) the peak is due to annealing. Under these conditions, the peak heights can be very large, and corrections for thermal transfer become important. Analysis of the published plot of $F(x)$ [91] reveals that it can be approximated as

$$F(x) = K((1/x) - 1). \tag{171}$$

The value of K is a weak function of the distribution of retardation times, decreasing from 0.87 for an exponential decay to 0.75 for a stretched exponential with $\beta = 0.456$. Most values of β exceed 0.46 (Table 1), so the approximation that $F(x)$ is independent of $g(\ln \tau)$ is a good one. Moreover, the variation that does occur does so in a region where $F(x)$ changes rapidly with x, so that estimates of x are insensitive to uncertainties in $F(x)$. An approximate mathematical analysis predicts $K \approx 1$ [91,168]. Hutchinson and Ruddy [91,163] applied this method to polystyrene, and obtained a value of 0.48 for x that is in excellent agreement with values obtained by other researchers, mostly by curve fitting (Section 4.5.).

4.4.4.3. Temperature step method. This method was proposed by Lagasse et al. [169] for the analysis of volume recovery data. It has not yet been applied to experimental volume or enthalpy relaxation data, and has been criticized by Hutchinson and Kovacs [170], but is included here for the sake of completeness. The method was originally described in terms of the KAHR phenomenology, which we augment here with the equivalent TN expressions. The method uses two temperature steps of different magnitudes but same sign, $T_1 \rightarrow T_2$ at $t = 0$ and $T_2 \rightarrow T_3$ at $t = t_a$ ($T_1 > T_2 > T_3$), and extracts x from the limiting ratios

$$\left(\frac{T_f(t_a) - T_3}{T_f(t_a) - T_2}\right)_{t_a \rightarrow 0} \text{ and } \left(\frac{\tau(T_2)}{\tau(T_3)}\right)_{t_a \rightarrow 0},$$

for different magnitudes of the second jump at t_a. The ratio of the relaxation times is given by

$$\left(\frac{\tau(T_2)}{\tau(T_3)}\right)_{t_a \rightarrow 0} = \exp(-x\theta\,\Delta T_2) = \exp\left(\left(\frac{x\,\Delta h^*}{R}\right)\left(\frac{1}{T_2} - \frac{1}{T_3}\right)\right). \tag{172}$$

4.4.4.4. Heating rate dependence of T_g. This method [171,172] has been criticized by Crichton and Moynihan [173], Hutchinson and Ruddy [174] and Hutchinson [175], but is included here to illustrate some of the pitfalls in analyzing non-exponential and non-linear enthalpy relaxations. The principal criticism is that the method does not properly account for the memory effect associated with non-exponentiality. The method centers around an equation derived from the simplification that T_f remains unchanged during scanning until $T \approx T_g \approx T_f'$ is reached, but this approximation is valid only for unannealed glasses formed at very slow cooling rates that are difficult or impractical to achieve. Using calculated dT_f/dT data, Crichton and Moynihan [173] obtained values of x using this method that differed greatly from the input values. For ($\Delta h^*/R = 5 \times 10^4$ K, $\beta = x = 0.5$), values of x evaluated by this method ranged between 0.63 and 0.97, depending on history. If T_g was defined as the inflection point of the heat capacity rise, slow cooled and annealed glasses produced values for x of 0.63–

0.65, consistent with each other but again different from the input value. Crichton and Moynihan observed that these estimated values of x would seem very reasonable to someone who did not know the correct input values. Hutchinson and Ruddy [174] showed that this method, using slow cooling rates, was equivalent to their peak shift method [91] using annealing (Section 4.4.4.2.). Both methods depend on the glass being close to equilibrium ($T_f \approx T_a$), but Hutchinson and Ruddy noted that this condition is difficult to achieve without annealing. This objection is consistent with the criticism of Crichton and Moynihan, because glasses that are close to equilibrium have almost erased the effects of their thermal history and therefore do not exhibit strong memory effects.

4.4.4.5. Adam–Gibbs T_2. Good estimates of T_2 can be made if T_g and the NM parameters are known, using Eqs. (113) and (116). The accuracy of these equations has been demonstrated by several researchers [86,113,130,133,154,157]. Values of T_2 can also be obtained by the curve fitting methods described next.

4.5. Curve fitting techniques

Enthalpy relaxation parameters can be obtained from experimental heat capacity data using computer assisted visual fitting [160], or nonlinear regression optimization methods [86,161]. The simplest technique is to compare experimental and calculated heat capacity curves with trial and error changes in parameters. This method was used in the early work of the Moynihan school and produced estimated uncertainties in x and β of ± 0.05. In the past few years it has become increasingly common to use the multidimensional Marquardt [176] optimization algorithm, first applied to enthalpy relaxation by Hodge and Huvard [177]. This optimization technique changes continuously from the method of steepest descents when the fit is far from optimum, to the Newton–Raphson method when the optimum is approached. A user-specified objective function, Φ, is minimized in a multiparameter search space that is bounded by user-specified parameter limits. A FORTRAN algorithm has been published [178]. To date, Φ has always been specified by the residual sum of squared differences between experimentally observed and calculated normalized heat capacities:

$$\Phi = \sum_{i=1}^{n} \left(C_{p;i}^{N}(obs) - C_{p;i}^{N}(calc) \right)^2. \tag{173}$$

This objective function places most weight on the largest values of C_p^N that occur in the overshoot region, which is not entirely satisfactory because thermal transfer problems are most significant for high overshoot heat capacity data. A better expression for Φ that would not introduce other problems, for example sensitivity to the choice of $C_{pg}(T)$ for small values of C_p^N, is not evident, although defining Φ as the logarithm of the sum of squared residuals is an interesting possibility (set to zero for sums less than unity, so that an appropriate scaling factor would be needed). Sales [86] applied an optimization algorithm due to Bevington [179]. The Marquardt and Bevington algorithms are hard-pressed to optimize all four parameters of the standard TN formalism, because the parameters are strongly correlated [130,161]. Reliable and history invariant values of β can usually be obtained from four parameter optimizations, but the parameters x and Δh^* often vary with thermal history. A better procedure is to use a three-parameter optimization by fixing one of the parameters, preferably Δh^* obtained from Eq. (161). When Δh^* is fixed, the value of $\ln A$ is tightly constrained because variations in it shift the heat capacity curve along the temperature axis, and even small shifts produce large changes in Φ because of the steepness of the heat capacity curves near T_g. In addition, $\ln A$ and Δh^* together determine T_f', which should be matched to the experimental value to ensure consistency. The parameter search space is then two-dimensional, and x and β can be obtained quickly. If desired, the fourth parameter can be estimated from the minimum in Φ, although this is often quite broad, and its position can shift with thermal history. In these cases, it is commonly found that β is fairly constant across the minimum, but that x changes systematically

with Δh^* to produce values of $x\,\Delta h^*$ that are almost constant.

Hodge and Huvard [177] found that the best fit value of Δh^* for PS, obtained from the minimum in Φ, was the same as that found from the cooling rate dependence of T_f'. Hodge [161] also observed consistent values obtained by the two methods. Others have reported that values of Δh^* obtained by curve fitting are less than those determined from Eq. (161). Substantially smaller values were reported by Prest et al. [153] for PS. They found that Δh^* obtained by several methods of analysis of the cooling rate and heating rate dependences of T_f' were self-consistent, but were about a factor of 2 larger than those found by curve fitting. The only significant difference between the data sets of Hodge and Huvard and of Prest et al. is the ratio of heat to coding rates (0.25 and 1, respectively), so it seems that thermal transfer effects may be significant.

Adam–Gibbs parameters can also be obtained using Marquardt or similar optimizations [86,113,130,133,154,157] but, as with the NM equation, four parameter optimizations are not practical. For three parameter optimizations, it is not clear whether Q or T_2 should be fixed, because both Q and T_2 determine x and Δh^*_{eff}. Hodge [130] reported that three-parameter Marquardt optimizations performed by fixing T_2 were less dependent on starting estimates of the parameters, and less likely to become caught in local minima, than optimizations in which Q was fixed. Sales [86] also fixed T_2 in his optimizations using the Bevington algorithm, and obtained a best fit T_2 from the minimum in Φ.

4.6. Thermal transfer effects and high overshoot data

The experimental sources for these effects were discussed in Section 2.1.3. They are most severe for the highest overshoot data, although as noted earlier Hutchinson and co-workers have raised questions about the validity of applying curve fitting methods to all experimental data. These investigators found that heat transfer effects shift T_{max} to higher temperatures for heating rates greater than about 20 K min^{-1} (in addition to the well-recognized effect of heating rate on temperature calibration), and calculations by the present writer using Eqs. (57)–(60) confirm this shift [111]. Thermal transfer effects were also recognized by Hodge [130,161], who averaged parameters from low overshoot data obtained at 10 K min^{-1}, and assessed predictions of long aging time behavior by comparing experimental and calculated values of T_f'. O'Reilly and Hodge [89] observed that x and β for PS varied strongly with thermal history, and that these variations occurred using a heating rate (1.25 K min^{-1}, with signal averaging) at which heat transfer effects were negligible. They concluded that the phenomenology was deficient, and suggested that the methods for describing non-linearity were incorrect. Moynihan et al. [113] also concluded that the treatment of non-linearity is imperfect (see Section 7).

High overshoot data also provide challenges to the approximations inherent in numerical integrations, and other simplificaions. These include the following.

(1) Selection of a suitably small time subinterval during long anneals. In some cases 0.2 decades is too long (Section 4.2.).

(2) Temperature steps used for Boltzmann summations must be sufficiently small. The need for small temperature steps is especially important in the overshoot region (see Eq. (146), for example) but, in some circumstances, temperature steps of 1 K can also be too large during cooling, or heating below the main transition temperature range.

(3) The approximate equivalence between dT_f/dT and C_p^N may break down. However, it is unlikely that any difference is more than a few percent (Section 1.2.3.).

The relative importance of experimental and computational difficulties in handling high overshoot data is not known with any confidence. Thermal transfer effects may be smaller for inorganics than for polymers, because their glass transitions occur over a wider temperature range [113] and their thermal conductivities are higher. However, there is increasing agreement that the thermal history dependence of model parameters is due to a real deficiency in the current phenomenologies, rather than thermal transfer ef-

fects. Nevertheless, a better quantitative assessment of thermal transfer effects is desirable before the accuracy of alternative phenomenologies can be properly assessed.

4.7. Non-thermal histories

4.7.1. Hydrostatic pressure

Hodge and Berens [180] used a simplified method for introducing hydrostatic pressure, P, that was adequate for their purposes but is not rigorous enough to be regarded as a general method. They noted that P lengthens the enthalpic retardation time, and suggested three ways for introducing this. The logarithm of the pre-exponential factor, $\ln A$, or the NM activation energy, Δh^*, can be increased in direct proportion to P, or a shift in T_f can be used. In the last case, the equilibrium condition is redefined as $T_f = (T - K)P$, where K is a positive constant, so that the usual equilibrium condition $T_f = T$ only holds for $P = 0$. It was assumed that the non-linearity parameter, x, and the stretched exponential parameter, β, were independent of P. The shift in τ_0 with P was estimated from the enthalpic Ehrenfest relation, Eq. (49), repeated here in a modified form for convenience:

$$(\partial T_g/\partial P)_H = V_g T_g(\Delta\alpha/\Delta C_p), \tag{174}$$

where V_g is the volume at T_g. The constancy of H in Eq. (174) corresponds to fixed T_f, and in the approximation $T \approx T_f \approx T_g$ one has

$$\left(\frac{\partial T_g}{\partial P}\right)_H \approx \left(\frac{\partial T_g}{\partial P}\right)_{\ln\tau_0} = \frac{-(\partial \ln \tau_0/\partial P)_T}{(\partial \ln \tau_0/\partial T)_P}. \tag{175}$$

Partial differentiation of the NM equation under these conditions yields

$$\mathrm{d}\ln\tau_0|_{T_f} = \frac{-x\,\Delta h^*}{RT^2}\mathrm{d}T \approx \frac{x\,\Delta h^* V_g\,\Delta\alpha}{RT_g\,\Delta C_p}\,\mathrm{d}P. \tag{176}$$

The corresponding changes in $\ln A$, Δh^* and T_f are

$$\mathrm{d}\ln A \approx \frac{x\,\Delta h^* V_g\,\Delta\alpha}{RT_g\,\Delta C_p}\,\mathrm{d}P, \tag{177}$$

$$\mathrm{d}\,\Delta h^* \approx \frac{x\,\Delta h^* V_g\,\Delta\alpha}{\Delta C_p}\,\mathrm{d}P, \tag{178}$$

and

$$\mathrm{d}\,T_f \approx \left(\frac{-x}{1-x}\right)\frac{T_g V_g\,\Delta\alpha}{\Delta C_p}\,\mathrm{d}P. \tag{179}$$

For $T = T_a < T_f \approx T_g$, the right-hand sides of Eqs. (176)–(179) are multiplied by a factor of order $(T_g/T_a)^2$ [180], obtained by replacing T^2 with T_a^2 in Eq. (176) and retaining T_g in Eq. (174). None of these equations are readily generalized to arbitrary temperature and pressure histories, although pressure scans at constant temperature could presumably be approximated by ramping $\ln A$.

Ramos et al. [181] adopted a more rigorous method for introducing pressure into the KAHR formalism. They wrote

$$\begin{aligned}\mathrm{d}\delta = &-\delta\,\Delta\alpha\,\mathrm{d}T + \delta\,\Delta\kappa\,\mathrm{d}P \\ &+ \sum_{i=1}^{N}\left(\frac{\partial\delta}{\partial\xi_i}\right)_{T,P;\xi_j\neq i}\mathrm{d}\xi_i \\ &- \sum_{i=1}^{N}\Delta\alpha_i\,\mathrm{d}T + \sum_{i=1}^{N}\Delta\kappa_i\,\mathrm{d}P,\end{aligned} \tag{180}$$

where ξ is an order parameter, and then neglected the first two terms for small δ. The time dependence of the components δ_i is given by

$$\frac{\mathrm{d}\delta_i}{\mathrm{d}t} = -\Delta\alpha_i\frac{\mathrm{d}T}{\mathrm{d}t} + \Delta\kappa_i\frac{\mathrm{d}P}{\mathrm{d}t} + \frac{\delta_i}{\tau_i} \quad (1 \le i \le N), \tag{181}$$

where the exponential decay of each δ_i has been introduced. For changes in both T and P, the shift factor, a_δ, is given by

$$a_\delta = \exp\left(-1(1-x)\theta_T\frac{\delta}{\Delta\alpha} + (1-x)\theta_P\frac{\delta}{\Delta\kappa\,(P)}\right), \tag{182}$$

$$\theta_P = \left(b\kappa_f/f_g^2\right)P, \tag{183}$$

where b is a constant and κ_f is the pressure coefficient of the free volume $f_{T,P}$. Gupta [80] introduced pressure into structural relaxation phenomenology by considering a fictive pressure in addition to the fictive temperature.

4.7.2. Mechanical stress and vapor induced swelling

The only attempt to introduce these perturbations into enthalpy relaxation phenomenology was made by Hodge and Berens [180]. They considered annealing of poly(vinyl chloride) (PVC) that had been exposed to mechanical stress (near or above the yield stress), or to swelling induced by solvent vapor absorption followed by rapid desorption. Annealing took place after the release of these non-thermal perturbations. It was assumed that the treatments increased T_f instantaneously (a reasonable assumption given the rapid application and release of stress or solvent vapor), by an amount ΔT_f that decayed with reduced time during subsequent annealing and reheating. This decay was assumed to be described by the same relaxation parameters as the thermal history, and was superimposed on the response to the purely thermal history. Good agreement with experimental data was obtained using values of ΔT_f that increased linearly with the applied perturbation (stress or solvent vapor pressure). In particular, the calculations reproduced the experimental result that only the sub-T_g endotherm peak heights, and not the peak temperatures, were affected by the applied perturbations.

5. Experimental results

In this section, we restrict our attention to qualitative experimental results, and defer a discussion of relaxation parameters to Section 6.

5.1. Scanning calorimetry

5.1.1. Enthalpy recovery near T_g

Simple cooling and reheating histories produce heat capacity curves during heating that exhibit an increase in C_p over the glass transition range, followed by a maximum and a decrease to the equilibrium liquid or rubber value. Exceptions to this are seen in glasses with high values of T_f' produced by very fast cooling rates, such as in splat quenching, vapor deposition or quenching of fine fibers. Slow scans of these glasses exhibit exothermic dips in the heat capacity just before the increase in C_p at T_g. These exotherms occur because the relatively high value of T_f' produced by a fast quench greatly shortens the average retardation time, and during the slow reheat T_f has time to relax towards the equilibrium state defined by $T_f = T$ from values $T_f > T$. This relaxation produces negative values of dT_f/dT and an exothermic excursion below the glassy heat capacity. The phenomenon is illustrated in Fig. 1(B). The exotherm can be suppressed by decreasing the high initial values of T_f' by annealing below T_g. For the more common simple overshoot, the equilibrium condition $T_f = T$ is reached before any relaxation can occur, and dT_f/dT remains positive as T_f approaches the equilibrium state $T_f = T$ line from values $T_f < T$ (Fig. 1(A)).

5.1.2. Isothermal annealing

Enthalpy lost during annealing is usually (but not always) recovered near T_g during reheating, producing the familiar high overshoot in annealed glasses. Pioneering studies of this phenomenon were made by Volkenstein and Sharonov [182], Foltz and McKinney [183] and Petrie [184], all of whom demonstrated that the magnitude of the overshoot was a quantitative measure of the enthalpy relaxation that had occurred during annealing. Other quantitative studies were reported by Straff and Uhlmann [185], O'Reilly [186], Ali and Sheldon [187] and Ophir et al. [188]. The number of papers containing qualitative statements about annealing peaks near T_g, either as the primary area of study or as part of a larger investigation, is immense, and no useful purpose would be served by citing them all. Every study of which this writer is aware reveals that enthalpy recovery near T_g responds to changes in annealing conditions the same as enthalpy recovery in the glassy state, discussed in the next section. Thus, we discuss here only those studies of enthalpy recovery near T_g that are of special interest or novelty, or illustrate the variety of materials studied. The selection is inevitably subjective.

Ten Brinke and co-workers [189,190] applied results from enthalpy relaxation phenomenology to blends of PVC/poly(isopropyl methacrylate) (PVC/P(iPr)MA), PVC/poly(methyl methacrylate) (PVC/PMMA), and PS/poly(2-vinyl pyri-

dine) (PS/PVP), and showed that the miscibility or immiscibility of components with closely similar T_g could be established if appropriate annealing histories were used. For the PS/PVP blends [190], for which the T_g of the PS and PVP used were 106 and 100°C, respectively, annealing at 91°C for longer than 6 h produced two heat capacity maxima that became increasingly better resolved as annealing times increased to a month or so, demonstrating that PS and PVP are immiscible. The better resolution at longer annealing times occurred because PVP reached its equilibrium state after only relatively short annealing times at 9°C below its T_g, producing an annealing peak that did not shift with further annealing, whereas the annealing peak for PS continued to move to higher temperatures, even after long annealing times at 15°C below its T_g. For the PVC blends [189], a separate PVC phase could easily be identified because annealing of PVC produced sub-T_g peaks that were easily distinguished from the more usual overshoots for PMMA and P(iPr)MA. Quan et al. [191] used enthalpy relaxation to experimentally characterize the interfacial regions of a styrene-hydrogenated butadiene–styrene triblock copolymer. Ten Brinke [192] showed that Quan's results could be reproduced by the TN formalism, but noted some complications associated with estimating the amount of interfacial material. Cowie and Ferguson [57] investigated annealing in blends of PS and poly(vinyl methyl ether) (PVME). They observed heat capacity maxima in the middle of the glass transition, and reported that the PVME component annealed independently of the PS component. Mijovic and co-workers [193,194] investigated blends of PMMA and SAN (styrene-co-acrylonitrile). The annealing rates for SAN-rich blends were slightly faster for anneals 20 and 35°C below T_g, but at 50°C below T_g the rates were independent of composition. The response to different annealing temperatures also changed with blend composition. Gomez-Ribelles et al. [55] studied enthalpy relaxation in PVC plasticized with dioctyl phthalate (DOP). They reported that only some of the polymer was plasticized (i.e., showed a decrease in T_g with increasing DOP content), with the remainder showing a concentration-independent T_g (albeit very weakly, with $\Delta C_p(T_g) \approx 0.01$ J g^{-1}). Their plots also exhibited the extremely broad melting endotherms just above T_g associated with the crystallinity of this material [195]. The breadth of the melting endotherm is due to the extremely small average size, but not unusual size distribution, of crystallites that are subject to large surface contributions to the crystal free energy. (The small amount of crystallinity is responsible for the toughness of PVC, and crystallinity is not reduced by plasticization of the predominant amorphous phase.)

Johari and Mayer and co-workers [196–198] annealed vapor-deposited water and hyperquenched aqueous solutions just below their T_g to remove the large exotherm resulting from the high initial T_f'. This enabled the observation of glass transitions in the presence of large ice crystallization exotherms just above T_g. Gupta and Huang [199] investigated enthalpy relaxation and recovery in slowly cooled bulk samples and rapidly cooled fibers (8–12 μm diameter) of a soda–lime–silicate glass. They observed the usual exotherm below T_g for the rapidly quenched and slowly reheated fibers, but were unable to fit the TN model to these histories. Warner [200] observed enthalpy relaxation in some thermotropic anthraquinone polymers, and Hedmark et al. [201] reported annealing endotherms in a liquid crystalline polyester copolymer. Petrie [202] reported enthalpy relaxation effects in non-polymeric mesogens. These observations are consistent with other parallels between the glass transition and thermotropic transitions in liquid crystals [20]. Stephens [203] described annealing endotherms in amorphous Se as a function of annealing time and temperature. The enthalpy loss on annealing increased linearly with log t_a, in the usual manner (see next section), and a plot of data taken from the published figure exhibits the usual approximately linear increase with T_a (also see next section). Ma et al. [204] observed annealing endotherms and shifts in T_g with annealing time, in a series of chalcogenide glasses containing Te as a common component. Changes in T_g, the breadth of the glass transition and in annealing behavior were observed as a function of average coordination number (defined by composition). Tatsumi-

sago et al. [205] observed a minimum in the enthalpic activation energy as a function of average coordination number in a series of Ge–As–Se glasses. Koebrugge et al. [206] observed annealing endotherms in a metallic glass of composition $Pd_{40}Ni_{40}P_{20}$, that increased in magnitude with annealing time. Sommer et al. [207] studied the enthalpy lost during annealing of amorphous alloys of composition $Cu_{67}Ti_{33}$, $Cu_{50}Ti_{50}$, $Cu_{34}Ti_{66}$, $Ni_{33}Zr_{67}$ and $Pd_{26}Zr_{74}$ as a function of annealing time. The lost enthalpy increased linearly with log t_a at short annealing times and reached constant values at long times, consistent with the annealed glasses reaching the equilibrium state at long times.

5.1.3. Sub-T_g endotherms

5.1.3.1. Thermal histories. The occurrence of heat capacity peaks well below T_g, defined for present purposes as the midpoint of the glass transition for unannealed glasses (Fig. 1(A)), was first reported (for PVC) by Illers in 1969 [208]. Gray and Gilbert [209] also observed sub-T_g heat capacity peaks in annealed PVC. Chen and Wang [210] reported a well-developed shoulder just below T_g in PS annealed for 260 h at 320 K (50 K below T_g). Hutchinson and Ruddy [166] observed sub-T_g peaks in PS, as did Ruddy and Hutchinson [211] in rapidly quenched PS that had been annealed at 333 K for more than about 48 h. Wysgoski [212] observed sub-T_g endotherms in annealed ABS (acrylonitrile–butadiene–styrene) and SAN (styrene–acrylonitrile) copolymers, and found that they became more intense and moved to higher temperatures with increased annealing temperature, until at $T_a \approx T_g - 20$ K the endotherms merged with the familiar T_g overshoot. Berens and Hodge [213] observed similar behavior in rapidly quenched and annealed PVC, and reported an increase in both peak height and peak temperature with increasing annealing time. Qualitatively similar, but smaller, sub-T_g peaks have been observed in B_2O_3 [214], and sub-T_g shoulders have also been reported in zirconium fluoride based glasses [112,164]. Hodge [130,161] observed a well-developed sub-T_g heat capacity peak and a shoulder just below T_g for two annealing histories in atactic PMMA, as did Ribelles and co-workers [215,216]. Ribas [217] observed sub-T_g peaks in epoxy resins. Hofer et al. [218] observed sub-T_g peaks in annealed hydrogel glasses of aqueous lithium chloride and ethylene glycol solutions imbibed in poly(2-hydroxy-ethyl methyacrylate). The bulk solutions exhibited the more common overshoots in the glass transition range. Senapati and Angeli [219] observed sub-T_g endotherms in mixed anion glasses in the system $60AgI–(40 - y)Ag_2SO_4–yAg_2WO_4$ for y values near 20, after annealing well below T_g. For y values near 0 and 40, annealing produced overshoots above T_g. McGowan et al. [220] observed sub-T_g peaks in some main-chain nematic polymers. Altounian et al. [221] observed endothermic peaks in annealed Fe–B metallic glasses, and Chen [222] observed annealing induced sub-T_g shoulders in an amorphous metal alloy (composition $Pd_{48}Ni_{32}P_{20}$). Sub-T_g endothermic peaks with exothermic minima between them and the glass transition have been observed in several metallic glasses. The exotherm results from the non-equilibrium glass approaching the equilibrium $T_f = T$ line from above, commonly observed in rapidly quenched glasses heated at relatively slow heating rates (Fig. 1(B) and Section 5.1.1.). The annealing endotherm is superimposed on, and thus attenuated by, this exotherm. Representative examples of these effects have been reported in a series of papers by Inoue, Chen and Masumoto for $(Pd_{0.86}Ni_{0.14})_{83.5}Si_{16.5}$ [223], a series of $(Fe, Co, Ni)_{75}Si_{10}B_{15}$ alloys [224], several Zr–Cu–Fe and Zr–Cu–Ni compositions [225] and in $(Fe_{0.5}Ni_{0.5})_{83}P_{17}$ and $(Fe_{0.5}Ni_{0.5})_{83}B_{17}$ [226].

These observations testify to the occurrence of sub-T_g endotherms in a wide variety of glasses. Such behavior was first explained in terms of enthalpy relaxation and recovery by Kovacs et al. [47]. Quantitative fits of the TN phenomenology to experimental data were first given by Hodge and Berens [152], who found that the endotherms were most easily produced in materials with the most extreme non-exponentiality (broadest distribution of retardation times). These authors, as well as others [48], suggested that the phenomenon was a manifestation of the memory effect. Sufficient data have been published to

establish some clear experimental trends [130,161].

(1) The sub-T_g peak temperature, T_{max}, the decrease in T_f during annealing, ΔT_f, and the peak height, C_{pmax}^N, all increase approximately linearly with log t_a (at constant T_a and short t_a). At long t_a, these quantities approach limiting values as the annealed glass approaches the equilibrium state, and the sub-T_g peaks evolve into overshoots.

(2) The quantities T_{max}, ΔT_f and C_{pmax}^N increase linearly with T_a at constant t_a when $T_a \ll T_g$. At $T_a \approx T_g - 20$ K, ΔT_f and C_{pmax}^N pass through a maximum. These maxima occur because at higher T_a the annealed glasses reach the equilibrium state ($T_f = T_a$) and the difference between T_f' and T_a decreases to zero as T_a approaches T_g.

(3) Faster cooling rates before annealing increase C_{pmax}^N but have little effect on T_{max}. Non-thermal perturbations applied and released before annealing produce similar behavior (see next section).

Sub-T_g endotherms are superimposed on the glass transition heat capacity 'background', observed at the same cooling and heating rates but without intervening annealing. This superposition is clearly seen in published heat capacity curves, such as those for PS [210], zirconium fluoride-based glasses [112,164], and PVC [213,227]. It is also evident in calculated curves [32,152]. This phenomenon is surprising at first glance, since it might be expected that the non-linear kinetics would couple the glass transition to changes in T_f induced by annealing. The apparent absence of coupling can be rationalized by noting that the effective reduced times for the annealing and glass transition processes are different. The glass transition and sub-T_g peaks are Boltzmann superimposed responses to two separate perturbations: cooling through the glass transition, and annealing. The long average retardation times associated with low annealing temperatures produce short reduced times, and these promote sub-T_g peaks. In these circumstances, only the shorter retardation time components of the distribution relax and partial recovery occurs in the glassy state. Thus, materials with more non-exponential decay functions, corresponding to broader distributions with a greater proportion of very short retardation time components, show an increased tendency to produce sub-T_g endotherms. At longer reduced times, produced by longer anneals and/or by higher annealing temperatures and shorter average retardation times, the reduced timescale for annealing lengthens and approaches the characteristically long reduced times associated with the glass transition. In these circumstances, the sub-T_g annealing peak merges with the glass transition and the glass transition begins to be affected by annealing, as noted by Hutchinson and Ruddy [91], for example. At still longer reduced annealing times, enthalpy recovery is manifested as the familiar high overshoot above T_g.

The reproduction of sub-T_g endotherms and their behavior with respect to annealing conditions by the KAHR and TN phenomenologies indicates that these endotherms are indeed a manifestation of enthalpy relaxation and recovery, and are not due to changes in crystallinity or the development of qualitatively different molecular structures. Nor are they the result of secondary relaxations that are somehow manifested as heat capacity anomalies by annealing, since the endotherms can be calculated assuming unimodal distributions.

5.1.3.2. Non-thermal histories. Sub-T_g endotherms also occur in polymeric glasses that have experienced hydrostatic pressure perturbations, undergone mechanical deformation, or been exposed to solvent or vapor treatments. Weitz and Wunderlich [228] observed sub-T_g peaks in PS and PMMA samples that had been cooled under pressure to form densified glasses, and reheated under atmospheric pressure. At low pressures, a simple reduction in overshoot was observed, with the sub-T_g peaks appearing only at pressures above 200 MPa. At the highest pressures (345 MPa) a broad exotherm developed between the sub-T_g peak and T_g. Although annealing was not intentionally introduced in these experiments, the samples were stored in a freezer for a day or more between cooling and heating, or were at or near room temperature for at least the time required to transfer samples from the pressure vessel to the

calorimeter. Modeling calculations suggest [32] that unusually high fictive temperatures can be attained following pressure release, and that significant relaxation can occur in a few minutes at room temperature, so it seems reasonable to speculate that some annealing could have occurred during sample transfer. The exotherms observed for the highest pressure-densified glasses are characteristic of rapidly cooled and slowly reheated glasses, and are also consistent with a high fictive temperature being generated by release of the high pressures applied during cooling. These data are qualitatively similar to those found in splat quenched and annealed metals, discussed earlier. Non-polymeric materials (phenolphthalein, sucrose, $KNO_3/Ca(NO_3)_2$) exhibited only a decrease in overshoot with increasing pressure, presumably because of the less non-exponential decay functions (narrower distributions) for these materials. Similar results to those observed by Weitz and Wunderlich for PS and PMMA were reported for PS by Richardson and Savill [227], Yourtee and Cooper [229], Dale and Rogers [230] and Brown et al. [231], and for PMMA by Kimmel and Uhlmann [232] and Price [233]. Wetton and Moneypenny [234] observed sub-T_g peaks in pressure-densified PVC, PMMA, PS, poly(4-methoxystyrene), poly(3-chlorostyrene) and poly(4-chlorostyrene). Prest and co-workers [235,236] reported sub-T_g endotherms in pressure-densified PVC, and observed that they became more asymmetric and moved to slightly lower temperatures with increasing pressure. Hutchinson et al. [237] observed a sub-T_g endotherm in an annealed sample of a pressure-densified silver iodomolybdate glass.

Sub-T_g endotherms have also been observed in polymers subjected to various mechanical stresses. Prest and Roberts [235] reported them in mechanically compacted PS, and Berens and Hodge [238] observed them in PVC samples that had been cold drawn to near or beyond the yield stress, or subjected to simple powder compaction (thought to generate localized shear stresses between the powder particles that exceeded the yield stress). Brady and Jabarin [239] observed sub-T_g endotherms in tensile drawn PVC. Vapor- or solvent-induced swelling stresses have also been reported to accelerate the development of sub-T_g endotherms in polymers. Shultz and Young [240] reported such an effect for freeze-dried PS and PMMA, and Berens and Hodge [213] observed that vapor-induced swelling of PVC accelerated the development of sub-T_g peaks.

Very few data are available on the effects of non-thermal perturbations applied during annealing, but released before heating. Berens and Hodge [213,238] observed that vapor-induced swelling, pressure (approximately hydrostatic), and mechanical stress all decreased the rate of annealing in PVC when applied during annealing. Chan and Paul [241] found that exposure of BPAPC to high CO_2 pressure during annealing reduced the magnitude of the annealing endotherm.

The results obtained to date suggest that it is the release of the non-thermal perturbations before annealing, rather than the perturbations per se, that increases T_f' [32]. An increase in enthalpy following pressure release is known to occur in pressure-densified PS [242], and could well be a general phenomenon. The reduction in annealing endotherms by some form of stress applied after annealing has sometimes been referred to as 'rejuvenation', and it seems likely that this rejuvenation is caused by the increase in T_f induced by the application and release of stress compensating for the decrease in T_f during annealing. It appears that the application and release of non-thermal perturbations, particularly when applied to polymers, can elevate T_f' to higher values than those achievable by rapid thermal quenches. Thus, the tendency of many materials to produce sub-T_g endotherms after long anneals well below T_g may simply be accelerated by the application and release of non-thermal stresses, and that non-thermal histories do not produce any qualitatively new effects. Modeling results [32] support this hypothesis.

6. Enthalpy relaxation parameters

Opalka [112] and Moynihan et al. [113] determined the best functional forms for $\phi(t)$ and $\tau(T, T_f)$ for several inorganic glasses, including

B_2O_3 and a series of ZBLA [243] fluoride glasses. They compared the stretched exponential and a truncated stretched exponential form for $\phi(t)$, and the Davidson–Cole, log Gaussian, box and wedge distributions. For $\tau(T, T_f)$ they compared NM, AGL and AGF. The stretched exponential and AGF gave the best overall fits to heat capacity data. When the fits were within or close to probable experimental uncertainty, the NM, AGL and AGF forms for $\tau(T, T_f)$ were indistinguishable when combined with the stretched exponential form for $\phi(t)$. When the best fits were well outside experimental uncertainty, the AGL and AGF forms for $\tau(T, T_f)$ gave better fits than NM. Here, we discuss the KAHR, NM and AG phenomenologies for non-linearity. For almost all parameterizations the non-linear stretched exponential decay function has been used.

6.1. KAHR equation

The activation energy, θ, and non-linearity parameter, x, have been determined for PS by Hutchinson and Ruddy [91]. For a monodisperse sample with $M_n = 30.1 \times 10^3$, they found $\theta = 0.52$ K^{-1} (corresponding to $\Delta h^*/R = 70$ kK) and $x = 0.48$. These x and Δh^* values agree within typical experimental uncertainties (about $\pm 10\%$ in Δh^* and ± 0.05 in x) with those obtained by others using the NM equation and TN formalism (see below). Prest et al. [153] also obtained KAHR parameters for PS, and found $\theta = 0.47$ K^{-1} using curve fitting, and $\theta = 1.0$ K^{-1} from the cooling rate dependence of T_f'. As discussed in section 4.5., the reason for the large discrepancy is not known, but we note here that the curve fitting value is close to the average value obtained by other groups. Hutchinson et al. [244] determined θ and x for three glasses in the AgI–$AgPO_3$–Ag_2MoO_4 system. The average value of x was 0.68, and θ increased with AgI content from 0.21 K^{-1} for 0% AgI, to 0.31 K^{-1} for 50% AgI. Ingram, et al. [245] reported values of θ, Δh^* and x for three AgI/Ag_2MoO_4 glasses. By contrast with the phosphate containing glasses, the values of θ and Δh^* decreased, and x increased, with increasing AgI content.

6.2. Narayanaswamy–Moynihan equation

Simple thermal histories involving only cooling and reheating were the first to be parameterized, and a large number of results have been published. Many types of material have been studied, with most classes being represented. A compilation of all published (and some previously unpublished) NM parameters, averaged over histories that include only rate cooled and heated glasses with small or no amounts of annealing, is given in Table 1 (on p. 213). Examples of how well the TN phenomenology fits experimental data for B_2O_2 and 5P4E are shown in Fig. 3.

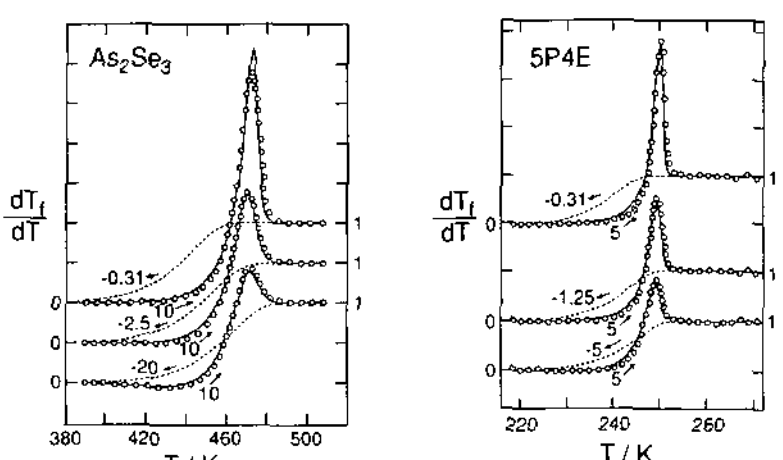

Fig. 3. Fits of TN formalism to experimental data for As_2Se_3 and 5P4E, using Eqs. (143) and (144). From Ref. [42].

Parameters for PS obtained by different groups are in good agreement for low molecular weight monodisperse samples ($M_n \leq 40 \times 10^3$), and polydisperse samples with $M_n \sim 85 \times 10^3$. Averages are $\Delta h^*/R = 78 \pm 7$ kK, $x = 0.48 \pm 0.06$ and $\beta = 0.67 \pm 0.08$. The stated uncertainties are standard deviations for the eight or nine histories for which only modest departures from equilibrium were generated. The spreads in values for $\Delta h^*/R$ and x are comparable with typical individual experimental uncertainties, but the variability in β is somewhat larger. Values of $\Delta h^*/R$ lying outside the range cited above were reported by Privalko et al. [246] for higher molecular weights (101 and 110 kK for $M_n = 110 \times 10^3$ and 233×10^3, respectively). The value of $\Delta h^*/R$ reported by Stevens and Richardson [247] for a monodisperse sample of $M_n = 36 \times 10^3$ is higher still (125 kK), but this result was heavily weighted by a single datum at a very slow cooling rate obtained outside the DSC. Although there is no apparent reason for questioning this datum, the remaining data lie within the DSC cooling rate range of the other experiments and are consistent with $\Delta h^*/R = 80$ kK. An increase in $\Delta h^*/R$ with increasing M_n for monodisperse samples was observed by Privalko et al. [246] and Aras and Richardson [248], but the absolute values observed by the two groups differ, particularly at lower molecular weights. The differences are illustrated by the parameters of the equation used by Aras and Richardson to fit their data:

$$\Delta h^*/R = A - (B/M_n). \tag{184}$$

For 29 M_n values ranging between 5.16×10^2 and 1.5×10^7, Aras and Richardson obtained $A = 131$ kK and $B = 1.05 \times 10^8$. Fitting the Privalko data ($M_n = 9 - 233 \times 10^3$) to the same equation yields $A = 106$ kK and $B = 2.88 \times 10^8$. For $M_n = 10^6$, these two sets of parameters give $\Delta h^*/R = 130$ kK and 106 kK, respectively, almost the same with experimental uncertainty. For $M_n = 10^4$, on the other hand, the values are 121 kK and 77 kK, a difference of 60% that is well outside experimental uncertainty. If the highest M_n data of Privalko and lowest M_n data of Aras and Richardson are discarded, leaving M_n values in the overlapping range ($1–17 \times 10^3$), the average value of $\Delta h^*/R$ is 79 ± 11 kK. With the high and low M_n values included, $\Delta h^*/R = 83 \pm 20$ kK. Fictive temperature data tabulated by Wunderlich et al. [249] for PS yield a value for $\Delta h^*/R$ of 78 kK, in agreement with the averages just cited. Hodge and Huvard [177] and Hodge [130,161] found {$\Delta h^*/R = 80$ kK, $x = 0.43–0.49$, $\beta = 0.68–0.74$} for a polydisperse PS, and Hutchinson [96] reported {$\Delta h^*/R = 70$ kK, $x = 0.46$, $\beta = 0.46$} for a monodisperse sample. Prest et al. [153] reported parameters for a total of 17 thermal histories, the averages being $\Delta h^*/R = 81 \pm 14$ kK, $x = 0.62 \pm 0.09$ and $\beta = 0.81 \pm 0.16$. These last variabilities in $\Delta h^*/R$ and x are comparable with typical experimental uncertainties, but the spread in β values is substantially larger than the typical uncertainty of ± 0.05, principally because some of the reported values of β were greater than 1. These all occurred for the highest overshoots (where thermal transfer effects are greatest, and the departure from equilibrium largest), and if these histories are excluded the average becomes $\beta = 0.74 \pm 0.09$. The averages and variabilities for the other parameters, after exclusion of the histories for which $\beta \geq 1$, are $x = 0.58 \pm 0.07$ and $\Delta h^*/R = 66 \pm 8$ kK, both uncertainties being comparable with experimental uncertainty. No systematic trends with thermal history or overshoot ($C_{p\max}^N$) were observed. Tsitsilianis and Mylonas [60] observed that a star PS had similar parameters to linear PS, although their value of β was obtained from a linear decay function and is therefore unreliable (see discussion of the Scherer relations in Section 1.2.3.). The PS parameters obtained from an analysis [177] of the data of Chen and Wang [210] are inconsistent with the values cited above. The discrepancy could arise from the relatively low annealing temperature used in this study, although the $\Delta h^*/R$ parameter (175 kK) is still much larger than the next largest value reported by Stevens and Richardson [247] (125 kK). It is possible that larger values of $\Delta h^*/R$ result in some way from the low values of T_f' induced by long aging times [210] or very slow cools [247].

For PVAc, there is good agreement between the data of Sasabe and Moynihan [250] and Hodge

[130,161], which improves if the values of $\Delta h^*/R$ are forced to be equal [130] (the two reported values of 71 and 88 kK are statistically indistinguishable at about the 60% confidence level, for typical standard deviations of ±10%). For $\Delta h^* = 71$ kK, the differences of 0.06 in both β (0.57 and 0.51) and x (0.35 and 0.41) are close to experimental uncertainty, and can reasonably be attributed to sample differences (such as molecular weight distribution). The values of β are in good agreement with linear dielectric values, when these are extrapolated to the same temperature [250]. However, the activation energy at $T_g = 304$ K for enthalpy relaxation is higher than that for dielectric relaxation by a factor of 1.8.

There is also good agreement between the best fit parameters reported for a-PMMA by Hodge [130,161] and Ribelles et al. [215], when compared for similar thermal histories. The Ribelles group reported a thermal history dependence for their parameters, but their best fit values for one particular history agreed with the averaged set reported by Hodge, that was itself heavily weighted by a single thermal history that produced a similarly shaped sub-T_g heat capacity peak: Hodge reported {$\Delta h^*/R = 138$ kK, ln $A(s) = -355.7$, $x = 0.22$, $\beta = 0.37$}, and Ribelles et al. found {$\Delta h^*/R = 125 - 150$ kK, $x = 0.18 - 0.21$, $\beta = 0.33 - 0.35$}. Mijovic and co-workers [193,194] reported $\Delta h^*/R = 132$ kK, in agreement with Hodge and Ribelles et al. Ott [251] reported a lower value of $\Delta h^*/R = 60.6$ kK for a-PMMA. Tribone et al. [162] found $\Delta h^*/R = 106$ kK, $x = 0.15 - 0.40$ and $\beta = 0.35 - 0.45$ for a-PMMA. The difference between the $\Delta h^*/R$ values of Hodge/Ribelles et al. and Tribone et al. can reasonably be attributed to the different methods for determining it. Hodge reported that the parameter set found by him produced a value of $\Delta h^*/R$ very similar to that found by Tribone et al., if it was defined in the same way (from the heating rate dependence of T_g at fixed Q_c). Avramov et al. [252] reported that the activation energies obtained from Q_h at constant Q_c, and from Q_c at constant Q_h, differed substantially even when determined on the same sample of the same material (a bismuth germanate). The activation energy determined from Q_h was smaller than that obtained from Q_c by a factor (2.4) that was larger than, but in the same direction as, the discrepancy between the Hodge/Ribelles et al. and Tribone et al. activation energies for aP-MMA (a factor of 1.3). The values of β obtained by Hodge, Ribelles et al. and Tribone et al. are all similar to values obtained by linear techniques such as dielectric relaxation spectroscopy. For example, $\beta = 0.31 \pm 0.02$ is estimated from the data of Ishida and Yamafuji [253], using Eq. (75). By contrast with PVAc, the average enthalpic activation energies reported by Hodge, Mijovic et al. and Ribelles et al. are somewhat smaller than the dielectric value of 155 kK at $T_g = 375$ K (again estimated from the data of Ishida and Yamafuji). Tribone et al. also determined the parameters for hydrogenated and deuterated isotactic and syndiotactic PMMA. The activation energies for these tacticities differed substantially from that of the atactic form (see Table 1), which as expected lay between the isotactic and syndiotactic values. No significant differences were found between the parameters for hydrogenated and deuterated samples, for any of the tacticities. A dependence of x on thermal history, and an invariance of β, were observed for all three tacticities.

Parameters for PVC have been reported by Hodge and Berens [152], Hodge [130,161] and Pappin et al. [254]. Both groups used material from the same source. The exceptionally low values for β obtained by Hodge and co-workers, 0.23–0.27 depending on details of the data analysis, were consistent with average values extracted from the extraordinarily broad dielectric loss peaks (which were strongly temperature-dependent, however). It is the lowest value of β yet reported for enthalpy relaxation. The extremely low value of β may be caused by the small amount of crystallinity in PVC, and a corresponding heterogeneous structure, giving rise to a physically significant distribution of relaxation times in addition to inherent non-exponentiality. The value of x obtained by Hodge and Berens, 0.10–0.11, is also extraordinarily small. These x and β parameters were determined from the behavior of sub-T_g peaks for different histories, and did not produce a particularly good fit to the heat

capacity in the glass transition region. However, the experimental uncertainties in the data were rather high, especially for data near the minima between the sub-T_g peak and the heat capacity rise at T_g. Uncertainties near these minima are determined largely by the extrapolated glassy heat capacity, which for the powder samples was quite noisy, and the rubbery heat capacity was rendered unusually uncertain by the broad melting endotherm that almost overlaps with the glass transition. The cooling rate was also estimated rather than controlled. Thus, the relatively poor fits to the glass transition were less significant than usual, although it seems a problem does exist. Pappin et al. [254] reported $x = 0.27$ (almost three times larger than the Hodge and Berens value), and $\Delta h^*/R = 135$ kK (65% lower than the value 225 kK found by Hodge and Berens). Ott [251] reported an intermediate value of $\Delta h^*/R \approx 168$ kK for PVC. The origin of the discrepancies, particularly in Δh^* obtained from integrated heat capacities, is not known, but is conceivably due to experimental uncertainties that are larger than claimed by both groups. There are also possible differences in sample crystallinities due to different stabilization protocols above T_g before cooling [195], and differences in $C_{pe}(T)$ could also have arisen from different assessments of the melting endotherm. Crystallinity has been reported to affect the amorphous phase [255,256], and as noted above, could affect the β parameter. The difference in x cannot be ascribed to the different values of Δh^*, however, because the values of x $\Delta h^*/R$ are very different, ~ 36 kK for Pappin et al. [254] and 25 kK for Hodge and Berens [152].

For BPAPC, Hodge [130,161] reported $\Delta h^*/R = 150$ kK, $x = 0.19$ and $\beta = 0.46$. Except for β, these parameters are similar to those reported by the same author for a-PMMA. The value of β is about 0.10 larger than that of PMMA, and this difference probably accounts for the infrequent observation of sub-T_g endotherms in BPAPC. Ott [251] reported $\Delta h^*/R = 207$ kK for BPAPC.

The values of $\Delta h^*/R$ for inorganic glasses such as B_2O_3 [86,160], As_2Se_3 [257], $Ca/K/NO_3$ [258], $NaKSi_3O_7$ [259], NBS 710 (a soda–lime–silicate) [129,141] and lead silicate (NBS 711) [260], are generally smaller than those observed for polymers, and the values of x and β are generally larger (see Table 1). The parameters for the monomeric organic material 5P2E [42,261] are similar to those of the inorganics. Three materials stand apart from this trend, however. The parameters for polystyrene are similar to those observed for many inorganics, while those for a series of inorganic ZBLA fluoride glasses [243] and lithium acetate (LiAc) are similar to those for polymers. The parameters for LiAc are very uncertain, however, because of the inability to obtain an independent value of $\Delta h^*/R$ (the samples crystallized at slow cooling rates). For alkali, mixed alkali and lead silicates [259,260], the values of x (0.65–0.70) are much higher than for any other material, but the values for $\Delta h^*/R$ and β are not unusual. Enthalpic values of β cannot be compared with dielectric values for many inorganics because of the high conductivity of the latter, although Moynihan et al. [42] compared enthalpy, volume, strain and stress relaxation parameters for 5P2E, B_2O_3, As_2Se_3 and a mixed alkali silicate. They found that the values of β for different relaxation properties were, with a couple of exceptions, within the typical uncertainty of ± 0.05. Activation energies generally agreed to within 10%, with the largest difference being 20%. There is excellent agreement between the parameters for B_2O_3 obtained by Sales [86] and DeBolt et al. [160].

Hofer et al. [218] reported parameters for aqueous solutions of ethylene glycol (22 mol%) and lithium chloride (16 mol%), both in the bulk and imbibed in poly(hydroxyethyl methacrylate) (PHEMA) as a hydrogel. The x parameters changed somewhat with thermal history, but the values of Δh^* and averaged x for the bulk and hydrogel materials were the same within uncertainties. The values of β changed less with history, but their averages were substantially smaller for the solutions imbibed in PHEMA than for the bulk: β decreased from 0.64 to 0.39 for ethylene glycol, and from 0.93 to 0.68 for lithium chloride.

As noted in the Introduction, the values of $\theta = \Delta h^*/RT_g^2$ are similar for a wide variety of materials, generally being of the order of unity for polymers and 10^{-1} for inorganics. The aver-

age ± standard deviation for all materials listed in Table 1 is 0.57 ± 0.32.

The enthalpic activation energies for inorganics are for the most part the same as those determined from viscosity data above T_g. An exception to this occurs for the ZBLA glasses, for which the enthalpic activation energy is 40% larger than the average of two viscosity measurements [112,113].

Hodge [161] reported correlations between all four TN parameters for all materials analyzed up to that time, and these correlations have been confirmed in more recent compilations [130,133]. Low values of $\Delta h^*/R$ are associated with high values of x and β, and high values of $\Delta h^*/R$ are found with low values of x and β. They have been rationalized in terms of the Adam–Gibbs phenomenology, discussed next.

6.3. Adam–Gibbs–Fulcher (AGF) equation

This equation has been discussed in Section 2.3.3. It was noted in that section that the accuracy of Eqs. (110) and (112)–(116), relating the AGF parameters Q and T_2 to the NM parameters x and Δh^*, has been established by Hodge [130], Opalka [112], Moynihan et al. [113], Scherer [129], Sales [86] and Ribelles et al. [215]. Thus, the AGF non-linearity parameters for materials subjected only to NM analyses can be estimated with some confidence. This confidence is reinforced by the finding that the β parameter is the same within uncertainties for both NM and AGF analyses, where these have been performed on the same materials and for the same thermal histories. Published AGF parameters are summarized in Table 2, together with values of the

Table 2
Adam–Gibbs–Fulcher parameters

Material	Q (kK)	T_2 (K)	β	$-\ln A(s)$	Ref. [a] (AGF)	T_K [Ref.] (K)	T_0 [Ref.] (K)
PVAc	6.23	225	0.55	66.60	[130]		238 [250]
PVC	2.61	320	0.28	59.74	[130]	290 [130]	350 [266]
BPAPC	7.03	325	0.54	70.30	[130]	(220) [85]	
PS	17.1	210	0.74	100.3	[130]	260 [265]	
						280 [264]	
aPMMA	3.43	325	0.34	55.45	[130]	335 [263]	222 [253]
B_2O_3	11.6	286	0.65	25.68	[113,260]	335 [65]	402 [65]
As_2Se_3	9.82	237	0.67	43.10	[130]	236 [203]	
5P2E	6.16	147	0.70	63.0	[130]		
$40Ca(NO_3)_2$–$60KNO_3$	6.73	238	0.46	62.90	[130]		
$24.4[yNa_2O\cdot(1-y)K_2O]$–$75.6SiO_2$ ($y = 0$–1.0)	24.0	222	0.66	46.30	[130]		
NBS711 [b]	18.9	248	0.67	34.95	[260]		
NBS710 [c]	8.06	494	0.63	32.83	[260]		
ZBLA	5.96	525	0.50	53.00	[130]		
	12.5	425	0.46	61.38	[113]		
Glycerol [d]	2.18	134	0.51	34.20	[113]	135 [64]	132 [65]
Glycerol [e]	3.37	120	0.51	43.41	[113]		
LiAc	5.8	335	0.56	–	[133]	370 [62]	
$yPbO\cdot(1-y)P_2O_5$	13–19	150–350	0.49–0.77	23.7–69.2	[86]		
xFe_2O_3–$(1-x)Pb(PO_3)_2$	19–25	300–420	0.60–0.68	53.7–69.2	[86]		

[a] Parameters obtained directly using the AGF Eq. (109) for $\tau_0(T, T_f)$.
[b] Lead silicate.
[c] Soda-lime-silicate.
[d] $Q_h = 5$ K min^{-1}.
[e] $Q_h = 20$ K min^{-1}.

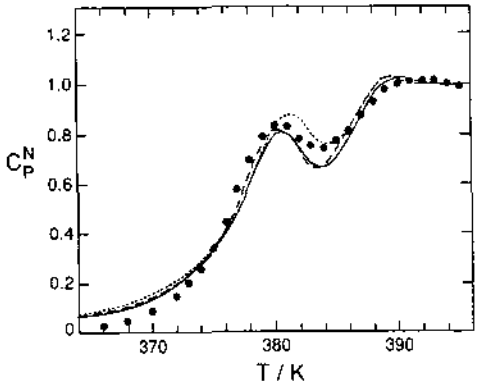

Fig. 4. Fits of NM (Eq. (88)), AGL (Eq. (108)) and AGF (Eq. (109)) expressions for $\tau(T,T_f)$, to data for atactic poly(methylmethacrylate). From Ref. [130].

Kauzmann temperature, T_K, and VTF T_0 parameter where these are known.

In assessing the AGF formalism, we consider first the quality of fits relative to NM. Following this we discuss the parameter T_2 and its relation to the Kauzmann temperature, T_K, and to the VTF temperature, T_0, obtained from linear relaxation data above T_g (most often dielectric). Enthalpic activation energies are then compared with values obtained by dielectric and other linear relaxation techniques, followed by a discussion of the 'primary' activation energy, $\Delta\mu$.

The goodness of fits afforded by AGF is comparable with that given by NM, although modest improvements of AGF fits over those of NM have been reported by Hodge for PS [130], Opalka and co-workers for some ZBLA glasses [112,113] and Ribelles et al. for a-PMMA [215]. A comparison of the NM, AGL and AGF best fits to atactic PMMA, for a single thermal history that produces a heat capacity peak in the middle of the glass transition range, is shown in Fig. 4. Because of the similarity in fits, almost none of the fitting problems found for NM are significantly improved by the AGF formalism. The advantages of AGF are restricted to the physical significance of its parameters, and its ability to rationalize the correlations observed between the NM and β parameters. The reasons for the similarity in fitting quality of the NM and AGF equations have been discussed by Moynihan et al. [113]. They observed that the ratio of non-linear to linear retardation times at temperature, T, is approximately proportional to the departure from equilibrium, $(T - T_f)$, for both NM and AGF expressions. For NM

$$\ln\left(\frac{\tau}{\tau_e}\right) \approx \left(\frac{(1-x)\,\Delta h^*}{RTT_f}\right)(T - T_f), \tag{185}$$

and for AGF

$$\ln\left(\frac{\tau}{\tau_e}\right) \approx \left(\frac{QT_2}{T(T_f - T_2)(T - T_2)}\right)(T - T_f). \tag{186}$$

The AGF derived values of T_2 are within 1 K of T_K for the inorganic materials B_2O_3 and As_2Se_3. This agreement is unusually significant, both because $\Delta C_p(T)$ for these materials closely follows the hyperbolic form of Eq. (55) from which the AGF equation is derived, and because the values of T_K are particularly reliable. The agreement for B_2O_3 is significant in another regard. It has been a long-standing puzzle why the viscosity of B_2O_3 becomes Arrhenius slightly above T_g, by contrast with the VTF behavior of enthalpy relaxation indicated by the equality of T_2 and T_K. Angell [21,262] has argued that the processes responsible for viscosity at temperatures just above T_g can decouple from the longer time processes probed by enthalpy relaxation. The AGF enthalpy relaxation parameters for B_2O_3 support this view.

For a-PMMA, Hodge [130] reported $T_2 = 325$ K. A Kauzmann temperature cannot be calculated for the uncrystallizable atactic polymer, of course, but a value of 285 K has been estimated for isotactic PMMA by O'Reilly et al. [263]. The measured values of $\Delta C_p(T)$ are the same for isotactic and atactic PMMA [263], so the difference in T_K is the same as the difference in T_g if the residual entropies at T_g are assumed to be equal. For i-PMMA, $T_g = 325$ K, $T_K = 285$ K and $T_g - T_2 = 40$ K. Thus, $T_K \approx T_g - 40 \approx 335$ K is estimated for a-PMMA. This value for T_K is equal to the T_2 value reported by Hodge [130], within experimental and computational uncertainties. For PS, Hodge [130] found $T_2 = 210$ K, substantially lower than the values for T_K ob-

tained by Karasz et al. [264] (280 ± 15 K), and by Miller [265] (260 ± 15 K). This discrepancy is the best documented failure of the AGF formalism to date, both because of the relatively large number of published enthalpy relaxation parameters for PS and because of the reliable estimates of T_K. The cause of the discrepancy is unknown. Curiously, however, the value of $T_2 = 260$ K estimated from the anomalous NM parameters obtained from the Chen and Wang data [130] agrees very well with T_K. The AGF value of T_2 for BPAPC (325 K) is substantially above T_K (220 K), but since this value of T_K is almost 200 K below T_g [85] there is reason to doubt its reliability. It is possible that the Kauzmann analysis could be compromised by the parameters used to define $\Delta C_p(T)$, which as noted above (Section 1.3.4.) predict $\Delta C_p = 0$ near the melting point. Moynihan et al. [113] obtained AGF parameters for glycerol and propylene glycol. The averaged AGF parameters for glycerol were in excellent agreement with the ac calorimetry data of Birge and Nagel [100,101], but the stretched exponential parameters were very different. The AGF parameters changed systematically with cooling rate at fixed heating rate, for simple rate scans without annealing, and the authors concluded, as have other investigators, that the phenomenology is deficient, probably in the way non-linearity is handled.

In cases where T_K is unavailable, it is of interest to compare T_2 with the VTF T_0 parameter obtained from linear relaxation data above T_g. Part of this interest arises from the possible decoupling of enthalpy (and volume) relaxation from viscosity, diffusion, dielectric, viscoelastic or other dynamic processes, suggested by Angell [20,21, 262] and discussed for B_2O_3 above. Such decoupling manifests itself as differences in T_0 or T_2 for different processes. For PVAc, the enthalpic value of $T_2 = 182$ K obtained from the data of Sasabe and Moynihan [250] is less than $T_0 = 238$ K obtained dielectrically by the same investigators on the same sample. On the other hand, the enthalpic T_2 value obtained by Hodge [130] for a different sample of PVAc (227 K) agrees well with the dielectric T_0. Bearing in mind the uncertainties in both T_2 and T_0 associated with fitting the AGF and VTF equations, the two values are probably statistically indistinguishable.

For PVC, a least squares analysis of the dielectric data of Ishida [266] shown in Ref. [267] produces a good VTF fit with $B = 290$ K and $T_0 = 351$ K. The value for T_0 is larger than the enthalpic value for T_2 of 320 K estimated by Hodge [130], but forcing $T_0 = T_2 = 320$ K produces a fit almost as good as the best fit (see discussion of VTF parameter uncertainties in Section 1.2.1.). Both values far exceed the value for T_2 of 193 K estimated from the NM parameters obtained by Pappin et al. [254]. An approximate value of $T_K = 290 \pm 20$ K has been reported by Hodge for PVC [130], using the calorimetric data of Gouinlock [268] but requiring uncertain corrections for crystallinity and syndiotacticity. This value for T_K agrees with T_2, within the (considerable) uncertainties in each. For a-PMMA, analysis of the dielectric data of Ishida and Yamafuji [253] yields $T_0 = 222$ K, considerably below both the enthalpic value $T_2 = 325$ K cited by Hodge, and the estimated Kauzmann temperature of 290 K cited above. It is possible that this difference reflects a decoupling of the dielectrically active relaxation processes from the broader, more inclusive enthalpic processes, similar to that proposed for the viscosity of B_2O_3.

Estimates of the 'primary' activation energy, $\Delta\mu$, have been published for polymers by Hodge [130,133]. The numerical factor relating $\Delta\mu$ to the AGF parameter, Q, contains the minimal entropy, s_c^*, and the heat capacity change at T_g (or T_2), both of which depend on mass. Using the Wunderlich bead as the mass unit and putting $s_c^* = k_B \ln 2$ and $k_B \ln 3!$ yields values for $\Delta\mu/k_B$ in the range 3.6–18 (for $s_c^* = k_B \ln 2$) and 1.4–7.0 kK (for $s_c^* = k_B \ln 3!$). The values for $s_c^* = k_B \ln 3!$ are comparable with rotational energy barriers. The rationale for choosing $s_c^* = k_B \ln 3!$ was that three chain segments are involved in crankshaft motions, and that these motions are reasonable candidates for the localized rearrangements involving the smallest number of chain segments. Thus, the AGF Q parameters are consistent with intersegmental rotational energy barriers being the primary excitation barrier for cooperative motions near T_g for polymers.

For inorganic glasses, Scherer [129], Opalka [112] and Moynihan et al. [164] obtained sensible values of $\Delta\mu$ comparable with bond energies, assuming $s_c^* = k_B \ln 2$.

Sales [86] studied a series of lead and iron phosphate glasses in which the number of non-bridging oxygens per PO_4 tetrahedron was varied systematically by changing chemical composition. The AGF equation was used to analyze structural relaxation in the glass transition, for histories without annealing. This work is particularly revealing, because of the detailed correlation it establishes between the AGF parameters and well-defined chemical and structural changes. As already noted (Section 6.3.), Sales found that Eq. (114) relating the AGF parameter Q and NM parameter $\Delta h^*/R$ was a good approximation for all materials studied. The AGF equation could be well-justified for these materials, because of the approximate equivalency of the hyperbolic and linear forms for ΔC_p (Section 1.3.4.). The NM activation energy, Δh^*, increased smoothly with the number of non-bridging oxygens (defined as Q by Sales but referred to here as R to avoid confusion with the AGF parameter). The increase was due largely to changes in the ratio T_2/T_g, and was accompanied by an increase in $\Delta C_p(T_g)$, consistent with Angell's 'fragility' increasing with R (Section 6.5.). The product $\Delta\mu s_c^*$ was independent of composition except for the most iron-rich glasses. Assuming $\Delta\mu$ to be determined by a P–O chemical bond energy that is independent of composition (about 100 kcal mol^{-1}), the estimated value of W^* that determines s_c^* (Eq. (102)) was found to be about 4.6, or $2^{2.2}$. Both W^* and T_g/T_2 increased with increasing iron content, which was interpreted in terms of different coordination numbers and geometries for the Fe^{3+} and Pb^{2+} cations. It was suggested that the structural constraints imposed by the crystal-field-stabilized octahedral Fe^{3+} moieties increased the values of both $\Delta\mu s_c^*$ and T_g/T_2, compared with the less geometrically constrained Pb^{2+} species. As discussed below in Section 6.5. with regard to the NM parameter correlations, the increases in both $\Delta\mu s_c^*$ and T_g/T_2 are consistent with the idea that $\Delta\mu$, and possibly s_c^*, determine the ratio T_g/T_2. The values of β did not exhibit any significant variation with R. Further interesting speculations about the relationship between coordination number and geometry, the pre-exponential factor, strong and fragile behavior and viscosity above T_g, can be found in the original paper [86].

6.4. AC calorimetry

This experimental technique has been described in Section 2.2. Real and imaginary components of the complex heat capacity C_p^* are obtained as a function of temperature and frequency, and it is found that the temperature dependences of the fixed frequency real compo-

Table 3
AC calorimetry parameters

Material	β	$-\log_{10} A$	T_0 (K)	B (K)	Ref.	Comment
Glycerol	0.65 ± 0.03	14.6 ± 0.9	128 ± 5	2500 ± 300	[100,101]	
(Non-linear	0.505	18.85	120	3372	[113]	(5 K min^{-1})
AGF)	0.510	14.85	134	2179	[113]	(20 K min^{-1})
Propylene glycol	0.61 ± 0.04	13.8 ± 0.4	114 ± 7	2020 ± 130	[100]	
$OTP_{1-x}OPP_x$	[a]					
$x = 0$ (extrap.)				184 ± 13	[269]	
$x = 0.09$	[b]	18.7 ± 1.3	117 ± 6	3175 ± 320	[269]	
0.16		16.9 ± 2.1	186 ± 12	2397 ± 590	[269]	
0.22		20.2 ± 2.3	172 ± 13	3436 ± 820	[269]	
0.33		22.2 ± 2.8	164 ± 14	4154 ± 900	[269]	

[a] OTP, o-terphenyl; OPP, o-phenylphenol.
[b] Temperature-dependent: $\beta = -0.81 - 425/T$ (K).

nent resemble the heat capacity scans during cooling observable with some DSC instruments. As with other linear relaxation techniques, stretched exponential (or other functional) parameters can be obtained from the real and imaginary components (e.g., by applying Eqs. (75) or (82) to the loss peaks), and VTF parameters can be obtained from the temperature dependence of the position of the peak in the imaginary component, or of the relaxation time obtained from stretched exponential fits. It is of considerable interest and importance to compare the linear parameters obtained by ac calorimetry with the non-linear parameters obtained by scanning calorimetry on the same materials. Unfortunately, ac calorimetry has so far been applied to only three materials: propylene glycol [101], glycerol [101,102], and orthoterphenyl/orthophenylphenol mixtures [269–271]. The linear relaxation parameters for these materials are collected in Table 3. AC calorimetric and non-linear DSC enthalpy relaxation parameters have been directly compared only for glycerol [113], and the non-linear AGF parameters for this material from Table 2 are included in Table 3 for convenience. Excellent agreement between the linear VTF and non-linear AGF parameters is observed, but the stretched exponential parameter β is significantly different for the two techniques. It is curious that the discrepancy lies in the non-exponentiality, which is believed to be well described, rather than in the description of non-linear behavior, about which doubts are mounting. The discrepancy in β could perhaps be caused by a frequency-dependent thermal conductivity $\kappa(\omega)$, since the stretched exponential was fitted to $C_p(\omega)\kappa(\omega)$ rather than $C_p(\omega)$ (Section 2.2.). Such a frequency dependence would not have to be very strong to modify the shape of the real and imaginary components, from which β is found, and could be sufficiently weak that the peak frequency in C_p^* and the retardation time are not significantly affected, therefore accounting for the agreement in VTF parameters. However, κ has been found to be independent of frequency for o-terphenyl and its mixtures [269].

For o-terphenyl, the ac calorimetric value of T_0 (184 ± 13 K by extrapolation) agrees with T_K (200 ± 10 K) [272]. For glycerol, the linear ac calorimetric and non-linear AGF values of T_2 (128 ± 5 and 127 ± 7 K, respectively) also agree with T_K (135 ± 3 K) [64]. The stretched exponential parameter, β, is independent of temperature for glycerol and propylene glycol, but is strongly temperature-dependent for o-terphenyl. Extrapolation of the latter trend [269] indicates that β would be zero at or near T_K and T_0. The stretched exponential β parameters for glycerol and propylene glycol obtained calorimetrically are smaller by about 0.15 than the dielectric values [103].

6.5. Parameter correlations

Strong correlations between β, x and Δh^* have been reported by Hodge [130,133], and were rationalized in terms of the AGF phenomenology. Major conclusions from this work are that the correlations can be consistently mapped onto the classification of strong and fragile behavior in liquids advocated by Angell [5,20,21,62] (the origins of which can be traced to the work of Laughlin and Uhlmann [123]), and that a high degree of non-linearity is associated with fragile liquid behavior. The mapping arises from (i) the link between non-linearity and the ratio T_g/T_2 (Eqs. (113) and (116)), (ii) the VTF result that deviations from Arrhenius behavior increase with decreasing T_f/T_2 (Eq. (114)) and (iii) the fact that the strong and fragile classification rests on T_g/T as a scaling variable. If it is hypothesized that $\Delta\mu$ determines the ratio T_f'/T_2, i.e., that a high primary activation energy prevents T_f' from approaching T_2, it can be shown that $x\,\Delta h^*$ is approximately constant:

$$Q \approx K_1\,\Delta\mu \approx K_2\left(\frac{T_f'}{T_2} - 1\right) \approx K_2\left(1 - \frac{T_2}{T_f'}\right) \approx K_2 x \tag{187}$$

$$\Rightarrow \frac{\Delta h^*}{R} \approx \frac{Q}{x^2} \approx K_2/x \Rightarrow \frac{x\,\Delta h^*}{R} \approx K_2. \tag{188}$$

Eq. (188) is consistent with the experimental observation that $x\,\Delta h^*$ is relatively constant compared with Δh^* alone (see Table 1). It has been noted by Angell [21], however, that the VTF equation implies that Q and $T_g/T_0 = T_g/T_2 =$

T_g/T_K should be linearly related, if the pre-exponential factor and the relaxation time at T_g are material-independent. For hydrogen bonded materials, Angell found $T_g/T_0 = 1.0 + 0.0255\ Q/T_0$, consistent with $T_g \to T_0 = T_2 = T_K$ when $Q \to 0$. On the other hand, the assumption that $\Delta\mu$ determines T_g/T_2 could also be regarded as being vindicated by the correct prediction that $\tau(T_g)$ is relatively constant for different materials. Angell [5,20,21,83] has also argued that the thermodynamic contribution to the AG Q parameter, $[\Delta C_p(T_g)]$, as well as the kinetic factor, $\Delta\mu$, are both important in determining liquid state dynamics. Thus the assumption that $\Delta\mu$ is the dominant factor may only be valid for similar classes of material, and this would be consistent with the separate correlations observed for different classes of materials, discussed below. On the other hand, it can also be argued that the thermodynamic factor, ΔC_p, would be more consistently assessed at the thermodynamic temperature, T_K, rather than the kinetically determined T_g, although this would require longer extrapolations and introduce additional uncertainties. One analysis [83] has suggested that using $\Delta C_p(T_g)$ can generate spurious discrepancies.

If $\Delta C_p(T_g)$ is assumed constant rather than $\Delta C_p(T_2)$, the proportionality constant between Q and $\Delta\mu$, and the relation between Q and Δh^*, are both modified. Inserting $C = C'T_g/T_2$ (Eq. (55)) into Eq. (105) for Q yields

$$Q = (N_A s_c^*\ \Delta\mu/(k_B C'))(T_2/T_g) \tag{189}$$

$$= Q'(T_2/T_g), \tag{190}$$

so that

$$Q' = QT_g/T_2 \tag{191}$$

$$= \frac{x^2\ \Delta h^*}{R}\ \frac{T_g}{T_2} \tag{192}$$

$$= \frac{x^2\ \Delta h^*}{R(1-x)}. \tag{193}$$

Eq. (193) is identical to Eq. (110), obtained from $\Delta C_p = C =$ constant.

When $T_f'/T_2 = (1-x)^{-1}$ is plotted against $Q = x^2\ \Delta h^*/R$ [133], linear relations consistent with Eq. (187) are observed. Separate correlation lines are observed for different classes of materials, corresponding to different groupings of constant $x\ \Delta h^*$, suggesting that K_2 of Eqs. (187) and (188) depends on material type. These correlations are shown in Fig. 5. The separate correlation lines could be due to the dependence of ΔC_p on the class of material, discussed above, or to a variable s_c^*, as in the iron-rich phosphate glasses studied by Sales [86]. These separate correlation lines must be regarded as provisional, however, since the correlations for different material types degrade into an uncorrelated broad scatter if T_f'/T_2 is plotted against $Q' = x^2\ \Delta h^*/(R(1-x))$.

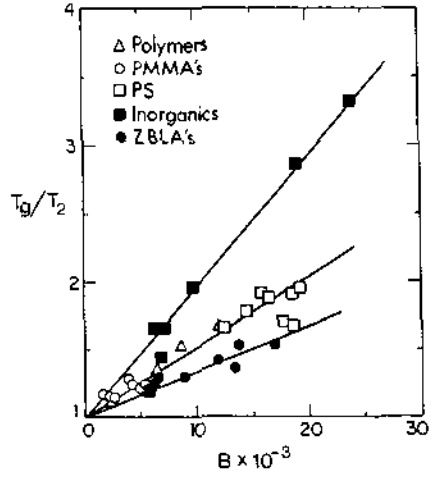

Fig. 5. Correlation between T_g/T_2 and AGF parameter B (equal to Q of Eq. (109)). From Ref. [133].

The stretched exponential parameter, β, also correlates with x and T_f'/T_2. The correlation between x and β is shown in Fig. 6. Hodge [133] used the long-standing idea, based on the Adam–Gibbs concept of increasing size of relaxing groups and increasing cooperativity with decreasing temperature, to suggest that β should approach 1.0 in the limit $T_f'/T_2 \to \infty$ $(x \to 1.0)$, and tend to zero as $T_f' \to T_2$ $(x \to 0)$. A simple functional relation that satisfies these limits, and which is consistent with the approximately linear correlation observed between x and β, is

$$\frac{T_f'}{T_2} \approx \frac{1}{(1-x)} \approx \frac{1}{(1-\beta)}. \tag{194}$$

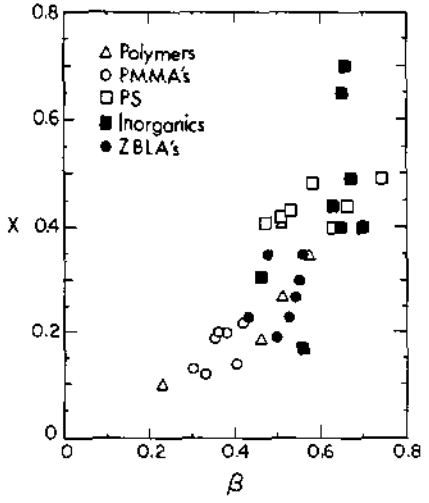

Fig. 6. Correlation of NM parameter, x, with non-exponentiality parameter β. From Ref. [133].

As already noted, independent experimental evidence for $\beta \to 0$ as $T \to T_2$ exists for o-terphenyl and salol [269]. Two objections to Eq. (194) have been raised, however. First, although its equilibrium form ($T_f' = T$) is consistent with the strong temperature dependence of β observed in many (but not all) materials (the o-terphenyl mixtures observed by Dixon and Nagel [269], for example), it is inconsistent with the TN assumption that β is constant. This criticism can be countered by appealing to the same reasoning used to explain the success of the generalized Arrhenius NM equation (Section 3.2.1.), namely that the range in thermodynamic and fictive temperatures over which relaxation occurs in a DSC scan is sufficiently small that β can be well approximated as being constant. A second objection [273] is that Eq. (194) is inconsistent for the many other materials for which the linear values of β are constant (glycerol and propylene glycol, for example [103]). In particular, the generally lower values of x for polymers implies a stronger temperature dependence for z^* and therefore of β, yet β is generally less temperature-dependent for polymers than for monomeric glasses. However, the temperature dependence of z^* from which Eq. (194) is derived is weaker for $T \gg T_g$ than for $T \approx T_g$. Also, the range in T_f'/T_2 over which significant changes in enthalpic β values occur (~ 1.11–2.5) is much larger than the typical ranges in T/T_2 over which linear data are acquired. Independent support for Eq. (194) has come from recent work by Moynihan and Schoeder [274], who described light scattering evidence for nanoscale inhomogeneities in glass-forming liquids that relax at different rates. They suggested that this could be the source of non-exponentiality. Expressions relating the non-linearity parameters to the size of these regions were derived, and the predicted sizes of the inhomogeneities were shown to be in excellent agreement with those determined by other methods. In this interpretation the physical significance of non-exponentiality lies in the distribution of retardation times associated with the inhomogeneities, rather than the inherent non-exponentiality of cooperative or collective molecular motions. A temperature-dependent β is predicted that is consistent with β approaching zero as $T \to T_2$.

Exceptions to Eq. (194) nevertheless occur. For bulk and hydrogel imbibed aqueous ethylene glycol (EG) and LiCl solutions [218], the value of β is much smaller for the solutions in gel than in the bulk, but the corresponding values of x and T_g/T_2 are very similar. The lower values of β for the solutions imbibed in gel support the interpretation of a low β as originating from a heterogeneous environment in the hydrogels, rather than from increased cooperativity, if it is assumed that these different environments have similar non-linear characteristics. Sales [86] observed that β was independent of composition in a series of phosphate glasses, for which T_g/T_2 changed systematically. The silicate glasses are also exceptional, in having by far the largest values of x and T_g/T_2 for any material, but normal values of β. The large values of T_g/T_2 can reasonably be attributed to high values of $\Delta\mu$ associated with the breaking of a covalent bond [275], and the relatively normal values of β can be attributed to the fact that, once the chemical bond is broken, geometric constraints make further relaxation normally cooperative. Thus, the unusually tight three-dimensional network structure of silicates may be the reason for their exceptional enthalpy relaxation parameters.

7. Summary and future considerations

The current phenomenologies give good to excellent descriptions of enthalpy relaxation near equilibrium. For many (perhaps most) engineering applications, such as those discussed in Scherer's book [9], they appear to be adequate. The Adam–Gibbs phenomenology provides valuable insights into the physical origin of non-linearity. It establishes a link between non-linearity and Angell's strong/fragile classification of liquid behavior, between non-linearity and the Kauzmann paradox, and provides a plausible rationalization of the correlations observed between the NM parameters. As with the empirical NM and KAHR equations, however, Adam–Gibbs does not provide a satisfactory description of relaxation far from equilibrium. Resolution of the failure of these formalisms must be counted among the most important goals of future research.

Moynihan [276] has attempted to modify the phenomenology in several ways to improve the quality of fits, without success. The attempted modifications were as follows.

(1) Make τ_i in $\phi(t) = \Sigma \exp[-t/\tau_i]$ depend partly on T_{fi}, in addition to its dependence on the global T_f (in KAHR terms, making τ_i a function of both δ_i and $\Sigma_i g_i \delta_i$:

$$\tau_i = \tau_{i,0} \exp\left(\frac{x\ \Delta h^*}{RT} + \frac{y(1-x)\ \Delta h^*}{RT_{f(\mathrm{avg})}} + \frac{(1-y)(1-x)\ \Delta h^*}{RT_{fi}} \right). \quad (195)$$

No improvement was observed (best fits were obtained with $y = 1$).

(2) Add a tail to the stretched exponential decay function:

$$\log\ g_i(\tau_i) = \log\ g_{i,\mathrm{KWW}}(\tau_i) + K\ \log^2(\tau_i/C). \quad (196)$$

Best fits were obtained when $K = 0$, i.e., when $g(\tau_i)$ was the stretched exponential distribution.

(3) Abandon thermorheological simplicity by making β depend on T or T_f. The introduction of such dependences did not improve the situation, presumably because the range in T and T_f over the glass transition is too small to significantly affect β (Section 6.5).

(4) Change the form of the non-linearity expression to make it more sensitive to $T - T_f$:

$$\tau = \tau_0 \exp\left(\frac{x\ \Delta h^*}{R} + \frac{(1-x)\ \Delta h^*}{RT_f} + K(T_f - T)^3 \right). \quad (197)$$

No improvement was found.

Ritland [11] also suggested a modification to $\tau(T, T_f)$:

$$\mathrm{d}T_f/\mathrm{d}t = \pm\left(|T - T_f| + k\,|K - T_f|^N \right)/\tau, \quad (198)$$

which was evaluated by Scherer [154] for volume relaxation in a $Na/Ca/SiO_2$ glass. Scherer found improved fits at large departures from equilibrium using $k = 1.0 \times 10^{-13}$ and $N = 7$, corresponding to a modification of only one part in 10^6 in $\mathrm{d}T_f/\mathrm{d}t$ for $T_f - T \approx 10$. Scherer also noted that the stretched exponential parameter, β, decreased at smaller reduced times but that, although incorporating this into the calculation improved most of the fits, not all of the data could be described within uncertainties. Gupta and Huang [199] also noted a failure in the TN phenomenology for rapidly quenched silicate fibers that were far from equilibrium, although satisfactory fits could be made to slowly cooled bulk and fiber data obtained relatively close to equilibrium. Rekhson and Ducroux [277] have described a phenomenology based on the AGF equations in which a distribution in $\{Q_i\}$ is assumed. The fastest time constants in $g(\ln \tau_i)$ are characterized by the smallest Q_i. These authors showed that this phenomenology removed the inconsistencies observed by Scherer.

Since none of the modifications listed above allow all histories to be fit with a single set of parameters, it seems that a more fundamental change in the phenomenology is needed. However, any modification must converge to the present phenomenology in the limit of small depar-

tures from equilibrium, because the current methods for describing non-linearity are consistent with behavior seen near and above T_g. The search for a new phenomenology is made particularly challenging by the fact that a rigorous theoretical derivation of non-linearity, and of the glass transition in general, is not yet in sight. The heuristic Adam–Gibbs approach is probably still the best account available.

A more modest short-term goal is to parameterize more materials in more detail. The validity of the correlations between x, Δh^* and β needs to be tested for many more material types. More systematic studies of the type made by Sales [86] for lead and iron phosphate glasses need to be made, and the relationship between the AGF T_2, VTF T_0, and Kauzmann T_K temperatures needs to be better defined. For polymers, the effects of crystallinity and cross-linking density need further exploration.

A rigorous and fully satisfactory account of experimental thermal transfer effects has not yet been given. Although the data of O'Reilly and Hodge [89] at very slow heating rates indicate that thermal transfer cannot account for all the observed fitting problems, a standard and rigorous procedure for correcting for thermal transfer is needed. To date, only Hutchinson and coworkers [90,91] have explicitly addressed this issue.

Despite the fact that enthalpy relaxation should now be considered to be a standard experimental technique, its inherent non-linearity is too often not fully appreciated, or is incorrectly handled, by many practitioners. There are too many literature reports that contain incorrect data analyses. It is to be hoped that this situation will improve, and that the field will continue to advance in the future.

It is a pleasure to thank J.M. O'Reilly, W.M. Prest Jr. and A.J. Kovacs for valuable and stimulating discussions, G.W. Scherer and J.M. Hutchinson for their valuable comments and sharing some of their preprints and unpublished observations, and C.T. Moynihan for valuable discussions and permission to cite some results in advance of publication.

8. References

[1] S.M. Rekhson, J. Non-Cryst. Solids 95&96 (1987) 131.
[2] P.K. Gupta, Rev. Solid State Sci. 3 (1989) 221.
[3] G.W. Scherer, J. Non-Cryst. Solids 123 (1990) 75.
[4] J. Wong and C.A. Angell, Glass: Structure by Spectroscopy (Dekker, New York, 1976).
[5] C.A. Angell, Pure Appl. Chem. 63 (1991) 1387.
[6] L.C.E. Struik, Physical Aging in Amorphous Polymers and Other Materials (Elsevier, Amsterdam, 1978).
[7] A.R. Cooper, Glastech. Ber. 56K Bd.2 (1983) 1160.
[8] A.R. Cooper and P.K. Gupta, Phys. Chem. Glasses 23 (1982) 44.
[9] G.W. Scherer, Relaxation in Glass and Composites (Wiley–Interscience, New York, 1986).
[10] I.M. Hodge and C.A. Angell, J. Phys. Chem. 67 (1977) 1647.
[11] H.N. Ritland, J. Am. Ceram. Soc. 37 (1954) 370.
[12] C.T. Moynihan, A.J. Easteal, M.A. DeBolt and J. Tucker, J. Am. Ceram. Soc. 59 (1976) 12.
[13] G.S. Fulcher, J. Am. Ceram. Soc. 77 (1925) 3701.
[14] G. Tamman and W. Hesse, Z. Anorg. Allg. Chem. 156 (1926) 245.
[15] H. Vogel, Phys. Z. 22 (1921) 645. The Vogel equation, $\eta(T)/\eta(T_1) = \eta_\infty^{((T-T_1)/(T-T_\infty))}$, is superficially different from the Fulcher and Tamman–Hesse equations, but is in fact equivalent to them, with $A = \ln \eta_\infty$, $B = \ln \eta_\infty (T_\infty - T_1)$ and $T_\infty = T_0$ [G.W. Scherer, J. Am. Ceram. Soc. 75 (1992) 1060]. It is common practice to refer to Eq. (3) as the Vogel–Tamman–Fulcher (VTF) equation, and with apologies to Hesse we continue this tradition here. A brief history of these equations has been given by Scherer in the paper cited above.
[16] G. Adam and H.J. Gibbs, J. Chem. Phys. 43 (1965) 139.
[17] M.L. Williams, R.F. Landell and J.D. Ferry, J. Am. Chem. Soc. 77 (1955) 3701.
[18] J.D. Ferry, Viscoelastic Properties of Polymers, 3rd Ed. (Wiley, New York, 1980).
[19] P.W. Anderson, comment in Ann. NY Acad. Sci. 484 (1986) 288.
[20] C.A. Angell, J. Phys. Chem. Solids 49 (1988) 863.
[21] C.A. Angell, J. Non-Cryst. Solids 131–133 (1991) 13.
[22] Proc. 1st Int. Discussion Meeting on Relaxation in Complex Systems, Crete, June 1990, J. Non-Cryst. Solids 131–133 (1991).
[23] Glasses can be in a (metastable) equilibrium state near T_g, although these are probably better called supercooled liquids.
[24] F. Simon, Ergeb. Exact. Naturw. 9 (1930) 225; Anorg. Allgem. Chem. 203 (1931) 220.
[25] M. Goldstein, Ann. NY Acad. Sci. 279 (1976) 68.
[26] M. Goldstein, J. Chem. Phys. 64 (1976) 4767.
[27] M. Goldstein, in: Modern Aspects of the Vitreous State, ed. J.P. MacKenzie, Vol. 3 (Butterworths, London, 1964) p. 90.
[28] H.N. Ritland, J. Am. Ceram. Soc. 39 (1956) 403.
[29] A.J. Kovacs, J. Polym. Sci. 30 (1958) 131.

[30] K. Hofer, J. Perez, and G.P. Johari, Philos. Mag. Lett. 64 (1991) 37.
[31] The observed scatter in the enthalpy results, obtained by integration of heat capacity curves, was comparable with that in adiabatic calorimetry [K. Adachi and T. Kotaka, Polym. J. 12 (1982) 959].
[32] I.M. Hodge, in: Relaxations in Complex Systems, ed. K.L. Ngai and G.B. Wright (Office of Naval Research, Arlington, VA, 1984) p. 65.
[33] S. Spinner and A. Napolitano, J. Res. Nat. Bur. Stand, 70A (1966) 147.
[34] H.R. Lillie, J. Am. Ceram. Soc. 19 (1936) 45.
[35] M. Hara and S. Suetoshi, Rep. Res. Lab. Asahi Glass Co. 5 (1955) 126.
[36] A.J. Kovacs, Fortschr. Hochpolym.-Forsch. 3 (1963) 394.
[37] A.Q. Tool and C.G. Eichlin, J. Am. Ceram. Soc. 14 (1931) 276.
[38] A.Q. Tool, J. Am. Ceram. Soc. 29 (1946) 240.
[39] A.Q. Tool and C.G. Eichlin, presentation at Am. Ceram. Soc. Meeting, Atlantic City, 1924.
[40] R. Gardon and O.S. Narayanaswamy, J. Am. Ceram. Soc. 53 (1970) 380.
[41] O.S. Narayanaswamy, J. Am. Ceram. Soc. 54 (1971) 491.
[42] C.T. Moynihan, P.B. Macedo, C.J. Montrose, P.K. Gupta, M.A. DeBolt J.F. Dill, B.E. Dom, P.W. Drake, A.J. Easteal, P.B. Elterman, R.P. Moeller, H. Sasabe and J.A. Wilder, Ann. NY Acad. Sci. 279 (1976) 15.
[43] M.J. Richardson and N.G. Savill, Polymer 30 (1975) 2246.
[44] J.H. Flynn, Thermochim. Acta 8 (1974) 69.
[45] Yu.A. Sharonov and M.V. Vol'kenshtein, in: Structure of Glasses, Vol. 6, ed. E.A. Porai-Koshits (Consultants Bureau, New York, 1966).
[46] R.O. Davies and G.O. Jones, Proc. R. Soc. (London) 217A (1953) 27.
[47] A.J. Kovacs, J.J. Aklonis, J.M. Hutchinson and A.R. Ramos, J. Polym. Sci. 17 (1979) 1097.
[48] J.M. Hutchinson and A.J. Kovacs, J. Polym. Sci.–Phys. 14 (1976) 1575.
[49] O.S. Narayanaswamy, J. Am. Ceram. Soc. 71 (1988) 900.
[50] O.V. Mazurin and Yu.K. Startsev, Sov. J. Glass Phys. Chem. (Eng. Trans) 7 (1981) 274.
[51] I.M. Hodge and J.M. O'Reilly, Polymer 33 (1992) 4883. Eq. (5) in this paper is mathematically incorrect, but this does not affect the qualitative arguments given there. The correct expression for τ' is given by Eq. (36) of the present paper.
[52] G.W. Scherer, personal communication.
[53] J.M.G. Cowie and R. Ferguson, Polym. Commun. 27 (1986) 258.
[54] J.M.G. Cowie, S. Elliot, R. Ferguson and R. Simha, Polym. Commun. 28 (1987) 298.
[55] J.L. Gomez-Ribelles, R. Diaz-Calleja, R. Ferguson and J.M.G. Cowie, Polymer 28 (1987) 2262.
[56] J.M.G. Cowie and R. Ferguson, Macromolecules 22 (1989) 2307.
[57] J.M.G. Cowie and R. Ferguson, Macromolecules 22 (1989) 2312.
[58] M. Oguni, H. Hikawa and H. Suga, Thermochim. Acta 158 (1990) 143.
[59] S.Z.D. Cheng, D.P. Heberer, J.J. Janimak, S.H.-S. Lien and F.W. Harris, Polymer 32 (1991) 2053.
[60] C. Tsitsilianis and I. Mylonas, Makromol. Chem. Rapid. Commun. 13 (1992) 207.
[61] W. Kauzmann, Chem. Rev. 43 (1948) 219.
[62] C.A. Angell, in: Relaxations in Complex Systems, ed. K.L. Ngai and G.B. Wright (Office of Naval Research, Arlington, VA, 1984) p. 3.
[63] P. Richet and J. Bottinga, Geochim. Cosmochim. Acta 48 (1984) 453.
[64] C.A. Angell and D.L. Smith, J. Phys. Chem. 86 (1982) 3845.
[65] C.A. Angell and K.J. Rao, J. Chem. Phys. 57 (1972) 470, and references therein.
[66] A.A. Miller, Macromolecules 11 (1978) 859.
[67] F. Stillinger, J. Chem. Phys. 88 (1988) 7818.
[68] C.A. Angell, D.R. MacFarlane and M. Oguni, Proc. NY Acad. Sci. 484 (1986) 241.
[69] G. Vuillard, Ann. Chim. (Paris) 2 (1957) 223.
[70] E.J. Sare, PhD thesis, Purdue University (1970).
[71] J.H. Gibbs and E.A. DiMarzio, J. Chem. Phys. 28 (1958) 373.
[72] P.D. Gujrati and M. Goldstein, J. Chem. Phys. 74 (1981) 2596.
[73] E.A. DiMarzio and C.M. Guttman, Macromolecules 20 (1987) 1403.
[74] A.J.-M. Yang and E.A. DiMarzio, Macromolecules 24 (1991) 6012.
[75] P. Ehrenfest, Commun., Kamerlingh Onnes Lab., U. Leiden (1933) 756.
[76] C.A. Angell and W. Sichina, Ann. NY Acad. Sci. 279 (1976) 53.
[77] J.M. O'Reilly, J. Polym. Sci. 57 (1962) 429.
[78] G. McKenna, in: Comprehensive Polymer Science, Vol. 2, Polymer Properties, ed. C. Booth and C. Price (Pergamon, Oxford, 1989) ch. 10.
[79] C.T. Moynihan and A.V. Lesikar, Ann. NY Acad. Sci. 371 (1981) 152.
[80] P.K. Gupta, J. Non-Cryst. Solids 102 (1988) 231.
[81] B. Wunderlich and L.D. Jones, J. Macromol. Sci. Phys. B3 (1969) 67.
[82] V.B.F. Mathot, Polymer 25 (1984) 579.
[83] C. Alba, L.E. Busse and C.A. Angell, J. Chem. Phys. 92 (1990) 617.
[84] P.B. Macedo and A. Napolitano, J. Nat. Bur. Stand. 71A (1967) 231.
[85] Yu. Privalko, J. Phys. Chem. 84 (1980) 3307.
[86] B.C. Sales, J. Non-Cryst. Solids 119 (1990) 136.
[87] A.P. Gray, in: Analytical Calorimetry, ed. R.S. Porter and J.F. Johnson (Plenum, New York, 1968).
[88] M.A. DeBolt, PhD thesis, Catholic University of America (1976).